# Impact of static and dynamic load models on security margin estimation methods

Hannes Hagmar[a,*], Anh Tuan Le[a], Robert Eriksson[b]

[a] *Chalmers University of Technology, Gothenburg 412 96, Sweden*
[b] *Svenska kraftnät (Swedish National Grid), Sundbyberg 172 24, Sweden*

**Abstract**

The post-contingency loadability limit (PCLL) and the secure operating limit (SOL) are the two main approaches used when computing the security margins of an electric power system. While the SOL is significantly more computationally demanding than the PCLL, it can account for the dynamic response after a disturbance and generally provides a better measure of the security margin. In this study, the difference between these two methods is compared and analyzed for a range of different contingency and load model scenarios. A methodology to allow a fair comparison between the two security margins is developed and tested on a modified version of the Nordic32 test system. The study shows that the SOL can differ significantly from the PCLL, especially when the system has a high penetration of loads with constant power characteristics or a large share of induction motor loads with fast load restoration. The difference between the methods is also tested for different contingencies, where longer fault clearing times are shown to significantly increase the difference between the two margins.

*Keywords:* Dynamic security margins, dynamic security limits, load modeling, security assessment, security margin estimation

## 1. Introduction

Electric power systems are generally operated according to the $N$-1 contingency criterion, meaning that the system should be able to withstand the loss of any single system component, such as a transmission line or a generating unit, without losing stability. A system capable of handling this is said to be *secure* [1]. However, even when the system is secure for a given operation condition, system operators are also required to know how far the system can move from its current operating point and still remain secure. Therefore, system operators

*Corresponding author
*Email address:* hannes.hagmar@chalmers.se (Hannes Hagmar)

continuously compute *security margins*, which in turn represents the available transmission capacity in the system.

Two main approaches are used to compute the security margins of a power system: the post-contingency loadability limit (PCLL) and the secure operating limit (SOL) [1, 2]. The PCLL is evaluated by estimating the loadability limit of a post-contingency operating point, where a solution path is traced by iteratively increasing the system stress until the system's critical point is reached. The characteristics of the iteratively increased system stress in the post-contingency setting are similar to that of the slow load restoration that typically follows in a long-term voltage stability event. An alternative measure of the security margin is the SOL, which refers to the most stressed *pre-contingency* operating state in which the system can withstand a specified set of contingencies. The SOL, also referred to as the dynamic security margin, can account for the dynamic response after a contingency and it generally provides a more accurate measure of the security margin of the system. However, the SOL has been comparatively less documented in the literature, likely due to the practical difficulties required in its estimation. The SOL requires numerous full time-domain or quasi steady-state (QSS) simulations to trace the security limit for a set of different contingencies, a task that is generally too time-consuming to meet the near real-time monitoring requirements of system operators.

A security margin's capability to account for the dynamic response after a disturbance is likely to become increasingly important in the future. Electric power systems are experiencing a significant transformation; primarily characterized by increased penetration of power electronic converter interfaced technologies [3]. This type of components may have a significant influence on system stability, and includes the impact of dynamic load models [4], converter interfaced generation [5, 6], high-voltage direct current (HVDC) systems [7], as well as battery energy storage devices and flexible ac transmission systems [8, 9]. With the significant integration of such technologies, the dynamic response of power systems will in general become more dependent on fast-response devices, altering the power system dynamic behavior.

Although the SOL would provide a better measure of the security margin in a future with a higher share of fast-acting loads and generation, the high computational effort required in its estimation limits its possible applications. Several studies have attempted to provide solutions to the high computational effort required in estimating the SOL. Methods based on QSS simulations work by replacing the short-term differential equations of generators, motors, compensators with the corresponding algebraic equilibrium equations, thus significantly simplifying the general dynamic model of the power system [1]. Estimation methods for the SOL that are based on QSS simulations, as found in [10], can reduce the simulation time significantly compared to full time-domain simulations, but cannot fully incorporate the impact of short-term and transient effects. In [11], a method that combined QSS and time-domain simulations was proposed to include the impact of short-term effects. In [12], the authors used real synchrophasor data from the Hydro-Québec's transmission system to baseline phase-angles versus actual transfer limits across system interfaces. A

method for forecasting the SOL was then developed using ensemble decision trees where medoid clustering of the phase shift data was used as predictive features. In [13, 14, 15], various machine learning approaches based on training neural networks were proposed to allow real-time estimation of the SOL, with a specific focus on voltage stability. In [16], a combined methodology based on validating the estimations of neural networks with actual time-domain simulations was proposed to overcome the robustness issues that are commonly related to machine learning methods.

Despite ongoing efforts in improving the computational efficiency of the SOL, the circumstances when the SOL is to prefer to the PCLL have been relatively unexplored in the literature. In [17], it was shown that if a system starts at a stable equilibrium and is slowly stressed towards a critical point without encountering oscillations or other limit-induced events (e.g. reactive power limits for generators), static estimation methods are sufficient to locate the exact critical point experienced by the dynamic system. Thus, in such circumstances, the security margin computed by PCLL would essentially be equal to the one computed using the method of the SOL. In [16], a theoretical comparison between the two security margins was performed with respect to voltage stability, where the difference between the two measures was illustrated using a concept called "transient $P$-$V$ curves". The study highlighted the importance of load restoration dynamics on the difference between the two methods but provided no numerical results. In [18], the SOL was numerically compared to another type of security margin computed by static $V$-$Q$ curves, in which variations in the reactive power injection at a bus would affect the voltage at that same bus. The study concluded that the SOL (or generally a dynamic simulation approach) is a superior method compared to $V$-$Q$ curves, but since the two methods are so conceptually different, the results of the two methods could not directly be compared. In [10], the SOL computed by QSS simulations was compared to the PCLL, where primarily the impact of post-disturbance control was studied. No variations in the load composition were analyzed in the study.

A direct comparison between the SOL and PCLL is however not trivial, as one is computed using a static model of the system, while the other is generally estimated using a dynamic model. Thus, although it is well-known that the PCLL and the SOL may produce significantly different estimations of the security margin, the difference in the results can be caused by both in *how* the simulations were conducted, as well as owing to the fact that the SOL can account for the system's dynamic response after a disturbance. To address the above-mentioned lack of an accurate comparison between the methods, this study aims to develop a methodology that allows the two security margins to be fairly compared and to isolate the root cause of the difference between the two security margins. Further, we also provide a comparison for a large range of different static and dynamic load configurations and disturbance scenarios that are based on the developed methodology. We focus on the impact that different load model configurations and disturbances have on the two defined security margins. It should be noted that other aspects such as post-disturbance controls and generation characteristics of, for instance, converter-interfaced gen-

eration, will also have a significant impact on the difference between the two security margins and such studies deserves further attention in future research. The stability criteria that the two security margin methods are analyzed with respect to are mainly short-term and long-term voltage instability and rotor (transient) angle stability. The impact that frequency stability may have on the two security margins has not been analyzed in the study.

The main contributions of this study can be summarized as:

- A methodology to allow a fair comparison between the PCLL and the SOL is developed. The purpose of the developed methodology is to isolate the root cause of the difference between the two security margins; that is, that the PCLL is computed by the loadability limit of a *post-contingency* operating state, whereas the SOL is computed by the loadability limit to the final *pre-contingency* operating state in which the system is still secure. Any difference between the security margins caused by differences in the simulations and the simulation setups is compensated for.

- An extensive numerical comparison between the SOL and the PCLL under a range of both static and dynamic load model configurations is performed. Different fault scenarios are examined and discussed in the study. The purpose is to examine under what circumstances that the SOL is preferable to the PCLL. While the results are specific for the used test system, they are used to illustrate for which load and disturbance scenarios the difference between the PCLL and the SOL becomes most significant.

The rest of the paper is organized as follows. In Section II, the security margin definitions for the SOL and the PCLL are presented. In Section III, the methodology used in computing the margins is presented along with the simulation platform and the adaptations used to allow a fair comparison between the security margins. Results and discussion are presented in Section IV. Concluding remarks are presented in Section V.

## 2. Security margin definitions

In this section, a theoretical comparison between the PCLL and the SOL is presented. The conceptual difference of computing the two security margins is first presented, which is followed by a theoretical analysis of the circumstances and the instability mechanisms that can cause the two methods to differ.

### *2.1. PCLL versus SOL*

The security margin estimation processes for the PCLL and the SOL are illustrated in Fig. 1. Pre-contingency and post-contingency $P$-$V$ curves are used where a receiving end voltage in a stressed area is a function of an increasing (active) power transfer from the system to this receiving end. An initial, unstressed, operating condition (OC) is the starting point for the security margin estimation. The security margin is then defined as the change in loading from

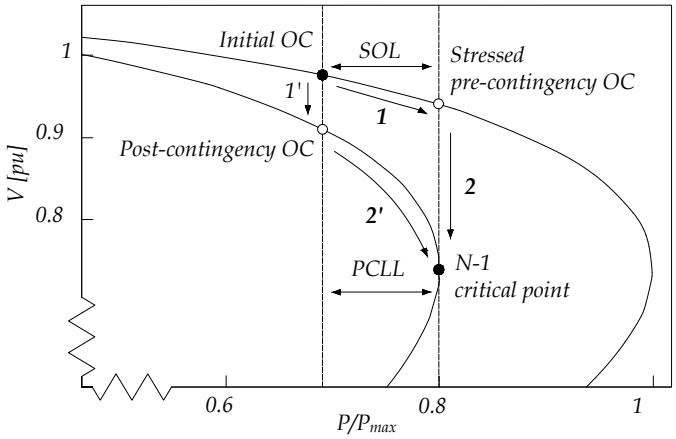


Figure 1: Security margin estimation for PCLL and SOL. **1'** and **2'** illustrates the computation path for the PCLL; **1** and **2** illustrates the computation path for the SOL.

the initial OC to the $N$-1 critical point. It should be noted that in actual applications, the limit is often smaller due to the other stopping criteria such as too low system voltages. However, for better illustration purposes, the former limit is used here.

In PCLL estimation, a post-contingency operating point is found by first introducing a contingency on the initial OC, which is typically followed by solving the resulting power flow study. This is illustrated in Fig. 1 by moving along arrow $\mathbf{1'}$. The security margin is then traced along the solution path by iteratively and step-wise increasing the system stress until the critical point is reached, moving along the arrow $\mathbf{2'}$. Parameterized continuation methods based on static load flow solutions, generally referred to as continuation power flow (CPF), are commonly used to avoid convergence problems close to the critical point of the system [19]. The distance between the pre-contingency operating point and the $N$-1 critical point represents the PCLL.

In the estimation of the SOL, the dynamic security of the system is tested with an increasing stress level, illustrated by arrow **1** in Fig. 1 [10]. For every new stressed pre-contingency OC, the system response following the disturbance is studied. The final, pre-contingency OC that is tested and can provide a stable operating point is illustrated by moving along arrow **2** in Fig. 1. The state transition following arrow **2** can generally not be computed using static methods as it can result in numerical divergence. Instead, methods based on dynamic (or QSS) simulations are generally required. The increased loadability between the initial OC and the most stressed pre-contingency OC that can still handle a dimensioning contingency without causing instability represents the SOL. It should be noted, that while the PCLL and the SOL are illustrated to result in the same level of security margin in Fig. 1, this is generally *not* the case. The difference between the two security margins is further analyzed in the following sections and a typical case is exemplified in Fig. 2.

*2.2. System dynamics and instability mechanisms*

Loads are often recognized to maintain constant power characteristics in a long-term *system* perspective but do not generally behave as such following a disturbance. Assuming a sudden voltage change, loads will initially drop according to their instantaneous characteristics [20]. Then, the impedance or the drawn current is adjusted to restore the load to its original level; a process that can be exemplified by the automatic changes in the slip of induction motors or by changes in tap positions to increase the voltage for loads behind load tap changers (LTCs). The overall load restoration after a disturbance is generally assumed to act significantly slower than the dynamics of other system components, such as the dynamics of generators and excitation systems. The PCLL is based on this time-scale decomposition, where short-term dynamics, such as the slip of induction motors, or generator and excitation dynamics, are assumed to be in equilibrium. Using this assumption, the loadability limit of the post-disturbance system can be found even though only static estimation methods are used to trace the security margin.

In [20] and [16], the concept of *transient* $P$-$V$ curves was used to allow visualization and analysis of short-term dynamics using $P$-$V$ curves. In the analysis, the post-disturbance $P$-$V$ curve is not fixed in time but is allowed to be affected by short-term system dynamics of, for instance, excitation systems. Nor is the load curve fixed in time, which allows the load restoration that follows after a disturbance to be illustrated. In Fig. 2, transient $P$-$V$ curves are used to illustrate a system that, when assuming the short-term dynamics are in equilibrium, could appear to be secure. However, when the short-term dynamics are taken into account, there is a loss of post-disturbance equilibrium of the short-term dynamics, and the disturbance would in fact cause the system to become unstable. The load restoration curves and the transient $P$-$V$ curves are illustrated using different shades of grey, where a lighter shade indicates closer in time after the disturbance. The time just after a disturbance is indicated by $t_1$; $t_2$ relates to a short time after the disturbance; $t_3$ relates to the time when all short-term dynamics are in equilibrium. The load is assumed to have long-term constant power characteristics, but just after a disturbance, the load will initially change to a constant impedance characteristic. Then, by fast load restoration, the load is quickly restored to the pre-disturbance level.

The initial OC is found in point $\boldsymbol{A'}$. Just after the disturbance, the short-term dynamics of system components such as generators or excitation systems will not yet have stabilized, which has the effect of shifting the post-disturbance $P$-$V$ curve to the left. As a result of the initial load characteristics and the shifted transient $P$-$V$ curve, the operating point moves along the arrow to operating point $\boldsymbol{B'}$. After this transition, both the load and the post-disturbance $P$-$V$ curve are shifted towards their stable counterparts. However, due to the fast load dynamics, there exists no intersection between the load curve and the post-disturbance $P$-$V$ curve at $t_2$ (the area indicated with the red dotted circle), and without any emergency control actions, the system stability would be lost. Thus, even though the post-disturbance $P$-$V$ curve and the load characteristic at $t_3$ still intersect in this case, the system would have become unstable.

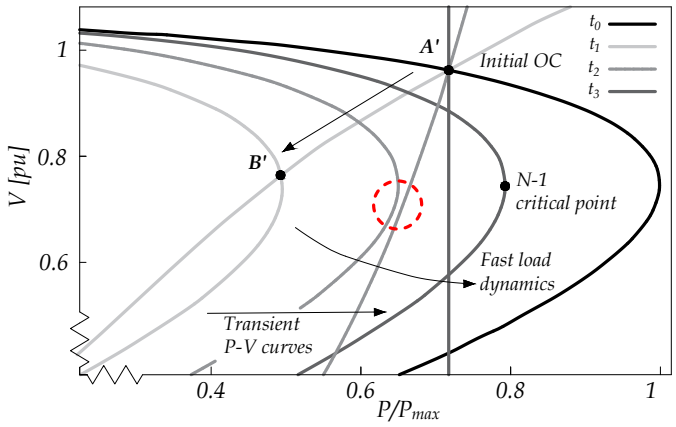


Figure 2: Transient $P$-$V$ curves illustrating a short-term instability event [16].

Instability caused by the short-term dynamics that follows a disturbance can generally be divided into three different instability mechanisms [1, 3]:

- Loss of post-disturbance equilibrium of short-term dynamics: Typically exemplified by the stalling of induction motors after a disturbance causing the transmission impedance to increase. Due to the increased transmission impedance, the mechanical and electrical torque curves of the motor may not intersect, causing the system to lack a post-disturbance equilibrium, similar to the case illustrated in Fig. 2.

- Lack of attraction towards the stable post-disturbance equilibrium of short-term dynamics: Typically exemplified by transient angle instability and the loss of synchronism by one (or several) generators following a too slow fault clearing.

- Oscillatory instability of the post-disturbance equilibrium: Typically exemplified by rotor angle stability, in which the equilibrium between electromagnetic torque and mechanical torque of synchronous machines in the system is disturbed. Instability may be caused by increasing angular swings of some generators leading to their loss of synchronism with other generators [3].

Typically, time-domain simulations are required to capture the short-term dynamics after a large disturbance. SOLs computed using QSS simulations can not account for the short-term dynamics that follow after a disturbance and are thus better suited to only monitor long-term voltage instability phenomena. Extensions of the QSS model have been proposed that are capable of also incorporating frequency dynamics that take place over the same time scale as a long-term voltage instability event [21, 11]. Combinations of time-domain simulations and QSS, as proposed in [11], can use time-domain simulations to model the system during the short-term period following a disturbance, followed by QSS simulations used to simulate the long-term interval after the short-term effects are finalized. However, short-term instability may also be induced by long-term dynamics, where the system degradation caused by long-term instability

eventually can trigger the above-mentioned short-term events [1]. It should be noted that SOLs computed by combinations of time-domain simulations and QSS, as proposed in [11], cannot capture this type of event.

## 3. Methodology for security margin computations

In this section, the methodology used in the comparison between the PCLL and the SOL is presented. The load models and a description of the test system are presented along with the required adaptions. Finally, the methodology used to allow a fair comparison of the PCLL and the SOL is presented.

### *3.1. Load models*

The power consumption of loads is generally affected by the system voltages and different load models are often used to characterize this relationship. A traditional load model used in both static and dynamic stability analysis is the ZIP model, which is made up of three components: constant impedance ($Z$), constant current ($I$), and constant power ($P$). The characteristics of the ZIP model is given by [1]:

$$P = zP_0 \left[ a_P \left( \frac{V}{V_0} \right)^2 + b_P \frac{V}{V_0} + c_P \right] \tag{1a}$$

$$Q = zQ_0 \left[ a_Q \left( \frac{V}{V_0} \right)^2 + b_Q \frac{V}{V_0} + c_Q \right] \tag{1b}$$

where $a_P + b_P + c_P = a_Q + b_Q + c_Q = 1$, $P_0$ and $Q_0$ are the real and reactive powers consumed at a reference voltage $V_0$, given that $z = 1$. $V$ is the actual voltage and $z$ is a variable indicating the actual loading of the system [1]. The constants $a_x$, $b_x$, and $c_x$ represent the share of constant impedance, constant current, and constant power of the load, respectively.

Although simple and widely used in security analysis [22], the ZIP model cannot model any dynamic behavior of the loads themselves. The significance of induction motor loads and other fast-acting dynamic loads are often highlighted in system stability studies. Induction motors (IM) are characterized by fast load restoration dynamics (often in the time frame of a second) and have a high reactive power demand. Induction motors are also prone to stalling, which may cause the motor to draw high reactive currents from the grid, resulting in a deteriorating effect on the system stability [1]. In PSS®E, a complex load model (CLOD) can be used to represent a bundled mix of loads with different dynamic load characteristics into a single model. The CLOD models a composition of various load types including induction motors and several static loads but requires only eight parameters, which is achieved by internally using typical manufacturer data for each load type. The CLOD model was chosen as it provides a simple yet efficient solution to model different configurations of common load types, including induction motors, when no detailed dynamics data were available. In Fig. 3, a schematic of the CLOD model is presented. The

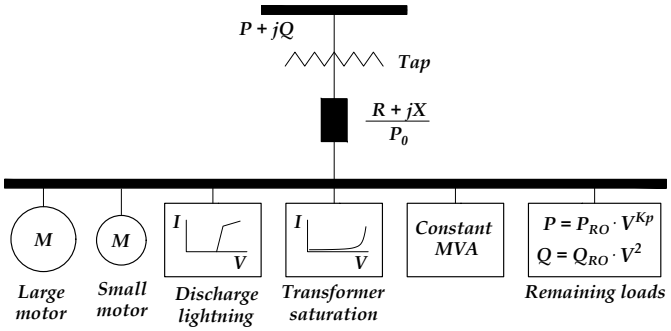


Figure 3: Overview of the complex load model (CLOD) [23].

transformer and feeders connecting the system bus to the load bus are modeled as a single impedance. At the load bus, different percentages of large and small IMs, discharge lighting loads, transformer saturation, and constant power loads can be modeled. The remaining part of the load is modeled as a polynomial load where the voltage dependency of the active load is controlled through a constant $K_p$. The performance curves of the two motor models, the discharge lightning model, and the transformer saturation model is further detailed in [23].

It should be noted, that all constant power loads in PSS®E are modeled as constant power only for a certain range of load voltages. When voltages drop below a threshold, by default 0.7 per unit in PSS®E, the constant power loads instead follow a function based on the magnitude of the bus voltage, further detailed in [24].

### *3.2. Simulation test system*

All simulations have been tested on the slightly modified version of the Nordic32 test system, detailed in [25]. The main characteristic of the system is sensitivity towards long-term voltage instability, although the system can exhibit other types of instabilities as well. A single-line diagram of the test system is presented in Fig. 4. The security margins are computed by increasing the loading in the area "*Central*", while the generation in the area "*North*" is increased by a corresponding quantity. The starting point for all scenarios is the secure "operating point B" as defined in [25].

All simulations were carried out using PSS®E version 35.0. To ensure numerical stability during the dynamical simulation runs, a short integration step of 0.0005 seconds was used in the simulations. In certain sensitive scenarios, such as when the simulations resulted in a non-converging dynamic simulation, the integration step was at times varied to provide a converging simulation.

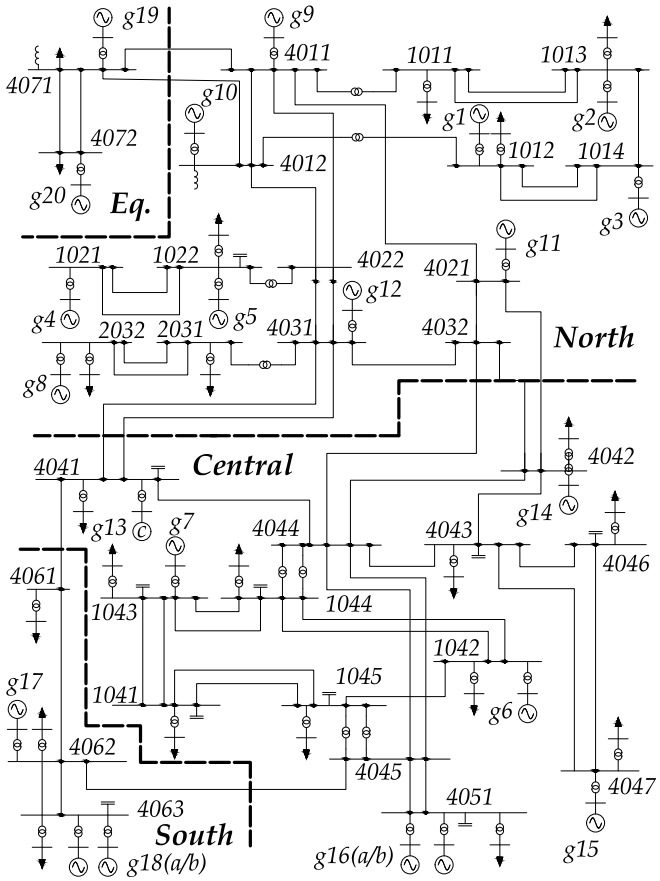


Figure 4: Single-line diagram of the modified Nordic32 system [25].

### *3.3. Methodology and adaptations*

To compare the two conceptually different methods of PCLL and SOL is not trivial; one is computed using a static model of the system, while the other is generally estimated using a dynamic model. To ensure that the difference in the computed security margins was not caused by differences in how the simulations were conducted, but rather by the fact that the SOL could better account for the system's dynamic response after a disturbance, a few adaptations of the methods were required. Instead of using CPF methods to compute the PCLL, we adopted a method that *slowly* ramps up the system stress in a dynamic simulation setting; an approach similar to the one used to compute the (pre-contingency) loadability margins in [25]. This approach allows the PCLL to be performed in a dynamic setting while mimicking how the system stress would have been increased if it would have been performed in a static setting. The advantage of adopting this methodology is that the loading and the generation

set points could be increased in the *exact* same way for both the computation of the PCLL and the SOL.

In [25], when computing the PCLL, the authors increased the system stress in small increments over time, but did not evaluate whether the system had stabilized before continuing stressing the system. This could result in that additional system stress was added to an already unstable system and that the PCLL became overestimated. For instance, long-term voltage instability events typically last several minutes, and a significant amount of system stress could thus have been added to the system while it had already become unstable. To address this issue, we used an adaptive method to analyze whether the system had stabilized. To achieve this, the timer settings of LTCs and over-excitation limiters (OELs) were monitored continuously throughout the simulation. These two components have the longest timer settings in the test system, and if all timers were reset for a given time (3 seconds) after a disturbance (or a load increase), the system was assumed to have stabilized.

#### *3.3.1. Steps for PCLL computation*

The steps used in computing the PCLL were the following:

- **Initialization:** The PCLL computation was initialized by applying a chosen contingency in the system in a dynamic simulation from the base case. The dynamic simulation ran until the system was fully stabilized.

- **Increase system stress:** Once the system had stabilized after the initial disturbance, the system stress was increased in small increments of 1 MW, which was distributed among all the loads in the "*Central*" area. To reduce the required simulation time, the system stress was for certain fault scenarios (scenarios A and B) initially increased in larger increments (5 MW), since lower stress levels were found to not cause instability in the system. The different fault scenarios are further discussed in Section 4.1. The power factor of each load was kept constant. Simultaneously, the load change was compensated by the primary frequency response of the generators in the system. The added load for both the PCLL and SOL were computed as a nominal load increase at 1.0 pu voltage to ensure that the same amount of load was added for both methods regardless of the current load voltage in the dynamic simulation. Increased active line losses caused by the increased system stress were also automatically compensated by the generators' primary frequency response, while the reactive line losses were automatically compensated by the generators' excitation systems.

- **Check stability criterion:** After the increased system stress, the simulation continued to run until the system either stabilized or until the stability criterion was violated. The system was considered unstable if *any* bus voltage in the system was lower than 0.9 pu. Although the modified Nordic32 test system is characterized by sensitivity towards voltage instability, other types of instability can violate the stability criterion. For

instance, transient angle instability can cause locally low voltages due to lost synchronism of certain generators. Overloading of transmission lines and transformers were not included in the stability criteria, as it is not directly affected by the dynamics of the system, but mainly just the magnitude of the system stress. Thus, in those cases that overloading would affect the results and be limiting for the security margin, it would generally limit the PCLL and the SOL to the same degree.

- **Re-iterate:** The system stress was increased until the system eventually violates the stability criterion. The difference in loading from the base case to the final stable operating point in the stressed post-contingency system represents the computed PCLL.

*3.3.2. Steps for SOL computation*

The SOL was computed similarly to the PCLL, but by instead stressing the system in its pre-contingency configuration and *then* introducing the disturbance. The steps used in the computation of the SOLs were the following:

- **Initialize simulation and increase system stress:** When the ZIP model was used to model the loads, the dynamic simulation was initialized directly at the beginning of the simulation. The system stress was then increased in its *pre-contingency* base case in small increments of 1 MW, in the same way as was done for the PCLL computation in its post-contingency configuration. The small step size in system stress was chosen to allow the illustration of the security margins using $P$-$V$ curves. In more general applications, faster methods such as the binary search method described in [10] or the dual binary search method described in[16], can otherwise be used to compute the SOL.
  *Adjustments for the CLOD model:* For the scenarios using the CLOD model, the increased system stress was required to be added in a static load flow scenario, which was then converted for dynamical studies. The increased load was distributed in a similar manner as when using the ZIP load model, except that the load was added in a static load flow scenario instead of during a dynamic simulation. However, the increased load could now not be automatically compensated by the generators' primary frequency response, and the increased load was instead distributed and compensated by increasing the generation set-points of all the hydro generators in the "North" and "Eq" regions, see Fig. 4. The distribution of the increased generation was based on the rated capacity of each generator and a generator with a higher rated capacity received a larger share of the increased generation. Increased active line losses caused by the increased system stress were compensated by an increase in the generation of the slack bus generator, g20. While this distribution can be assumed to be relatively similar to how the primary frequency control of the governors would have compensated for the increased load, it will cause a small difference in how the system stress is increased between the two load models.

- **Introduce disturbance and check stability:** A disturbance was then applied in the system. A final end time of the dynamic simulation of 1000 seconds was used. The system was considered unstable if *any* bus voltage in the system was lower than 0.9 pu at the end of the simulation. The simulation was also stopped in advance if any bus voltage decreased below 0.7 pu (still allowing the system to first stabilize for 20 seconds after the disturbance).

- **Re-iterate:** If the system was stable, the system was reinitialized to the last pre-contingency state, followed by increasing the system stress by an additional 1 MW and applying the same disturbance. The SOL is then computed from the difference in loading from the base case to the final stable operating point in the stressed post-contingency system.

## 4. Simulation results and discussion

In this section, the results of the numerical comparison between the PCLL and the SOL are presented. Three different contingency scenarios were tested. The results of PCLL and the SOL computation are presented for each contingency scenario and each load model configuration. It should be noted that the different types of disturbances were chosen to exemplify the difference between the two security margin methods under various conditions. In real applications, all relevant contingencies that might be dimensioning for the security margin should be included when computing the security margin. Furthermore, the direction of the system stress and the load-generation configuration should be representative of the specific system in consideration.

### *4.1. Contingency scenarios and loading scenarios*

The following contingency scenarios were examined:

- **Scenario A:** A three-phased fault for 40 milliseconds, followed by tripping the faulted line. The faulted line is the one connecting the two areas "*North*" and "*Central*" between bus 4032 to bus 4044.

- **Scenario B:** A longer three-phased fault for 100 milliseconds, followed by tripping the faulted line. The faulted line is the one connecting the two areas "*North*" and "*Central*" between bus 4032 to bus 4044.

- **Scenario C:** Tripping the of generator "*g7*" located at bus 1043 in the "*Central*" area.

For each of the contingency scenarios, different combinations of the ZIP load were tested for both the PCLL and the SOL. In addition, the SOL was computed for different compositions when the CLOD model was used to model the loads in the system. Adjusting the load levels *during* a dynamic simulation, which was required when computing the PCLL, was not feasible when using the CLOD model, as it requires that its internal parameters are recomputed

whenever the load composition changes. Thus, the CLOD model was analyzed only with respect to the SOL. Furthermore, the CLOD model was found to be generally numerically unstable for longer fault clearing times. Thus, we only provide a comparison of the results for Scenario A with a fault clearing time of 40 milliseconds.

### *4.2. Simulation results*

The PCLL and SOL results for each scenario and each load configuration using the ZIP model are presented in Table 1. The SOL results for scenario A and different configurations of the CLOD model are presented in Table 2. The largest difference between the PCLL and SOL is found for cases with a high share of constant power characteristics of the active part of the loads. For instance, for scenario 1A with fully constant power characteristics for the active part of the load and fully constant impedance characteristics for the reactive part of the load, the SOL was only 28 MW, while the PCLL was found to be 275 MW. The difference between the two security margin methods then reduces rapidly with a decreasing level of constant power characteristics on the active part of the load. Already at slightly lower levels of constant power loads, for instance, in Scenario 4A, the difference between the SOL and the PCLL becomes close to negligible. In Fig. 5, the post-disturbance $P$-$V$ curves of the transmission side of bus 1041 are illustrated, respectively, for Scenario 1A. The $P$-$V$ curves are computed by sampling the voltage magnitude when the system had stabilized after each dynamic simulation. Here, with a fully constant power characteristic of the active part of the loads, the $P$-$V$ curves are almost identical for both the PCLL and the SOL up until the collapse point for the SOL.

Table 1: Computed PCLL and SOL for different loading and contingency scenarios

| | Constant | | | | | | | | |
|---|---|---|---|---|---|---|---|---|---|
| | **MVA** | **I** | **Z** | ***Scenario A*** | | ***Scenario B*** | | ***Scenario C*** | |
| **Scenario number** | (P/Q) [%] | (P/Q) [%] | (P/Q) [%] | **PCLL** [MW] | **SOL** [MW] | **PCLL** [MW] | **SOL** [MW] | **PCLL** [MW] | **SOL** [MW] |
| 1 | 100/0 | 0/0 | 0/100 | 275 | 28 | 275 | 4 | 351 | 71 |
| 2 | 95/0 | 5/0 | 0/100 | 340 | 88 | 340 | 86 | 353 | 128 |
| 3 | 90/0 | 10/0 | 0/100 | 341 | 146 | 341 | 144 | 357 | 196 |
| 4 | 80/0 | 20/0 | 0/100 | 364 | 362 | 364 | 260 | 365 | 362 |
| 5 | 50/0 | 50/0 | 0/100 | 387 | 386 | 387 | 387 | 380 | 378 |
| 6 | 95/0 | 5/50 | 0/50 | 280 | 55 | 280 | 48 | 283 | 85 |
| 7 | 80/0 | 20/50 | 0/50 | 359 | 240 | 359 | 233 | 357 | 356 |
| 8 | 50/0 | 50/50 | 0/50 | 382 | 382 | 382 | 381 | 375 | 372 |
| 9 | 0/0 | 100/0 | 0/100 | 425 | 424 | 425 | 425 | 407 | 405 |
| 10 | 0/0 | 50/0 | 50/100 | 465 | 464 | 465 | 456 | 439 | 438 |
| 11 | 0/0 | 20/0 | 80/100 | 488 | 488 | 488 | 489 | 457 | 458 |
| 12 | 0/0 | 0/0 | 100/100 | 504 | 504 | 504 | 505 | 471 | 471 |

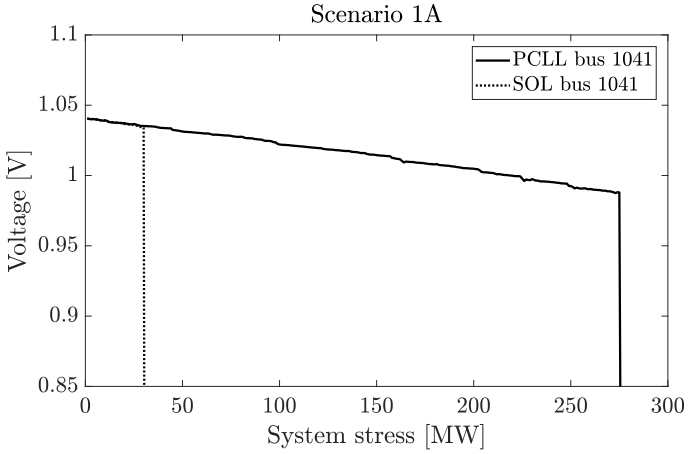


Figure 5: $P$-$V$ curves computed at bus 1041 for scenario 1A.

The difference between the PCLL and the SOL is more significant for Scenario B when a longer fault clearing time was used in the simulations. For instance, in Scenario 1B, the SOL was estimated to only 4 MW, compared to 275 MW for the PCLL. With reference to the discussion with the transient $P$-$V$ curves presented in Section 2.2, a longer fault clearing time would have the effect of shifting the post-disturbance $P$-$V$ curve for a longer time to the left, causing the system to lack attraction towards a stable post-disturbance equilibrium. Yet again, the difference between the two security margins decreases rapidly as the share of constant active power loads decreases. For instance, in Scenario 5B with a 50% share constant active power load, and the remaining part of the active load being of constant current characteristics, the SOL and the PCLL are almost identical. The post-disturbance $P$-$V$ curves of scenario 5B on the transmission side of bus 1041 are illustrated in Fig. 6. The figure shows that although the computed $P$-$V$ curves of the SOL are slightly below that of the PCLL, the two security margins find almost the same critical point of the system.

For all cases, except when the load is of constant power characteristics, the $P$-$V$ curves computed using the SOL are *slightly* below the ones computed using the PCLL. Although the initial response of the excitation systems used in the Nordic32 test system is fast, there is an integrating part of the control system which takes a longer time until the voltage magnitudes of the generators are restored to their pre-disturbance set-point (differing slightly due to the droop in the automatic voltage regulation). In the PCLL case, this voltage restoration is allowed to fully stabilize after the initial disturbance before the system stress is added to the system. This is not the case for the SOL, in which the system is stressed before the disturbance is applied to the system. In turn, this causes LTCs and OELs to act earlier for a lower level of system stress, causing the

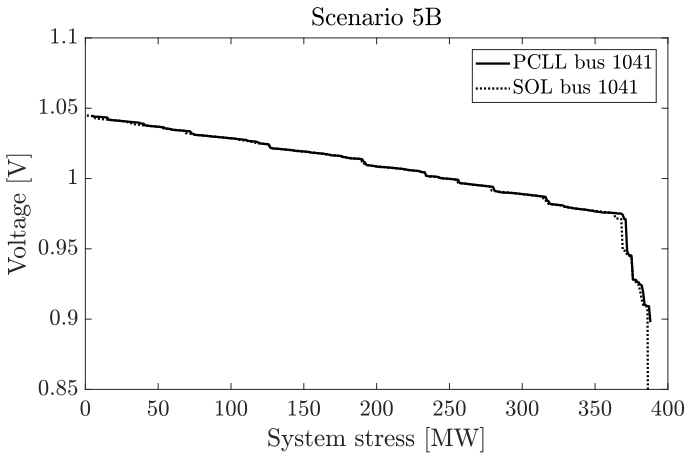


Figure 6: $P$-$V$ curves computed at bus 1041 for scenario 5B.

magnitude of the post-disturbance voltages to be generally lower.

In Scenario C, the chosen contingency was the disconnection of the generator "*g7*", located in the "*Central*" area. Once again, the largest difference between the PCLL and SOL is found for cases with a high share of constant power characteristics of the active part of the loads. For load scenarios with a larger share of either constant current or constant impedance characteristics of the active part of the load, the difference between the two security margins becomes negligible.

In Table 2, the computed SOLs for scenario A when using different configurations of the CLOD model are presented. The scenarios are generated by varying the load composition, consisting of large induction motors (LIMs), small induction motors (SIMs), discharge lightning (DL), transformer saturation (TS), constant power loads (MVA), and the remaining load which is of constant impedance characteristics ($K_p = 2$). Unsurprisingly, the computed SOL was the lowest when there was a large share of motor loads in the system. When the loads were modeled with a *too* high share of motor loads, such as scenario 13A, the computed SOL for the base case was negative. There was a relatively large difference between the computed SOL for scenario 17A with a 35% share of LIM loads and 25% share small motor loads, and scenario 20A with a 25% share of large motor loads and 35% share of SIM loads. LIM loads generally draw a higher reactive current during instances of low system voltages than SIM loads, which may have caused the computed SOL to differ from 47 MW for scenario 17A to 120 MW for scenario 20A.

In most scenarios where the CLOD model was used and for the level of system stress that made the system unstable, the system crashed during the transient state just after the disturbance. The CLOD models were found to be particularly sensitive towards long fault clearing times, and the Nordic32 test

Table 2: SOLs for different load configurations of the CLOD model

| | CLOD model parameters | | | | | | Scenario A |
|---|---|---|---|---|---|---|---|
| **Scenario number** | LIM [%] | SIM [%] | DL [%] | TS [%] | MVA [%] | Remaining ($K_p$=2) [%] | **SOL** [MW] |
| 13 | 35 | 35 | 5 | 5 | 10 | 10 | - |
| 14 | 30 | 30 | 5 | 5 | 10 | 20 | 60 |
| 15 | 25 | 25 | 5 | 5 | 10 | 30 | 372 |
| 16 | 35 | 30 | 5 | 5 | 10 | 15 | 28 |
| 17 | 35 | 25 | 5 | 5 | 10 | 20 | 47 |
| 18 | 35 | 20 | 5 | 5 | 10 | 25 | 59 |
| 19 | 30 | 35 | 5 | 5 | 10 | 15 | 37 |
| 20 | 25 | 35 | 5 | 5 | 10 | 20 | 120 |
| 21 | 20 | 35 | 5 | 5 | 10 | 25 | 365 |

system consistently crashed when using a longer fault clearing time (such as 0.1 seconds). The difference between the two security margins is thus likely even greater if breakers with longer fault clearing times can be assumed to dominate the system. However, in a few scenarios, the long-term load restoration in the system was the main driver for instability. One of these cases, scenario 15A, is illustrated in Fig 7, which shows the development of bus voltages over time for different levels of system stress. For the lower system stress levels of 150 MW and 372 MW, the system is able to satisfy the given stability criterion, although the 372 MW level causes the system voltages to drop significantly. However, for a system stress level of 373 MW, the long-term load restoration and the activation of OELs causes the system to loose stability after about 450 seconds.

### *4.3. Discussion*

The results in the previous section show that although the *same* operating point has been used as a starting point for all scenarios, the PCLL and the SOL differ significantly depending on the current load configuration and the type of fault that is considered. The largest difference between the two security margin methods was found when either the loads were of high constant power characteristics or consisted of a large penetration of induction motor loads. These results thus confirm the well-known fact that loads with fast restoration dynamics (where a constant power characteristic can be considered a theoretic extreme case) will deteriorate the system stability, and illustrate how significant this impact may be on the computed security margins.

The main conclusions of this study, that high penetration of loads with fast restoration dynamics will result in a difference between the PCLL and the SOL, should generalize well to other types of power systems. However, care should be taken when generalizing the *specific* results of this study to real power systems

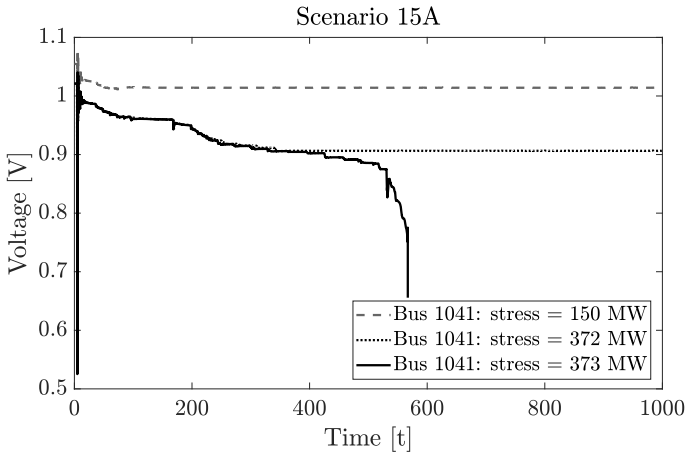


Figure 7: Voltage evolution for bus 1041 for Scenario 15A for different levels of system stress.

with different characteristics. For instance, although the difference between the SOL and the PCLL in this study was found to be negligible whenever the share of constant power characteristic of the active part of the loads was lower than 50%, this is not necessarily the case for other systems with different dynamics. System operators would thus be required to perform a similar analysis on their specific systems to analyze during what specific loading scenarios the PCLL and the SOL start to differ.

The stability assessment practice of many system operators is, to the authors' best knowledge, to compute security margin estimations computed by PCLLs, often in combination with dynamic security assessment (DSA). While DSA can provide certain types of security margins based on indices such as the transient energy functions [26], it does not provide an accurate measure of the loadability limit to the point where the system can no longer remain secure. We believe that if system operators continue to rely on conventional security margins computed by the PCLL, it is important to verify the reliability of those security margins to avoid either overly optimistic security margins or to avoid having to add unnecessary large reliability margins to the computed security margins. To account for modeling inaccuracies, transmission reliability margins are often added to ensure that modeling inaccuracies will not cause the system to be operated unknowingly in a non-secure operating state. Thus, if more accurate methods to determine security margins are used, such as the SOL, these reliability margins may theoretically be reduced and the system operators could more efficiently utilize the existing transmission capacity.

Dynamic load modeling may also become increasingly important in the future, as more loads are expected to be controlled through power electronically-controlled interfaces. These types of loads, such as electric vehicle chargers, inhibit very fast dynamic responses after disturbances [27]. Despite this, dy-

namic load models are still relatively unused in the industry. In a large survey study from 2013 on international industry practice on power system load modeling, it was shown that about 70% of system operators and utilities still only used static load models for power system stability studies [28]. A drawback of advanced load models is that the load composition is often partly unknown to system operators, and it is thus more straightforward to use the simplified static load models. Another drawback is the increase in computational requirement during simulations, which reduces their applicability in real-time applications. However, although complex load models do not necessarily need to be used in real-time applications, sensitivity analyses can preferably be performed using these models, so that the impact of various degrees of motor loads and other types of loads on the stability of a system can be studied.

While this study focused on the impact of different load models, converter-interfaced generation and other power electronic devices in the power system will also have a significant impact on the computed security margins. Although a growing share of renewable generation is often challenging from a planning perspective due to the intermittency of the energy source, the converter interface may in fact mitigate some of the short-term instability phenomena. For instance, with proper design of the converter controls, such components can contribute to provide fast voltage/reactive power control or active power control for fast frequency responses. We argue that the impact of such components, also in combination with loads with fast restoration dynamics, deserves further attention in the research.

## 5. Conclusions

In this paper, the PCLL and the SOL have been compared and studied under various load configurations and disturbance scenarios. A methodology was developed to allow a fair comparison between the two methods to ensure that the difference in the computed security margins was due to actual differences of the security margin approaches, and not caused by differences in the simulation setups. The numerical comparison shows that the two methods differ significantly under various load configurations and fault scenarios. The largest difference between the two methods was found when the loads were of high constant power characteristics or when the loads consisted of a large share of induction motor loads. Furthermore, the fault clearing time is found to be especially important and a longer fault clearing time caused the SOL to become significantly smaller than the PCLL. The results highlight the importance of load modeling and show that if a power system can be expected to have a large share of loads with fast restoration dynamics, the conventional method of using PCLL to compute the security margins can provide overly optimistic values of the actual security margin.

## References


[1] T. Van Cutsem, C. Vournas, Voltage stability of electric power systems, Kluwer Academic Publishers, Boston, 1998.

[2] C. Vournas, T. Van Cutsem, Online voltage security assessment, in: Real-Time Stability in Power Systems, Springer, 2014, pp. 305–333.

[3] N. Hatziargyriou, J. V. Milanovic, C. Rahmann, V. Ajjarapu, C. Canizares, I. Erlich, D. Hill, I. Hiskens, I. Kamwa, B. Pal, P. Pourbeik, J. J. Sanchez-Gasca, A. M. Stankovic, T. Van Cutsem, V. Vittal, C. Vournas, Definition and classification of power system stability revisited & extended, IEEE Transactions on Power Systems (2020) Early access. doi:10.1109/TPWRS.2020.3041774.

[4] A. Adrees, J. Milanović, Effect of load models on angular and frequency stability of low inertia power networks, IET Generation, Transmission & Distribution 13 (9) (2019) 1520–1526.

[5] T. Souxes, C. Vournas, System stability issues involving distributed sources under adverse network conditions, in: 2017 IREP Symposium Bulk Power System Dynamics and Control - X (IREP), 2017.

[6] B. Kroposki, B. Johnson, Y. Zhang, V. Gevorgian, P. Denholm, B. Hodge, B. Hannegan, Achieving a 100% renewable grid: Operating electric power systems with extremely high levels of variable renewable energy, IEEE Power and Energy Magazine 15 (2) (2017) 61–73. doi:10.1109/MPE.2016.2637122.

[7] R. F. Mochamad, R. Preece, Assessing the impact of vsc-hvdc on the interdependence of power system dynamic performance in uncertain mixed ac/dc systems, IEEE Transactions on Power Systems 35 (1) (2020) 63–74. doi:10.1109/TPWRS.2019.2914318.

[8] S. F. Santos, M. Gough, D. Z. Fitiwi, A. F. P. Silva, M. Shafie-Khah, J. P. S. Catalão, Influence of battery energy storage systems on transmission grid operation with a significant share of variable renewable energy sources, IEEE Systems Journal (2021) 1–12doi:10.1109/JSYST.2021.3055118.

[9] U. Datta, A. Kalam, J. Shi, Battery energy storage system to stabilize transient voltage and frequency and enhance power export capability, IEEE Transactions on Power Systems 34 (3) (2019) 1845–1857. doi:10.1109/TPWRS.2018.2879608.

[10] T. Van Cutsem, C. Moisse, R. Mailhot, Determination of secure operating limits with respect to voltage collapse, IEEE Transactions on Power Systems 14 (1) (1999) 327–335. doi:10.1109/59.744551.

[11] T. Van Cutsem, M.-E. Grenier, D. Lefebvre, Combined detailed and quasi steady-state time simulations for large-disturbance analysis, International Journal of Electrical Power & Energy Systems 28 (9) (2006) 634 – 642. doi:https://doi.org/10.1016/j.ijepes.2006.03.005.

[12] A. Kaci, I. Kamwa, L.-A. Dessaint, S. Guillon, Synchrophasor data baselining and mining for online monitoring of dynamic security limits, IEEE Transactions on Power Systems 29 (6) (2014) 2681–2695.

[13] A. Sittithumwat, K. Tomsovic, Dynamic security margin estimation using artificial neural networks, in: IEEE Power Engineering Society Summer Meeting,, Vol. 3, Chicago, IL, 2002, pp. 1322–1327. doi:10.1109/PESS.2002.1043583.

[14] N. Amjady, Dynamic voltage security assessment by a neural network based method, Electric Power Systems Research 66 (3) (2003) 215 – 226. doi:https://doi.org/10.1016/S0378-7796(03)00048-8.

[15] M. V. Baghmisheh, H. Razmi, Dynamic voltage stability assessment of power transmission systems using neural networks, Energy Conversion and Management 49 (1) (2007) 1 – 7. doi:https://doi.org/10.1016/j.enconman.2007.06.017.

[16] H. Hagmar, R. Eriksson, A. T. Le, Fast dynamic voltage security margin estimation: concept and development, IET Smart Grid 3 (4). doi:10.1049/iet-stg.2019.0278.

[17] I. Dobson, The irrelevance of load dynamics for the loading margin to voltage collapse and its sensitivities, in: Bulk power system voltage phenomena - III: Voltage stability, security & control, 1994, pp. 509–518.

[18] B. H. Chowdhury, C. W. Taylor, Voltage stability analysis: V-Q power flow simulation versus dynamic simulation, IEEE Transactions on Power Systems 15 (4) (2000) 1354–1359. doi:10.1109/59.898112.

[19] V. Ajjarapu, C. Christy, The continuation power flow: a tool for steady state voltage stability analysis, IEEE Transactions on Power Systems 7 (1) (1992) 416–423. doi:10.1109/59.141737.

[20] M. K. Pal, Voltage stability conditions considering load characteristics, IEEE Transactions on Power Systems 7 (1) (1992) 243–249. doi:10.1109/59.141710.

[21] M.-E. Grenier, D. Lefebvre, T. Van Cutsem, Quasi steady-state models for long-term voltage and frequency dynamics simulation, in: 2005 IEEE Russia Power Tech, 2005, pp. 1–8. doi:10.1109/PTC.2005.4524400.

[22] A. Arif, Z. Wang, J. Wang, B. Mather, H. Bashualdo, D. Zhao, Load modeling—a review, IEEE Trans. Smart Grid 9 (6) (2018) 5986–5999.

[23] Siemens Power Technologies International, Schenectady, NY, PSS®E 35.0.0 Program Application Guide: Volume II (Sep. 2019).

[24] Siemens Power Technologies International, Schenectady, NY, PSS®E 35.0.0 Program Application Guide: Volume I (Sep. 2019).

[25] T. Van Cutsem, M. Glavic, W. Rosehart, C. Canizares, M. Kanatas, L. Lima, F. Milano, L. Papangelis, R. A. Ramos, J. A. d. Santos, B. Tamimi, G. Taranto, C. Vournas, Test systems for voltage stability studies, IEEE Transactions on Power Systems 35 (5) (2020) 4078–4087.

[26] J. Jorge L, Online dynamic security assessment, in: Real-Time Stability in Power Systems, Springer, 2014, pp. 159–197.

[27] D. Mao, K. Potty, J. Wang, The impact of power-electronics-based load dynamics on large-disturbance voltage stability, in: 2018 IEEE Power Energy Society General Meeting (PESGM), 2018, pp. 1–5.

[28] J. V. Milanovic, K. Yamashita, S. Martínez Villanueva, S. Z. Djokic, L. M. Korunović, International industry practice on power system load modeling, IEEE Transactions on Power Systems 28 (3) (2013) 3038–3046.

IET Smart Grid

*Research Article*

IET Journals
The Institution of Engineering and Technology

# Fast dynamic voltage security margin estimation: concept and development

eISSN 2515-2947
Received on 1st October 2019
Revised 12th February 2020
Accepted on 25th March 2020
doi: 10.1049/iet-stg.2019.0278
www.ietdl.org

*Hannes Hagmar*[1] ✉, *Robert Eriksson*[2], *Le Anh Tuan*[1]

[1]*Chalmers University of Technology, Gothenburg 412 96, Sweden*
[2]*Svenska kraftnät (Swedish National Grid), Sundbyberg 172 24, Sweden*
✉ *E-mail: hannes.hagmar@chalmers.se*

**Abstract:** This study develops a machine learning-based method for a fast estimation of the dynamic voltage security margin (DVSM). The DVSM can incorporate the dynamic system response following a disturbance and it generally provides a better measure of security than the more commonly used static voltage security margin (VSM). Using the concept of transient *P* - *V* curves, this study first establishes and visualises the circumstances when the DVSM is to prefer the static VSM. To overcome the computational difficulties in estimating the DVSM, this study proposes a method based on training two separate neural networks on a data set composed of combinations of different operating conditions and contingency scenarios generated using time-domain simulations. The trained neural networks are used to improve the search algorithm and significantly increase the computational efficiency in estimating the DVSM. The machine learning-based approach is thus applied to *support* the estimation of the DVSM, while the actual margin is validated using time-domain simulations. The proposed method was tested on the Nordic32 test system and the number of time-domain simulations was possible to reduce with ∼70%, allowing system operators to perform the estimations in near real-time.

## 1 Introduction

Voltage instability is a key factor that limits the operation and transmission capacity of a power system [1]. An operation close to the physical limits enables an economic and efficient utilisation of the system, but may also make it more vulnerable to disturbances. The voltage security margin (VSM), also referred to as the post-contingency loadability limit, is estimated by system operators to evaluate the loadability margin of a post-contingency configuration of the system [2, 3]. The VSM is generally estimated by static assessments of the system where the stability limit up to the system critical point is traced [4, 5].

To handle the relatively computationally intensive process of estimating the VSM for large systems, machine learning (ML) has been proposed to transfer the majority of the computations from an online to an offline state. The algorithms are trained to correlate and learn the statistical patterns relating to the VSM with a certain operating condition in the system. Various learning techniques have been proposed, such as neural networks (NNs) [6–8], decision trees (DTs) [9, 10], and linear and local regression [11, 12].

Electric power systems are, however, becoming increasingly complex, with thousands of dynamic components such as nonlinear loads, converter-based generators, and other power electronic devices [13, 14]. The dynamic response following a contingency cannot be captured using static assessments, and studies have indicated that these might be insufficient when estimating the actual security margin [3, 15]. To ensure that the system is also dynamically secure, system operators often use an approach called dynamic security assessment (DSA). DSA includes time-domain analysis to test the power system's dynamic response after a set of contingencies to ensure its ability to reach a stable post-disturbance operating point [2]. The ML-based methods have also become increasingly popular in DSA due to the capability of providing system operators with tools to assess the dynamic security of the system in real-time. Examples of DSA methods based on ML are found in [14, 16–19], where mainly various NN or DT methods are utilised.

A drawback of DSA is that it only provides system operators with information about whether the *current* operating condition is dynamically secure. An alternative measure of the *margin* to security is the dynamic voltage security margin (DVSM). The DVSM, also referred to as the secure operating limit, is the margin to the most stressed pre-contingency operating point that can still withstand a set of credible contingencies [3, 13]. The concept of DVSM has received comparatively little interest in the literature, likely due to the practical difficulties in estimating the margin. DVSM estimation is computationally demanding, where multiple time-domain simulations are required to trace the security limit for a range of different contingencies. Despite recent progress in high-performance computing, it is generally not feasible to perform such estimations for large power systems in the time frame required by system operators.

To reduce the computation time, an approach using quasi-steady-state (QSS) simulations was proposed in [3]. In [20], the method was further developed and a combination of QSS and time-domain simulations was proposed to include the impact of short-term effects. Although this approach reduces the computational effort compared to a full time-domain simulation, it may still prove too slow for many real-time applications. In [21–24], different ML approaches based on NNs were proposed to allow real-time estimation of the DVSM. These ML-based approaches are promising in the sense that they, when properly trained, have the capability of providing an instantaneous estimation of the DVSM. However, the lack of robustness and the uncertainty when handling operating conditions not included in the training of the algorithms may deter system operators to implement them.

Although the concept of a DVSM is not new, the *circumstances* under which it is preferred to the conventional VSM are still somewhat undefined. Furthermore, existing methods to estimate the DVSM suffer from either being too time-consuming or lacking robustness in the case of the ML-based methods. As blackouts and other major failures are related to extremely high costs, it may thus be difficult to convince system operators to implement these ML-based methods. In this paper, we address the issues mentioned above by clearly establishing a general framework and providing a methodology for a robust near-real-time estimation of the DVSM. The main contributions are the following:

- The principles of the DVSM and the differences to conventional VSM are illustrated using a concept called transient *P* - *V* curves to allow better interpretation of the two measures. The aim is to summarise previous findings and to establish under which

circumstances a dynamic security margin is preferred to a static margin.

- A methodology for fast and robust computing of the DVSM is proposed and tested. The method is based on using NNs to provide both a qualified estimate of the actual DVSM and to determine the dimensioning contingency in the system with respect to the DVSM. The estimated values are used as a starting point for the estimation of the *actual* DVSM, aimed to improve the search algorithm and significantly reduce the computation time. The ML approach is thus proposed to *support* the estimation of the DVSM, while the actual margin is always validated using actual time-domain simulations.

The DVSM can easily be generalised to also include other stability related phenomena, such as rotor angle stability or inter-area oscillations. In these applications, the more general term of a *secure operating limit* can preferably be adopted. However, in this paper, we choose to specifically analyse the limit to voltage instability and the difference to the commonly used static VSM, and thus the more specific term of DVSM is adopted.

The remaining of the paper is organised as follows. In Section 2, the difference between static and dynamic voltage security is illustrated and discussed using the concept of transient $P$ - $V$ curves. In Section 3, a methodology for fast estimation of the DVSM is developed and aspects for efficient computing are proposed. In Section 4, results and discussion are presented, followed by concluding remarks in Section 5.

## 2 Static versus dynamic voltage security

In this section, the difference between static and dynamic voltage security is developed and the concept of transient $P$ - $V$ curves is adopted to illustrate *when* the DVSM is preferred to the conventional VSM. A small test system's dynamic response following a disturbance is used in the analysis.

### 2.1 Simple system model

In the following examples, the impact of load dynamics and the voltage control devices (e.g. excitation control for synchronous generators and synchronous condensers) are mainly taken into account in the analysis. The small 2-bus test system in Fig. 1 is used in the analysis. It consists of a controlled sending end voltage ($E\angle 0$), supplied by a voltage source through a reactance $X_f$. A complex load ($P + jQ$) is fed through a number of lines represented by inductances with the total reactance of $X_t$.

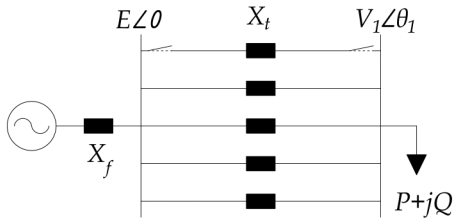


**Fig. 1** *Simple 2-bus system*

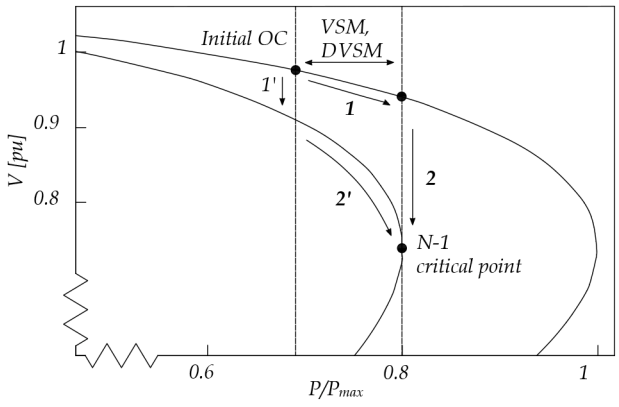


**Fig. 2** *VSM versus DVSM estimation*

A popular method in static voltage stability analysis is to use $P$ - $V$ curves, where the receiving end voltage is plotted with respect to an increasing active load transfer in the system. In the following figures in this section, $P$ - $V$ curves for the case when $E = 1.05$ pu, $X_t = 0.4$ pu, and a fully active power load are illustrated. The reactance $X_f$ is initially neglected, but will be introduced in Section 2.4. An additional $P$ - $V$ curve is plotted in each figure for a $N-1$ case when one line has been disconnected (increasing $X_t$ to 0.5 pu). Assuming lossless transmission, the curves are developed using the classic voltage equation, given below [2]:

$$V = \sqrt{\frac{E^2}{2} - QX_t \pm \sqrt{\frac{E^4}{4} - X_t^2P^2 - X_tE^2Q}} \tag{1}$$

where the upper part of each $P$ - $V$ curve corresponds to the solution of (1) with the plus sign, while the lower part of each curve corresponds to the solution with the minus sign.

The voltage instability mechanism is mainly driven by loads, and the impact of load modelling in voltage stability analysis is imperative [2]. The power consumption of loads is affected by the system voltages, and different load models are often used to characterise this relationship. A traditional model is the *exponential load model*, which is given below:

$$P = zP_0\left(\frac{V}{V_0}\right)^{\alpha} \tag{2}$$

$$Q = zQ_0\left(\frac{V}{V_0}\right)^{\beta} \tag{3}$$

where $P_0$ and $Q_0$ are the active and reactive power consumed when the voltage $V$ is equal to the reference voltage $V_0$, given that $z = 1$. $z$ is a dimensionless and independent variable indicating the actual loading of the system [2]. The voltage dependency is modelled by the $\alpha$ and $\beta$ parameters, where $\alpha = \beta = \{0, 1, 2\}$ represents constant power (MVA), constant current, and constant impedance characteristics, respectively.

### 2.2 Estimation of VSM and DVSM

The estimation methods for the VSM and the DVSM are illustrated in Fig. 2 using the developed $P$ - $V$ curves. The security margin is defined as the change in loading from an initial operating condition (OC) to the $N-1$ critical point. It should be noted that in real applications, the system loading is generally stopped before the $N-1$ critical point due to other stopping criteria such as too low system voltages. However, for better illustration purposes, the former limit is used.

In static VSM estimation, the initial post-contingency operating point is found by first introducing a contingency on the initial OC, which is followed by solving the resulting power flow study. This is illustrated in Fig. 2 by moving along the arrow **1**′. The stability limit is then traced along the solution path by iteratively increasing the system stress until the critical point is reached, moving along the arrow **2**′. What is known as continuation power flow methods are preferably used to avoid convergence problems close to the critical point [4, 5]. The loading between the pre-contingency operating point and the $N-1$ critical point constitutes the VSM.

The steps of estimating the DVSM are conceptually different from the VSM, where instead, the dynamic security of the system is being tested with an increasing stress level in the system, illustrated by the arrow **1** in Fig. 2 [3]. For every new pre-contingency OC (an increase in system stress), a time-domain simulation is initiated where the system response following a disturbance is studied. The simulation runs until the system stabilises or becomes unstable. The final pre-contingency OC that is tested and still provide a stable post-contingency operating point

is illustrated by moving along the curved arrow **2** in Fig. 2. The loading between the initial OC and the last pre-contingency OC that can still handle a dimensioning contingency without causing a voltage collapse, represents the DVSM.

In should be noted, that while the VSM and the DVSM are illustrated to be the same in Fig. 2, this is generally *not* the case. The difference between the methods is further discussed in the following sections.

### 2.3 Load response after a disturbance

Load dynamics plays an essential role in voltage instability phenomena [2]. In static VSM estimation, loads are often recognised to maintain a constant MVA characteristic [25]. This assumption is often true from a long-term *system* perspective, but does not necessarily mean that the loads themselves behave as constant MVA loads. Equipment and control mechanisms such as load tap changers (LTCs) and voltage regulators will restore load voltages following a disturbance, resulting in recovered load levels even for loads with constant impedance characteristics [26]. However, even though loads are considered to have long-term MVA characteristics, they do not necessarily behave as static MVA loads following a disturbance. Assuming a sudden voltage change, the loads will initially change according to their instantaneous characteristics, for instance a mix of constant impedance and constant current load [26]. Then, they will adjust their impedance or the drawn current to restore the load to their original level.

This load restoration event following a disturbance, tripping of a line in the system, is illustrated in Fig. 3. The initial OC is located at ***A***. Instantly after a disturbance, the load is assumed to have constant impedance characteristics, which results in a change in operating point from ***A*** to ***B***. Load dynamics then restores the load, moving the operating point from ***B*** to ***C***. The load is thus fully restored to the same initial load level as in point ***A***.

### 2.4 Transient P - V curves and fast load dynamics

In [27], it was shown that if the system starts at a stable equilibrium and is slowly stressed towards the critical point without encountering oscillations or other limit-induced events (e.g. reactive power limits for generators), the static equations are sufficient to locate the exact critical point experienced by the dynamic system. However, the majority of voltage collapse incidents experienced so far have resulted from large disturbances, typically by the loss of generation or transmission capacity [3]. In static VSM estimation, the transient state of such events can be neglected using the assumptions (i) that loads to do not behave as constant MVA loads just after a disturbance, and (ii) that load dynamics acts significantly slower compared to the voltage control dynamics of, for instance, excitation system of generators and synchronous condensers [26]. Hence, the transient impact of voltage control dynamics can be neglected and the assumptions developed in [27] would still be valid.

However, load dynamics of induction motors and power electronic loads, such as chargers for electric vehicles, are inherently fast. For these components, the load is often restored in a time frame within a second, similar to that of most excitation systems [2, 28], causing the assumptions used in conventional VSM estimation to falter. In [26], a concept called transient $P$ - $V$ curves was adopted to visualise the dynamic impact of voltage control on the static $P$ - $V$ curves. In this paper, we use the same approach when the difference between then VSM and the DVSM is illustrated. The transient $P$ - $V$ curves can be obtained by modelling and taking into account the dynamic impact of having the voltage source in Fig. 1 behind the reactance $X_f$. The assumption used in conventional VSM estimation, that excitation control instantly will restore $E$ to its pre-contingency value after a disturbance, will thus no longer be true. Instead, $E$ will initially be affected by events in the system but is controlled back to its nominal value by excitation control of the voltage source. As the main purpose here is to provide a principal understanding of the concept, the transient $P$ - $V$ curves in the following figures are hypothetical. Similarly, the curves illustrating the *fast* load restoration dynamics from a constant impedance load to a constant power load are drawn to allow a better understanding of the concept.

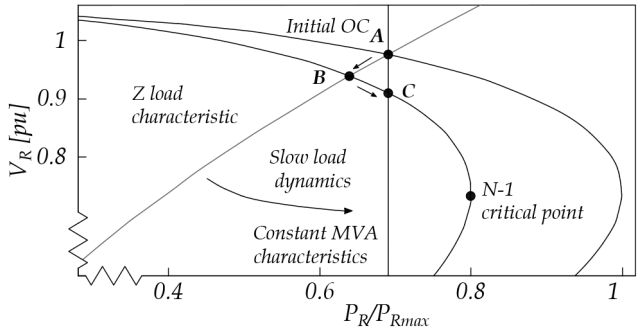


**Fig. 3** *Example of slow load restoration after a contingency*

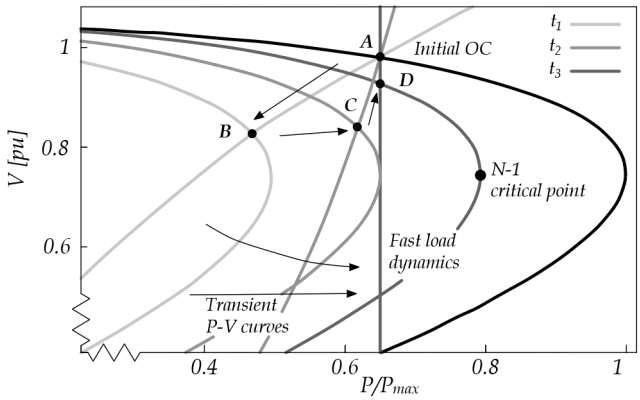


**Fig. 4** *Secure initial operating condition*

In Fig. 4, the dynamic response following a disturbance is illustrated for a secure initial OC. The transient $P$ - $V$ curves and the load restoration curves are illustrated using different shades of grey, where a lighter shade indicates closer in time to the disturbance. The time just after a disturbance is indicated by $t_1$, while $t_3$ relates to the time when all short-term dynamics have already taken place. The load is assumed to have long-term constant MVA characteristics, but just after a disturbance, the load will initially change to a constant impedance characteristic. Then, by fast load restoration, the load is quickly restored to a constant MVA characteristic.

The initial OC is found in point ***A***. Just after a disturbance (at $t_1$), the bus voltages drop caused by a larger current being transmitted through the remaining lines. The reactive power losses increase in the system, and a larger current is being transmitted through the reactance $X_f$ found in Fig. 1. The larger current causes the voltage $E$ to drop initially, resulting in the $P$ - $V$ curve being shifted to the left (the lightly shaded $P$ - $V$ curve). As a result of the initial load characteristics and the shifted $P$ - $V$ curve, the operating point moves along the arrow to the operating point ***B***. After the shifted operating point, two separate dynamic responses are initiated. The voltage control dynamics, here illustrating the excitation system response for a synchronous generator, is restoring the terminal voltage $E$ to its nominal value. This causes the transient $P$ - $V$ curve to shift back towards the $P$ - $V$ curve for the static $N-1$ case. Simultaneously, the fast load dynamics are restoring the load from the initial load characteristics back to a constant MVA characteristic. As an effect of the voltage control dynamics and the load restoration, the operating point moves along the arrows from ***B*** to ***C***, then finally, from ***C*** to ***D***. In this case, the system was found to be stable even after the disturbance with the new operating point ***D***.

In Fig. 5, the same system is slightly more stressed, with a higher level of initial transferred power. Just after the contingency, the operating point moves along the arrow from ***A***′ to ***B***′, by same the reasoning as in the previous case. However, due to the fast load dynamics, there exists no intersection between the curves at $t_2$, and without any emergency control actions, the system stability would

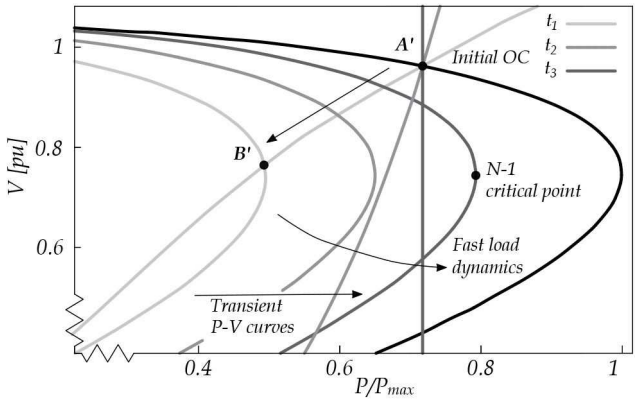


**Fig. 5** *Unsecure initial operating condition*

be lost. The example in Fig. 5 illustrates a type of event that the DVSM could identify and take into account, which is not possible using a static VSM. It should be noted that the $P$ - $V$ curve for the $N-1$ case and the load characteristic at $t_3$ still intersect in this case, indicating that a static VSM would still classify the initial OC as secure.

### *2.5 DVSM versus VSM*

The analysis in the previous section showed that the DVSM is to prefer over static VSM in power systems with a large share of loads with fast restoration dynamics. Furthermore, the closer power systems are being operated to the limits of operation, the event illustrated in Fig. 5, the more likely it is that the system will become unstable during the transient state after a disturbance. However, the advantages of using DVSM are not limited solely to the short time instance after a larger disturbance has occurred in the system. The same type of events may occur significantly later in a voltage instability event, triggered by larger drops in system voltages from, for instance by activation of overexcitation limiters (OELs), or undervoltage tripping of generators. These types of events are generally referred to as short-term instability events *induced* by long-term dynamics [2]. It should be noted that methods based on QSS and combinations of QSS and time-domain simulations, as was suggested in [20], cannot deal with these types of events.

A clear advantage of using the DVSM (which also applies for the methods based on QSS), is that in static VSM, the notion of time is fully ignored, and by that, the impact of, for instance, timer settings of OELs, LTCs, and switched reactive power components [15]. Furthermore, equipment such as air conditioners, induction motors, and undervoltage relays, may either stall or trip due to temporary low voltages, which is an effect that can better be taken into account in either time-domain simulations or QSS simulations.

## 3 Methodology for fast estimation of DVSM

In the previous section, the circumstances when the DVSM is preferred to the conventional VSM were presented. In this section, a methodology for a fast estimation of the DVSM is proposed to overcome the computational difficulties when estimating the margin. The method uses NNs to provide both an estimate of the actual DVSM at a specific OC, and to determine the dimensioning contingency for the system with respect to the DVSM. These *estimated* values are then used as starting points in a method called dual binary search to significantly reduce the required computational time in computing the *actual* DVSM.

The first step is the offline generation of OCs and estimations of the DVSM for a set of credible contingencies. It should be noted that the generation of a representative training set is a critical step in ML applications [29]. In this paper, a simplified approach is adopted to generate a data set with sufficient complexity to test the method. However, in actual applications, significantly more effort should be assigned to this step to ensure an efficient and accurate database generation. Generally, the training data would not be randomly generated but can be taken directly from either real or forecasted OCs in the system.

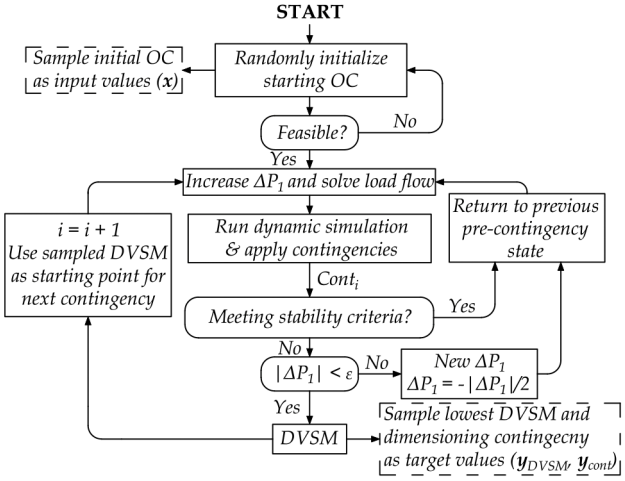


**Fig. 6** *Flowchart of the generation of training data for the DVSM and the NN*

The method is tested on the Nordic32 test system with all data and models, as presented in [30]. After a representative training set has been generated, the training scheme of the two NNs is presented. Each step in the methodology is described in the following subsections.

### *3.1 Generation of training data*

The training data for the NNs were generated using PSS®E34.2.0 with its in-built dynamic models [31]. In this paper, we have used full time-domain simulations, but the methodology could also be generalised for combinations of QSS and full time-domain simulations. The steps of generating the training data are illustrated in the flowchart in Fig. 6 and can be summarised as follows:

*3.1.1 Choose initial operating conditions:* All initial OCs were randomly generated around the secure operating point of the simulated Nordic32 system, denoted as 'operating point B' in [30]. The total load in the system for each initial OC was generated by multiplying *all* the active loads randomly from the *same* uniform distribution (80% of the original load as a lower limit, 95% of the original load as upper limit). Then, each *individual* load was varied by again multiplying the now updated load value with a random variable generated from a new uniform distribution (this time with 80% as the lower limit, and 120% as the upper limit). The power factor of all loads was kept constant. The total change in loading was then randomly distributed among all the generators in the system. The generated initial OCs were first solved using a conventional full Newton-Raphson load flow solution, which served as a starting point for the dynamical simulation. In the case the system was not found feasible, the initial OC was re-initialised.

*3.1.2 Increase system stress and solve load flow:* The system stress was then increased for the secure initial OC by increasing the power transfer between the two areas 'North' and 'Central'. The increased system stress was achieved by increasing the loads in the 'Central' area with a total of $\Delta P_1 = 200\,\text{MW}$, while simultaneously increasing the generation in the 'North' area with the same amount. The power factors of each load were again kept at the initial values. The distribution of the added load and generation was based on the initial load or the rated capacity of each generator. Thus, a bus with a larger initial load, or a generator with a higher rated capacity, received a larger share of the increased load and generation. All generation that could not be supplied by the regular generators were distributed to the slack bus generator in the system, g20, see Fig. 7. After the loads and the generation were updated, the load flow was reiterated, which then served as a starting point for the time-domain simulations. To avoid numerical and stability issues when increasing the system stress of the static system, the system

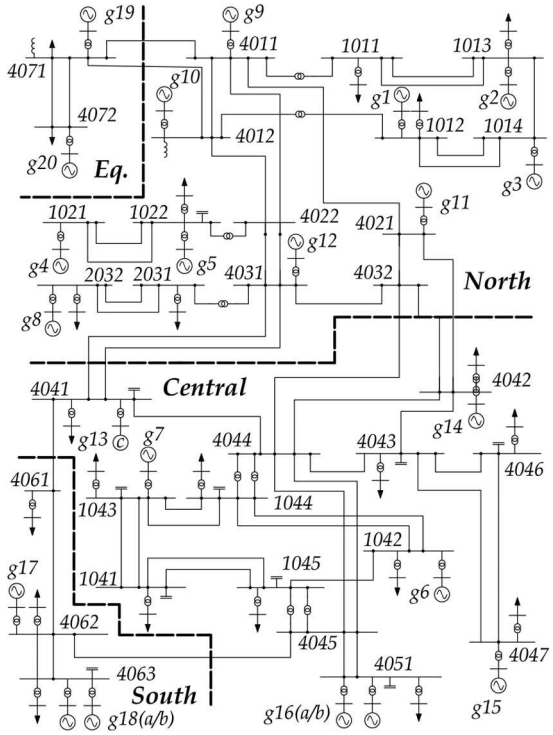


**Fig. 7** *One-line diagram of the Nordic32 test system*

stress was increased in small increments where a load flow solution was solved for each increment.

*3.1.3 Run time-domain simulation and test for security:* A time-domain simulation was then initialised for the first contingency. In the relatively small Nordic32 test system, the same single contingency was found to be dimensioning for almost all different initial OCs. To test the possibilities of using a NN to classify the dimensioning contingency, two different contingencies were handpicked as they were found to be dimensioning for different OCs. The tested contingency type was a three-phased fault on a transmission line during 0.1 s, followed by a tripping of the faulted line, which was kept tripped during the remaining time of the simulation. The lines between the buses '*4031–4041*' and '*4032–4044*', connecting the '*North*' and '*Central*' areas, were used, see Fig. 7 for a reference.

Each dynamic simulation ran for a total of 500 s, but was in the case of a major voltage collapse stopped in advance. The simulation time was chosen to ensure that the system either fully stabilised or collapsed. It should be noted that the required simulation time is dependent on the power system in consideration, and it is likely that different simulation times would be required in actual implementations of the algorithm. The system was considered secure if, at the end of each simulation, *all* transmission bus voltages were above 0.90 pu.

*3.1.4 Re-iterate and test other contingencies:* In case the system was found secure for the tested contingency, the system stress was increased again with $\Delta P_1$, followed by another security test. In case the system was *not* found secure, the previously added system stress was halved, and the process was re-initialised. This process of iteratively updating the system stress and testing for security continued until the increase in system stress was below a precision value of $\boldsymbol{\epsilon} = 5\,\text{MW}$. The DVSM was then computed by taking the difference in system loading between the initial OC and the secure system with the highest level of system stress.

Once the DVSM for the first contingency was computed, the same procedure was repeated for the second contingency. To save computational time, the estimated DVSM for the *first* contingency was used as a *starting point* for the estimation of the second contingency. If the system at that level of system stress was found secure for the second contingency, the simulation was stopped.

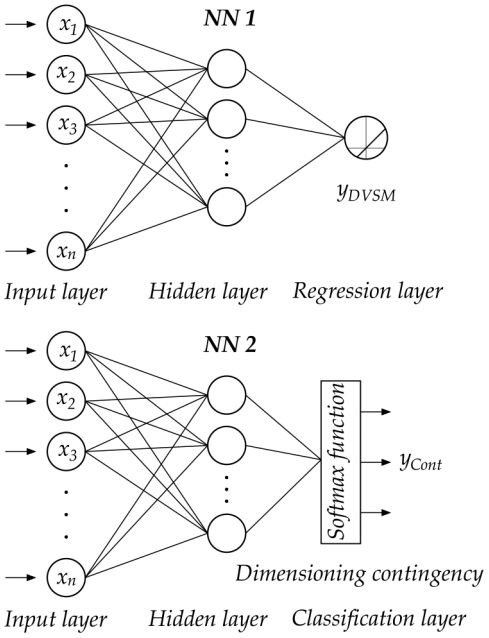


**Fig. 8** *Two NNs trained to estimate the DVSM and to classify the dimensioning contingency*

Otherwise, the search algorithm continued until a new smaller value of the DVSM was found.

*3.1.5 Sampling the input values and target values:* An input vector $\boldsymbol{x}$ consisting of measurements of all bus voltage magnitudes and angles, and active and reactive power flows were sampled from each one of the initial OCs. The choice of which input values to include in the training was based on the results in [8], which found that bus voltage magnitudes and angles were found to be the best combination of inputs when estimating the VSM using a NN. The active and reactive power flows were then added as additional inputs as this was found to increase the accuracy in the estimations even further.

Two target vectors $\boldsymbol{y}_{\text{DVSM}}$ and $\boldsymbol{y}_{\text{Cont}}$ were generated by sampling the DVSM for each case, and the contingency that was dimensioning for the specific case, respectively. The previously described steps were re-iterated until a sufficiently large training set was generated. Due to the random nature in which the training data was initialised and generated, some of the generated OCs were found to be correlated with very low DVSM values, despite being initialised with low system loading. To ensure that no anomalies were included in the training set, all OCs resulting in DVSM values below 150 MW was excluded from the training set.

### 3.2 Overview and design of the NNs

NNs have been successfully applied in a range of applications and their popularity have increased significantly in the last decades. NNs represents a class of ML algorithms which are inspired by the neurons in the human brain and its ability to classify and learn events from input data [32]. The strength of NNs lies in their capability of learning and approximating non-linear functions ($f$) from a set of input values ($\boldsymbol{x}$), and a corresponding vector of target values ($\boldsymbol{y}$).

*3.2.1 Architecture:* The architecture of the two NNs used in this paper is presented in Fig. 8 and the specific details regarding the architecture and the training parameters of the two NNs are specified in Table 1. In the training phase, the two NNs takes the same vector of input values, which are forwarded to each of the hidden layers through a set of weights, illustrated by the lines connecting each of the neurons. The output of each neuron in the hidden layer is computed using a non-linear activation function on the sum of all the inputs, which is then forwarded to the output layers. The rectified linear activation function (RelU) was used as

the non-linear activation function for the two NNs. For the NN estimating the DVSM, the outputs are forwarded to a regression layer with a linear activation function. For the NN responsible for ranking the contingencies, the outputs are forwarded to a layer with a softmax activation used for classification. The softmax activation function is generally used for multi-class classification but generally works well also for binary classification, as is the case in this paper. The softmax activation function outputs a probability vector, where each class is given a certain probability. The probability vector can then be used to rank the contingencies in order of which most likely will become dimensioning.

In the training phase, the networks use the true target vectors $\boldsymbol{y}_{\text{DVSM}}$ and $\boldsymbol{y}_{\text{Cont}}$, while during the test or prediction phase, the network estimates the DVSM and the ranked contingencies by generating the vectors $\hat{\boldsymbol{y}}_{\text{DVSM}}$ and $\hat{\boldsymbol{y}}_{\text{Cont}}$ for the current OC. The supervised training approach aims to update and learn the suitable values for the weights connecting each layer, implicitly modelling the non-linear relationship between the inputs and outputs.

*3.2.2 Training:* Different data sets were used in training, validation, and testing of the method. The training data has the dimension $(364 \times 6000)$, where the dimension represents the number of inputs, and the total number of training cases, respectively. Each network was trained for a maximum number of epochs, where an epoch is finished when all the cases in the training set have been used to update the network parameters. To reduce overfitting on the data, ridge regression (also known as L2 regularisation) was used to ensure the data does not rely too heavily on any single feature. To further reduce overfitting, a technique called dropout was applied where a certain percentage of the connections between each layer were masked/dropped, to ensure that the model does not rely too heavily on certain connections. The mean squared error (MSE) was used as a metric for the NN estimating the DVSM, while the categorical cross-entropy loss function was used for the NN classifying the dimensioning contingency. An adaptable algorithm for gradient-based optimisation, Adam, was used in training the network [33]. The learning rate ($\alpha$) was the only parameter that was tuned for the algorithm; the remaining used the default values according to [33].

It should be noted that both the training parameters and the architecture of the two networks have been iteratively tuned to increase the regression and classification accuracy. A deeper architecture with more hidden layers was found to not increase the performance for the specific test case and training set size. Other hyperparameters and network architectures would likely have better performance for other test systems than the Nordic32. By increasing the training set size further and spending even more effort in tuning the networks, an even better accuracy could be achieved.

### 3.3 Fast DVSM estimation and dual binary search

In [3], a binary search method was proposed to estimate the DVSM. In this paper, we propose an alternative approach denoted as the *dual binary search method*, which should be able to increase the computational speed of the DVSM. The trained NNs in Fig. 8 take the same set of measurements and generates: (i) an estimated value of the DVSM, and (ii) an estimated ranked order of the contingencies that most probably will be dimensioning for the current OC. The estimated DVSM is used as a qualified estimate of the real DVSM, which is validated through actual time-domain simulations. The dual binary search method is then used to take advantage of the estimated DVSM and the dimensioning contingency to reduce the computational time when validating the real DVSM for the system.

The dual binary search method is illustrated for two cases in Fig. 9. Case 1 illustrates the estimation process for an overestimated value of the DVSM, while Case 2 illustrates the estimation process for an underestimated value of the DVSM. Black dots indicate secure operating points and white dots indicate unsecure operating points. The estimated DVSM is always the starting point for the search of the *actual* DVSM of the system. The system stress is increased to this point iteratively using the approach explained in Section 3.1.2 to avoid convergence problems.

**Table 1** Design and hyperparameters used in training

| | Parameter | NN 1/NN 2 |
|---|---|---|
| Data | Number of inputs | 364/364 |
| | Training cases | 60006000 |
| | Validation cases | 400/400 |
| | Test cases | 400/400 |
| Architecture | Hidden layers | 1/1 |
| | Final activation function | Linear/Softmax |
| | Hidden cells | 128/32 |
| | Hidden layer activation | RelU/RelU |
| Training | Max epochs | 1000/3000 |
| | Learning rate ($\alpha$) | $1 \times 10^{-6}/1 \times 10^{-5}$ |
| | Dropout | 0%/50% |
| | L2 parameter | 0.01/0.01 |
| | Optimiser | Adam/Adam [33] |
| | Loss metric | MSE/categorical cross-entropy |

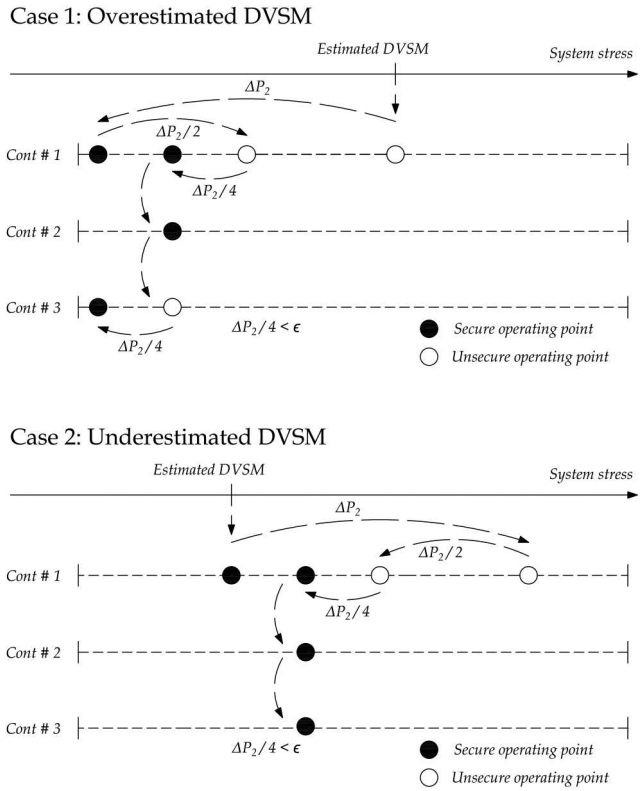


**Fig. 9** *Dual binary search for multiple contingencies*

Once the stressed static base case is found, a time-domain simulation is initiated for the *highest*-ranked contingency by the second NN, which is the contingency that most likely will be dimensioning for the DVSM. The initial estimated DVSM level is then tested for the chosen contingency. In case it is stable (respectively unstable), the system stress is increased (respectively decreased) with a certain value represented by $\Delta P_2$. We propose using a value of $\Delta P_2$ equal to the MSE of the estimated values for the DVSM, which should represent a reasonable uncertainty and step size for the estimation. If the new operating point is found to be secure, the system stress is again increased with $\Delta P_2$. In case it is not found to be secure, the system stress is reduced by $\Delta P_2/2$. The dual binary search is then continued until a secure operating point is found and when the step size in system stress change is smaller than a specified precision level ($\epsilon$).

This level of system stress is then tested for the other contingencies, in ranked order, until all lower-ranked contingencies have been tested and found secure. For both, the cases illustrated in Fig. 9, this level of system stress for the second-ranked contingency was found to result in a secure operating point. A third and final ranked contingency is then tested, which for Case 1 in Fig. 9 is found to be unsecure. The system stress is thus reduced further for this case, resulting in a secure operating point, which then constitutes the dimensioning DVSM for the system. It should be noted that for Case 1, the contingency ranking was not perfect, with the result that an extra time-domain simulation was required.

## 4 Results and discussions

In this section, the results from the regression and classification of the test set for the two NNs are presented. The reduction in computational effort is compared and presented between the conventional tracing method and the proposed dual binary search method. Furthermore, the capability of the method to handle unplanned topology changes and to estimate the security margin after a disturbance is tested. Finally, practical applications and discussions related to DVSM estimation are presented.

### *4.1 Regression and classification accuracy*

The prediction accuracy for the NN estimating the DVSM is presented in Fig. 10, where the estimated DVSM is plotted with respect to the real DVSM for the test set. The diagonal line indicates where the points should lie in case the estimated DVSM perfectly matches the real DVSM. Table 2 lists the mean and maximum errors of the estimations in percentage, as well as the MSE presented in MW. The results indicate that the NN is generally capable to accurately estimate the DVSM given an initial OC, with a mean error for the test set of 1.49%. The maximum estimation error was found to be 10.96%, while the MSE was estimated to 13.35 MW.

The classification accuracy of the NN used in ranking the dimensioning contingency is presented in Table 3 in the form of a confusion table. Each number in each row represents the instances of the real dimensioning contingencies, while each number in each column represents the instances of the predicted dimensioning contingencies. The conditional probabilities of correctly classifying the dimensioning contingency are presented in the column furthest to the right. Similarly, the conditional probabilities of a dimensioning contingency actually *belonging* to the predicted class are presented in the bottom row of the table. The total accuracy for the classification is presented in the rightmost corner of the table, and an accuracy of 91.3% was provided for the test set. Thus, in about nine instances of ten, the NN is capable of classifying which contingency that will be dimensioning for the DVSM for a specific OC. It should again be mentioned that it is possible that the estimation and classification results could be enhanced further by either increasing the training set size or by a more careful exploration of suitable hyperparameters for the training of the networks.

### *4.2 Computational efficiency*

In this section, the computational efficiency is compared between the proposed fast dual binary search method and the more conventional tracing method that was used in generating the training set (see Section 3.1 for reference). The proposed fast dual binary search method, explained in Section 3.3, uses the estimated DVSM value and the dimensioning contingency as a starting point to validate the real DVSM. The computational efficiency is measured as the average number of time-domain simulations required in estimating the DVSM. The results of using the two different methods are presented in Table 4. The average number of time-domain simulations required in estimating the DVSM using the *conventional* tracing method was found to be 15.3, while the corresponding number using the proposed dual binary search method was 4.7. The reduction in the average number of time-domain simulations required was thus −69.2% when the proposed method was applied.

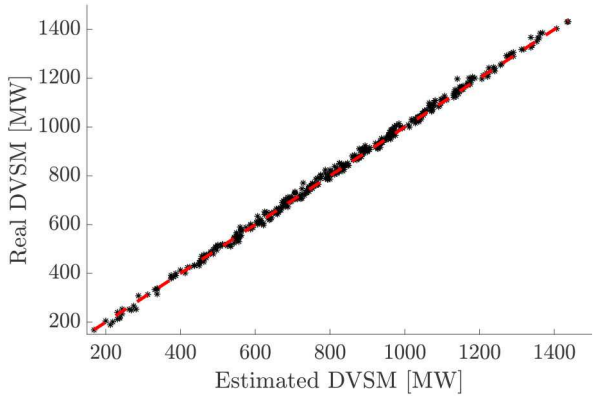


**Fig. 10** *Prediction accuracy of estimating the DVSM*

**Table 2** Regression results of the DVSM estimation

| Mean estimation error | Maximum estimation error | Mean squared error |
|---|---|---|
| 1.49% | 10.96% | 13.35 MW |

**Table 3** Confusion table showing real and predicted dimensioning contingencies

| | | Predicted | | |
|---|---|---|---|---|
| | | L4044–L4032 | L4044–L4032 | Accuracy |
| Real | L4044–L4032 | 104 | 23 | 81.9% |
| | L4044–L4031 | 12 | 261 | 95.6% |
| | Accuracy | 89.6% | 91.9% | 91.3% |

**Table 4** Reduction in the computational effort using the proposed method

| Average number of time-domain simulations | | |
|---|---|---|
| Conventional tracing method | Dual binary search method | Relative reduction in computations |
| 15.3 | 4.7 | −69.2% |

It should be noted that the *exact* comparison in computational efficiency between the two methods is of comparatively little interest, as it mainly applies to the specific test case used in this paper. For instance, it is probable that the computational savings are significantly higher in most real applications, where a larger range of contingencies may be dimensioning for the DVSM. Furthermore, in real applications where the range of the DVSM may be larger than what has been used in this paper, the conventional search algorithm would require significantly more time-domain simulations to find the true DVSM. Similarly, it is also possible to further enhance both the conventional search algorithm and the dual binary search algorithm by, for instance choosing more suitable values of $\Delta P_1$, or by increasing the precision value of $\boldsymbol{\epsilon}$. The most notable result is instead that the computational effort in estimating the DVSM can be reduced from requiring a large number of time-domain simulations, to only requiring a few. Although a few time-domain simulations would still take some time to compute for a real power system, it should be possible to provide sufficiently fast estimations of the DVSM to classify it as a '*near real-time*' estimation.

### *4.3 Impact of sudden topology change*

In any real application, the performance of a NN is dependent on its generalisation capability. This refers to the capability of the NN to generalise the learning from the actual training set to other, yet unseen, cases. In this section, we examine the performance of the NNs to generalise their estimations when subjected to test cases where unplanned topology changes have taken place. This also indirectly tests the capability of the method to estimate the security margin *after* the system has already undergone a disturbance. As

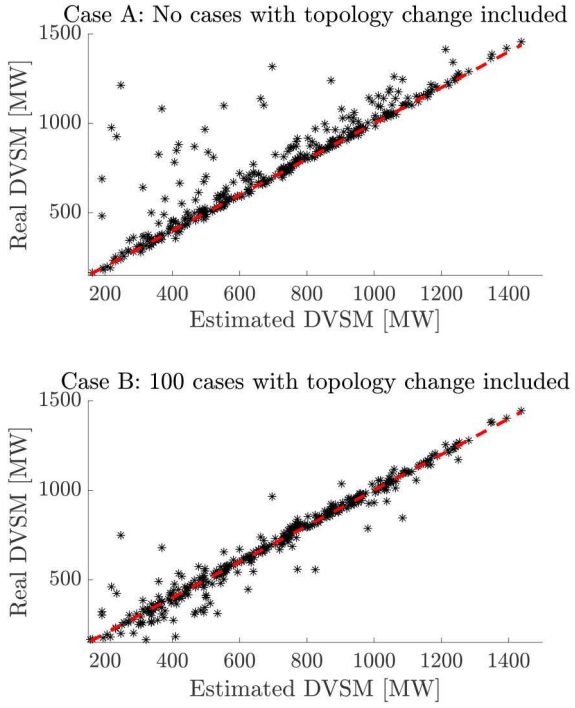


**Fig. 11** *Prediction accuracy of the DVSM during sudden topology changes, Cases A and B. With and without trained on a training set with 100 training cases with topology changes included*

most power systems are operated securely with respect to $N-1$, a single disturbance will likely not cause instability. However, following a disturbance, the system operator needs to ensure that the (post-contingency) system is again returned to a secure operation, so that if another contingency occurs ($N-1-1$), the system can withstand that disturbance as well. If not, restorative control needs to be issued to ensure that the system yet again fulfils the $N-1$ contingency criterion. For simplicity of notation, we will only refer to the case of unplanned topology change in the remaining part of this section.

In the following analysis, we only consider topology changes in the form of opened transmission lines. To ensure that the Nordic32 test system is still secure despite the topology changes, only topology changes in the 'North' region, see Fig. 7, were considered. Furthermore, only transmission lines between buses served by two parallel transmission lines were used in generating the test set with topology changes. A new test set of 400 cases was then generated in the same manner as explained in Section 3.1, with the difference that the topology changes were now added randomly.

Two different cases were then tested. For Case A, the NNs were trained on the previously developed training set and no unseen cases with topology changes were included in the training set. For Case B, the NNs were re-trained on a new training set where a few (100) training cases with topology changes had been included in the original training set. The exact same training procedure as before was used. The regression results for the two cases are presented in Fig. 11. Table 5 lists the mean error of the estimations in percentage for each case, as well as the MSE presented in MW. The result for Case 1 indicates that a sudden topology change will significantly affect the accuracy of the predictions. Although many cases were accurately predicted, the number of outliers increased significantly. The prediction accuracy was higher for Case B, even though only a very small number of cases with the topology changes were added to the training set. The classification accuracy of the NN used in ranking the dimensioning contingency was also affected significantly for the two cases, with a total classification accuracy of 55 and 78.5% for Case A and Case B, respectively.

The results highlight the importance of obtaining a representative training set and also taking into account the possibilities of unplanned topology changes. This would also allow system operators to better track the security margin after a disturbance has occurred. The results also showed that by the inclusion of even a very small set of training cases with various topology changes, the prediction accuracy could be increased significantly. Thus, in the event of an unplanned topology change in the system, the system operator could quickly generate a small training set on the new OC, and then retrain the NNs on the generated data. It should be noted that the proposed robust methodology of always validating the estimations of the NNs with *actual* time-domain simulations reduces the impact of these types of erroneous estimations. The main impact of a poor estimation of the DVSM will be that the time to validate it will increase.

**Table 5** Regression results of the DVSM estimation for Cases A and B

| | Mean estimation error, % | Mean squared error, MW |
|---|---|---|
| Case A | 12.97 | 134.38 |
| Case B | 7.33 | 63.59 |

### *4.4 Discussions and practical applications*

The proposed method is aimed to be used as an online tool for system operators to estimate a power system's DVSM. The method does not necessarily have to replace conventional VSM estimation, but may instead be used as an additional source of information to system operators to provide better and more accurate estimates of the total transmission capacity in their systems.

Theoretically, the DVSM estimates by the NNs could be used directly to provide real-time estimates of the security margin. However, despite years of research, examples where these methods have been practically applied in system operators' monitoring and control systems are, to the authors' best knowledge, very few. From a system operator's view, an inferior method that *always* works is generally preferred to a superior method that, in some instances, does not. The proposed method in this paper is thus suggested to utilise the advantages of ML, while still ensuring that the method always provides good estimates regardless of the current OCs.

An important factor in any ML-based application is the size of the training set. The required training set size is highly dependent on the complexity of the underlying problem, here represented by the power system in consideration. The required size of the training data set depends on several factors, such as the range of different possible operating conditions, the number of possible dimensioning contingencies, and, ultimately, the accuracy requirement of the system operator.

NNs were chosen as they have been proven to be very powerful in applications for both regression and classification, especially when trained on large sets of data [32]. A common criticism against NNs is that while they can accurately approximate any non-linear function, studying their structure will not give any insights on the function that is being approximated. However, since the proposed methodology use time-domain simulations to always *validate* the estimations provided by the NNs, the drawback of the lacking ability to interpret the estimations is of less significance.

The results in the previous section indicated that by using the proposed method, the number of required time-domain simulations to estimate the DVSM could be reduced to only a few, allowing system operators to estimate the DVSM in a time frame that could be defined as 'near real-time'. The update frequency of security margins will affect the required transmission reliability margins as the underlying system continuously change between the assessments. The actual estimation speed will still be affected by a range of different factors, such as the computational speed of the hardware being used, the size of the specific power system in consideration, or the required precision (i.e. the value of $\epsilon$).

In this paper, measurements of bus voltage magnitudes and angles, as well as active and reactive power, have been assumed to be available, either directly from measurements or from state estimations of the system. However, to ensure that missing values and errors are filtered out, all measurements should preferably be preceded by a state estimator. To adapt to the evolving operating conditions and self-rectify any bad predictions, the two NNs should

be trained continuously during operation. Using approaches such as stochastic gradient descent, the NNs weight parameters can continuously be tuned to increase the robustness and accuracy.

## 5 Conclusions

This paper presents a framework and a methodology for fast estimation of the DVSM. The difference between the DVSM and the conventional static VSM has been illustrated using a concept called transient $P$ - $V$ curves, where the advantages of using the DVSM have been established. Specifically, the DVSM will become increasingly important in power systems with an increasing share of loads with fast load restoration dynamics and in systems that are operated close to the physical limits.

Furthermore, a methodology for a fast estimation of the DVSM is proposed. The method uses a regression-based NN to provide a qualified guess of the actual DVSM. Moreover, a second NN is used to provide a classification of which contingency will be dimensioning for the system. The estimates from the NNs are used in a method called dual binary search, which is used to *validate* the actual DVSM using time-domain simulations. The ML-based approach is thus only proposed to *support* the estimation of the DVSM, while the actual DVSM is always validated through actual time-domain simulations. This two-step approach is proposed to overcome system operators' reluctance of using ML-based methods, while still allowing near real-time estimations of the DVSM.

The results presented in this paper are promising, and the trained NNs provided good estimations of both the DVSM and classifications for the dimensioning contingency. The accurate estimations used in combination with the proposed dual binary search method were found to successfully reduce the required number of time-domain simulations, which would allow system operators to overcome the main practical difficulties of estimating the DVSM.

In future research, the first step would be to test the developed method on a real power system to examine the capacity and limitations of the method. It would be highly relevant to examine if the proposed methodology is capable of increasing the computational efficiency sufficiently to allow system operators to use it in real-time monitoring and operation. Furthermore, generating a representative training set for a large power system is challenging. Thus, to examine the capability to generalise the learning from the actual training set to other, yet unseen, cases are of special interest. Finally, actual numerical comparisons between the DVSM and the VSM in real power systems would be of high interest, especially when considering high system penetration of loads with fast dynamic responses.

## 6 Acknowledgments

The work presented in this paper has been financially supported by Energimyndigheten (Swedish Energy Agency) and Svenska kraftnät (Swedish National Grid) within the SamspEL program with the project no. 44358-1.

## 7 References

[1] Glavic, M., Van Cutsem, T.: 'A short survey of methods for voltage instability detection'. Proc. (IEEE) PES General Meeting, Detroit, MI, 2011, pp. 1–8

[2] Van Cutsem, T., Vournas, C.: '*Voltage stability of electric power systems*' (Kluwer Academic Publishers, Boston, 1998)

[3] Van Cutsem, T., Moisse, C., Mailhot, R.: 'Determination of secure operating limits with respect to voltage collapse', *IEEE Trans. Power Syst.*, 1999, **14**, (1), pp. 327–335

[4] Ajjarapu, V., Christy, C.: 'The continuation power flow: a tool for steady state voltage stability analysis', *IEEE Trans. Power Syst.*, 1992, **7**, (1), pp. 416–423

[5] Chiang, H.-D., Flueck, A.J., Shah, K.S., *et al.*: 'CPFLOW: a practical tool for tracing power system steady-state stationary behavior due to load and generation variations', *IEEE Trans. Power Syst.*, 1995, **10**, (2), pp. 623–634

[6] El-Keib, A.A., Ma, X.: 'Application of artificial neural networks in voltage stability assessment', *IEEE Trans. Power Syst.*, 1995, **10**, (4), pp. 1890–1896

[7] Jeyasurya, B.: 'Artificial neural networks for on-line voltage stability assessment'. 2000 Power Engineering Society Summer Meeting (Cat. No.00CH37134), Seattle, WA, USA, 2000, vol. 4, pp. 2014–2018

[8] Zhou, D.Q., Annakkage, U.D., Rajapakse, A.D.: 'Online monitoring of voltage stability margin using an artificial neural network', *IEEE Trans. Power Syst.*, 2010, **25**, (3), pp. 1566–1574

[9] Van Cutsem, T., Wehenkel, L., Pavella, M., *et al.*: 'Decision tree approaches to voltage security assessment', *IEE Proc. C, Gener. Transm. Distrib.*, 1993, **140**, (3), pp. 189–198

[10] Zheng, C., Malbasa, V., Kezunovic, M.: 'Regression tree for stability margin prediction using synchrophasor measurements', *IEEE Trans. Power Syst.*, 2013, **28**, (2), pp. 1978–1987

[11] Fan, Y., Liu, S., Qin, L., *et al.*: 'A novel online estimation scheme for static voltage stability margin based on relationships exploration in a large data set', *IEEE Trans. Power Syst.*, 2015, **30**, (3), pp. 1380–1393

[12] Li, S., Ajjarapu, V., Djukanovic, M.: 'Adaptive online monitoring of voltage stability margin via local regression', *IEEE Trans. Power Syst.*, 2018, **33**, (1), pp. 701–713

[13] Savulescu, S.C.: '*Real-time stability in power systems. [electronic resource]: techniques for early detection of the risk of blackout', Power Electronics and Power Systems* (Springer International Publishing, USA, 2014)

[14] Konstantelos, I., Jamgotchian, G., Tindemans, S.H., *et al.*: 'Implementation of a massively parallel dynamic security assessment platform for large-scale grids', *IEEE Trans. Smart Grid*, 2017, **8**, (3), pp. 1417–1426

[15] Van Cutsem, T., Mailhot, R.: 'Validation of a fast voltage stability analysis method on the Hydro-Quebec system', *IEEE Trans. Power Syst.*, 1997, **12**, (1), pp. 282–292

[16] Mansour, Y., Chang, A.Y., Tamby, J., *et al.*: 'Large scale dynamic security screening and ranking using neural networks', *IEEE Trans. Power Syst.*, 1997, **12**, (2), pp. 954–960

[17] Sun, K., Likhate, S., Vittal, V., *et al.*: 'An online dynamic security assessment scheme using phasor measurements and decision trees', *IEEE Trans. Power Syst.*, 2007, **22**, (4), pp. 1935–1943

[18] Khoshkhoo, H., Shahrtash, S.M.: 'Fast online dynamic voltage instability prediction and voltage stability classification', *IET Gener. Transm. Distrib.*, 2014, **8**, (5), pp. 957–965

[19] Liu, C., Tang, F., Bak, C.L.: 'An accurate online dynamic security assessment scheme based on random forest', *Energies*, 2018, **11**, (7), p. 1914

[20] Van Cutsem, T., Grenier, M.E., Lefebvre, D.: 'Combined detailed and quasi steady-state time simulations for large-disturbance analysis', *Int. J. Electr. Power Energy Syst.*, 2006, **28**, (9), pp. 634–642

[21] Sittithumwat, A., Tomsovic, K.: 'Dynamic security margin estimation using artificial neural networks'. IEEE Power Engineering Society Summer Meeting, Chicago, IL, 2002, vol. 3, pp. 1322–1327

[22] Amjady, N.: 'Dynamic voltage security assessment by a neural network based method', *Electr. Power Syst. Res.*, 2003, **66**, (3), pp. 215–226

[23] Shang, J., Zhang, J., Zhao, W., *et al.*: 'ANN based dynamic voltage security assessment for a practical power system'. 2007 Int. Power Engineering Conf. (IPEC 2007), Singapore, Singapore, 2007, pp. 794–798

[24] Baghmisheh, M.V., Razmi, H.: 'Dynamic voltage stability assessment of power transmission systems using neural networks', *Energy Convers. Manage.*, 2007, **49**, (1), pp. 1–7

[25] Li, H., Chiang, H.D., Yoshida, H., *et al.*: 'The generation of zip-v curves for tracing power system steady state stationary behavior due to load and generation variations'. 1999 IEEE Power Engineering Society Summer Meeting. Conf. Proc., Edmonton, Canada, 1999, vol. 2, pp. 647–651

[26] Pal, M.K.: 'Voltage stability conditions considering load characteristics', *IEEE Trans. Power Syst.*, 1992, **7**, (1), pp. 243–249

[27] Dobson, I.: 'The irrelevance of load dynamics for the loading margin to voltage collapse and its sensitivities'. Bulk Power System Voltage Phenomena – III: Voltage Stability, Security & Control, Davos, Switzerland, 1994, pp. 509–518

[28] Dharmakeerthi, C.H., Mithulananthan, N., Saha, T.K.: 'Impact of electric vehicle fast charging on power system voltage stability', *Int. J. Electr. Power Energy Syst.*, 2014, **57**, pp. 241–249

[29] Thams, F., Venzke, A., Eriksson, R., *et al.*: 'Efficient database generation for data-driven security assessment of power systems', *IEEE Trans. Power Syst.*, 2020, **35**, pp. 30–41

[30] Van Cutsem, T., Glavic, M., Rosehart, W., *et al.*: 'Test systems for voltage stability analysis and security assessment'. PES-TR19, IEEE/PES Task Force, 2015

[31] PTI Siemens, '*PSS®e 34.2.0 model library*' (Siemens Power Technologies International, Schenectady, NY, 2017)

[32] Goodfellow, I., Bengio, Y., Courville, A.: '*Deep learning*' (MIT Press, USA, 2016). Available at http://www.deeplearningbook.org

[33] Kingma, D.P., Ba, J.: 'Adam: a method for stochastic optimization', arXiv eprints, 2014, p. arXiv:1412.6980

# Voltage Instability Prediction Using a Deep Recurrent Neural Network

Hannes Hagmar, *Student Member, IEEE*, Lang Tong, *Fellow, IEEE*, Robert Eriksson, *Senior Member, IEEE*, and Le Anh Tuan, *Member, IEEE*

***Abstract*—This paper develops a new method for voltage instability prediction using a recurrent neural network with long short-term memory. The method is aimed to be used as a supplementary warning system for system operators, capable of assessing whether the current state will cause voltage instability issues several minutes into the future. The proposed method uses a long sequence-based network, where both real-time and historic data are used to enhance the classification accuracy. The network is trained and tested on the Nordic32 test system, where combinations of different operating conditions and contingency scenarios are generated using time-domain simulations. The method shows that almost all N-1 contingency test cases were predicted correctly, and N-1-1 contingency test cases were predicted with over 95 % accuracy only seconds after a disturbance. Further, the impact of sequence length is examined, showing that the proposed long sequenced-based method provides significantly better classification accuracy than both a feedforward neural network and a network using a shorter sequence.**

***Index Terms*—Dynamic security assessment, long short-term memory, recurrent neural network, voltage instability prediction, voltage stability assessment.**

## I. Introduction

VOLTAGE instability is one of the main limitations for secure operation of a modern power system [1]. A voltage instability event can often be deceiving, where the system may seem stable for several minutes after a disturbance, only to end up in an unstable state within a short time [2]. When instability finally is detected, the system may already have become severely degraded and the risks of an extended blackout may have increased significantly.

Manuscript received August 16, 2019; revised January 30, 2020 and June 5, 2020; accepted July 5, 2020. Date of publication July 13, 2020; date of current version January 6, 2021. The work was supported in part by Energimyndigheten (Swedish Energy Agency) and in part by Svenska kraftnät (Swedish National Grid) within the SamspEL program with project number 44358-1. The work of L. Tong was supported by the U.S. National Science Foundation under grant 1932501 and 1809830. Paper no. TPWRS-01219-2019. *(Corresponding author: Hannes Hagmar.)*

Hannes Hagmar and Le Anh Tuan are with the Department of Electrical Engineering, Chalmers University of Technology, 41296 Göteborg, Sweden (e-mail: hannes.hagmar@chalmers.se; tuan.le@chalmers.se).

Lang Tong is with the School of Electrical and Computer Engineering, Cornell University, Ithaca, NY 14850 USA (e-mail: lt35@cornell.edu).

Robert Eriksson is with the Department of Market and System Development, Svenska kraftnät, 172 24 Sundbyberg, Sweden (e-mail: robert.eriksson@svk.se).

Color versions of one or more of the figures in this article are available online at https://ieeexplore.ieee.org.

Digital Object Identifier 10.1109/TPWRS.2020.3008801

To ensure a secure operation, system operators often use an approach called dynamic security assessment (DSA). DSA includes time-domain analysis to test a power system's dynamic response after a set of contingencies assure its ability to reach a stable post-disturbance operating point [3]. Time-domain analysis and assessment of the dynamic stability are complex tasks, and even with recent progress in high performance computing, it is generally not feasible to assess the dynamic stability in real-time [3].

To overcome this issue, various machine learning (ML) methods have been proposed in the literature. The main advantage of using ML is that high-cost computations can be performed off-line. Once the ML algorithm is trained, it can almost instantaneously provide estimations and warnings to operators that otherwise would require time-consuming computations. Examples of DSA methods based on ML are found in [3]–[8], where mainly various decision tree (DT) or neural network (NN) methods are utilized.

Voltage security assessment (VSA) is a branch in DSA that specifically examines the impact of voltage instability events [9]. This paper deals with the *emergency* applications of VSA, where the *current* system state is assessed. Here, the stability of the system is not tested with respect to a set of contingencies; rather, the system may already have suffered a disturbance. The aim of these methods is to perform voltage instability prediction (VIP) and to detect the *onset* of instability, rather than its consequences. Fast prediction of voltage instability would then allow system operators to trigger fast remedial actions to control the system back into stable operation again.

A method for VIP based on ML was first proposed in [4], where a DT was trained on a generated database consisting of the intermediate, short-term equilibrium that follows a disturbance. This post-contingency state, where the majority of the electromechanical transients have died out, was referred to as the "just after disturbance" (JAD) state. Extensions of the method utilizing phasor measurements have later been proposed in [10]–[12], where the performance of different attributes or input data have been tested. A method based on support vector machines (SVM) was proposed in [13], where generators' predicted reactive power output was used as an indicator for voltage collapse. A method based on training a NN to online monitor voltage security was proposed in [14], and in [15], a NN was used to also indicate where in the system instability would emerge.

Most previously developed methods for VIP have in common that only instantaneous measurements are used as inputs to the

VIP algorithms. These inputs represent the "state signal" that the ML algorithm uses to predict the future state. Ideally, the state signal should summarize all relevant information required to determine the future state of the system. A state signal achieving this is said to have Markov property [16]. However, the dynamic response of a power system cannot be modeled as a first-order Markov process using only the static states provided by available measurements in the power system. Rather, the future state of the system also depends on a range of unknown state variables such as the rotor speed of generators, tap positions, or rotor slips of induction motors.

An attempt to incorporate some time-related features to improve the performance in VIP was presented in [17], where a temporal decision tree (TDT) approach was proposed. The TDT method, further discussed in [18] and [19], could incorporate some time-related variables, such as the difference between two measurements for specific value of elapsed time ($\Delta t$). However, the proposed TDT method did not allow efficient modeling of more complex time-dependent features and also required the user to define a finite number of candidate values of $\Delta t$, thus limiting the capability of the algorithm.

In response to these limitations, we propose a new method based on a recurrent neural network (RNN) with long short-term memory (LSTM). LSTM networks excel at capturing long-term dependencies [20], which is an inherent aspect in long-term voltage stability [2]. The method is, to the authors' knowledge, the first of its kind to use sequences of both current and past data with the aim to enhance the available state signal and implicitly take into account unknown state variables.

The main contributions of this paper are the following:

- A methodology for VIP using an LSTM network is developed. The LSTM network can utilize previous measurements, such as the trend of bus voltage magnitudes, tap changes, or fault locations, to improve the accuracy for VIP. The performance using the sequence-based approach is compared with an LSTM network using a shorter sequence and a conventional NN.
- A new training approach is developed to provide operators with an *online* assessment tool for potential voltage instability. The training approach allows the network to not only be trained on the measurements gathered from the JAD state but during the full dynamic trajectory that the system takes following a disturbance. As time progresses during a voltage instability event, the network is capable of incorporating new observations and continuously updating the assessment.
- A methodology for including consecutive contingencies ($N$-1-1) into the training data is presented. The paper also examines the ability of the LSTM network to generalize for VIP under $N$-1-1 contingencies. Such ability is especially valuable in overcoming the combinatorial increase of complexity in training.

The rest of the paper is organized as follows. In Section II, the theory regarding RNNs and LSTM is presented. In Section III, the proposed method is presented along with the steps for developing the training data and the training of the LSTM network. In Section IV, the results and discussion are presented. Concluding remarks are presented in Section V.

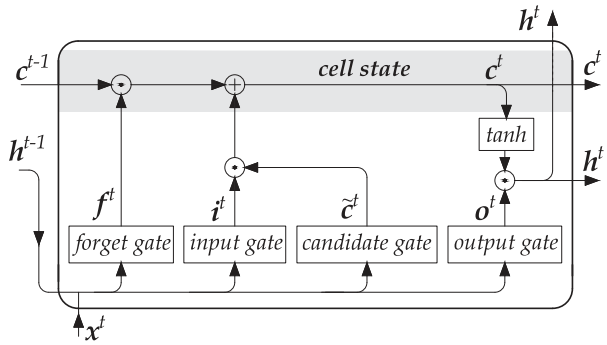


Fig. 1. Detailed schematics of an LSTM block.

## II. Long Short-Term Memory Networks

Neural networks are a class of machine learning algorithms, highly capable of accurately approximating nonlinear functions, mapping a set of inputs to a corresponding set of target values. RNNs represent a specific type of NNs adapted for processing *sequential* input data [21]. However, the standard implementation of RNN has difficulties in capturing long-term dependencies of events that are significantly separated in time. In an LSTM network, such information can be propagated through time within an internal state memory cell, making the network capable of memorizing features of significance [22].

A typical LSTM-block is illustrated in Fig. 1. The state memory cell, illustrated by the light grey area, is controlled by nonlinear gating units that regulate the flow in and out of the cell [20]. Following [22] and [20], the forward operation of an LSTM block is summarized below. It should be noted that each block consists of a number of hidden LSTM cells. Vector notation is used, meaning that, for instance, the hidden state vector $\boldsymbol{h}^t$ is not the output of a single LSTM-cell at time $t$, but the output of a vector of $N$ LSTM-cells. The operation of an LSTM block at a time $t$ may then be summarized by:

$$\boldsymbol{f}^t = \sigma\left(\boldsymbol{W}_f \boldsymbol{x}^t + \boldsymbol{U}_f \boldsymbol{h}^{t-1} + \boldsymbol{b}_f\right) \tag{1}$$

$$\boldsymbol{i}^t = \sigma\left(\boldsymbol{W}_i \boldsymbol{x}^t + \boldsymbol{U}_i \boldsymbol{h}^{t-1} + \boldsymbol{b}_i\right) \tag{2}$$

$$\tilde{\boldsymbol{c}}^t = \tanh\left(\boldsymbol{W}_c \boldsymbol{x}^t + \boldsymbol{U}_c \boldsymbol{h}^{t-1} + \boldsymbol{b}_c\right) \tag{3}$$

$$\boldsymbol{c}^t = \boldsymbol{f}^t \odot \boldsymbol{c}^{t-1} + \boldsymbol{i}^t \odot \tilde{\boldsymbol{c}}^t \tag{4}$$

$$\boldsymbol{o}^t = \sigma\left(\boldsymbol{W}_o \boldsymbol{x}^t + \boldsymbol{U}_o \boldsymbol{h}^{t-1} + \boldsymbol{b}_o\right) \tag{5}$$

$$\boldsymbol{h}^t = \boldsymbol{o}^t \odot \tanh(\boldsymbol{c}^t), \tag{6}$$

where element-wise multiplication is denoted by $\odot$, $\sigma$ is the logistic sigmoid function, $\tanh$ is the hyperbolic tangent function, and with the following variables:

- $\boldsymbol{x}^t \in \mathbb{R}^M$: input vector to an LSTM block
- $\boldsymbol{h}^t, \boldsymbol{h}^{t-1} \in \mathbb{R}^N$: output vector at time $t$ respectively $t$-1
- $\boldsymbol{f}^t \in \mathbb{R}^N$: activation vector of the forget gate
- $\boldsymbol{i}^t \in \mathbb{R}^N$: activation vector of the input gate
- $\tilde{\boldsymbol{c}}^t \in \mathbb{R}^N$: vector of the the candidate gate

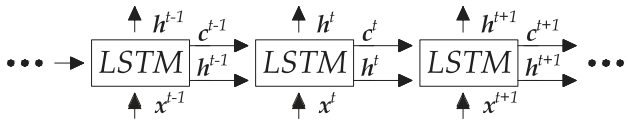


Fig. 2. An LSTM sequence with a directed connection between the blocks.

- $\boldsymbol{c}^t \in \mathbb{R}^N$: cell state memory vector
- $\boldsymbol{i}^t \in \mathbb{R}^N$: activation vector of the output gate

where $\boldsymbol{W}$, $\boldsymbol{U}$, and $\boldsymbol{b}$ represent the weight matrices and bias vectors for each gate. The superscripts $M$ and $N$ refer to the number of inputs and hidden LSTM cells in each LSTM block, respectively.

The information stored in the state memory cell is regulated by the operation of the different gates, as illustrated in Fig. 1. By the operation of (1), the forget gate controls what information should be stored from the previous memory cell state, and what can be discarded as irrelevant. The input gate and candidate gate control and update the memory cell state with new information by the operation of (2)–(3). In (4), the state memory cell is first updated by an element-wise multiplication of the previous cell state memory vector and the resulting vector of the forget gate. Then, the state memory cell is updated with new values provided by an element-wise multiplication of the resulting vectors from the input gate and the candidate gate. Equations (5)–(6) show how the hidden state is updated by the operation of the output gate, modulated by the updated cell state memory vector.

An LSTM *network* may then be constructed by creating a sequence of several LSTM blocks. A partition of an LSTM sequence is illustrated in Fig. 2, where each block has a directed connection to the following block in the sequence. If the block is the first one in the sequence, the past system state is initialized with a preset value. For a deep LSTM network, with several stacked layers, the inputs to the deeper layers consist of the hidden states of LSTM blocks of previous layers. The cell state memory is only passed along the time sequence between LSTM blocks of the same layer. Typically, for classification purposes, an output vector $\boldsymbol{y}$ is generated by applying a nonlinear function of the hidden state implemented by a separate feedforward NN. Depending on the application of the network, output vectors may be computed for a single, or for several, LSTM block's hidden states.

The LSTM network can then be trained using a supervised approach, where a set of training sequences and an optimization algorithm are used to update and learn suitable values for the weights matrices and bias vector parameters. The training of an LSTM network is discussed in further detail in Section III-C.

## III. Methodology

The proposed method for real-time VIP is based on off-line training of an LSTM network on a large data set consisting of time-domain simulation responses following a set of credible contingencies. The method is aimed to be used as a supplementary warning system that can assess the current state of the system in real-time. The LSTM network takes real-time and historic measurements and attempts to assess whether the *current* state will cause voltage stability issues several minutes into the future. As time progresses and if new events occur in the system, the network updates the assessment continuously. The network is also adapted to be able to indicate *where* in the system instability emerges, following the approach developed in [15], allowing more cost-effective countermeasures.

The first step of the method is the off-line generation of credible operating conditions (OCs) and contingency scenarios using time-domain simulations. The method is tested on a modified version of the Nordic32 test system with all data and models as presented in [23]. The load restoration following the contingencies is modelled by the actions of load tap changers that in steps restore the voltage-dependent loads. The corresponding generation changes are controlled mainly through governors that control the output of the hydro generators in the system. Schemes for automatic generation control or more dynamic load restoration models could be added in the dynamic models in the system but for the results to be more easily replicable, the same system as was presented in [23] was used. After a representative training set is generated, training of the LSTM network is performed. Each step in the methodology is described in the following subsections.

### A. Generation of Training Data

The generation of a training set is a critical step and a range of different initial OCs and contingencies were included to generate a representative training set. Dynamic simulations were performed using PSS®E 34.2.0 with its built-in models [24]. The steps of generating the training data are illustrated as a flowchart in Fig. 4 and can be summarized as follows:

*1) Initial OCs:* For the Nordic32 system, the initial OCs were randomly generated around the stable operation point denoted as "operating point B" in [23]. A large number of possible OCs were simulated by randomly initiating the loads from a uniform distribution around the base case load levels (80 % of the original load as a lower limit and 120 % as an upper limit), while the power factor of the loads was kept constant. The total load change was distributed among the generators based on a weighted random distribution, where a higher rated capacity of a generator results in a higher probability to cover a larger share of the total load change. All generation that could not be supplied by the regular generators were distributed to the slack bus generator g20, see Fig. 3.

In real applications, more delicate methods for efficient database generation and more careful generation of relevant OCs should be used [3], [25], where for instance the impact of unit commitment and topology changes are taken into account.

*2) Solve and Check for Feasibility:* The generated OCs were solved with a power flow simulator, which served as a starting point for the dynamical simulation. If the system load flow did not converge, the initial OC was re-initialized.

*3) Start Dynamic Simulation and Introduce Contingencies:* Two separate dynamic simulations were then initiated for the $N$-1 and the $N$-1-1 cases. The process is illustrated in Fig. 5. For each of the two cases, the system runs without any contingencies

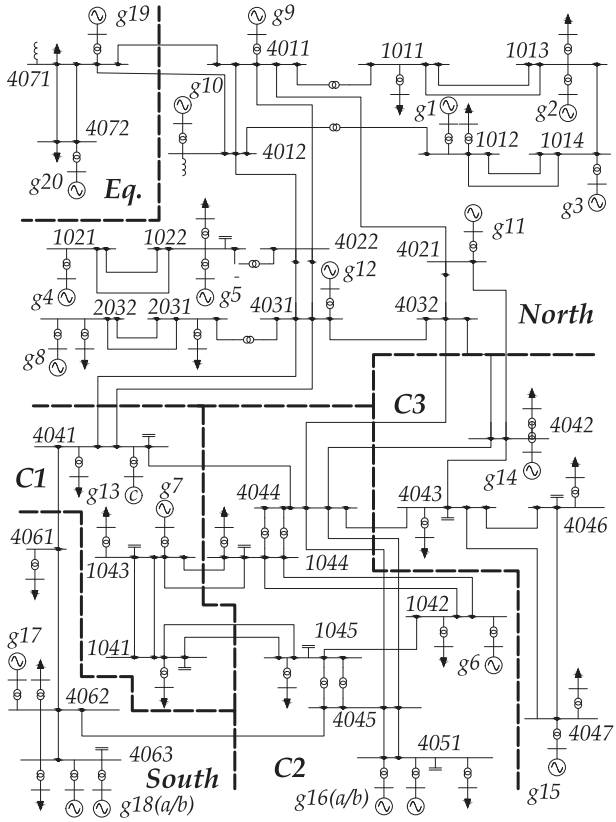


Fig. 3. One-line diagram of the modified Nordic32 system with subareas.

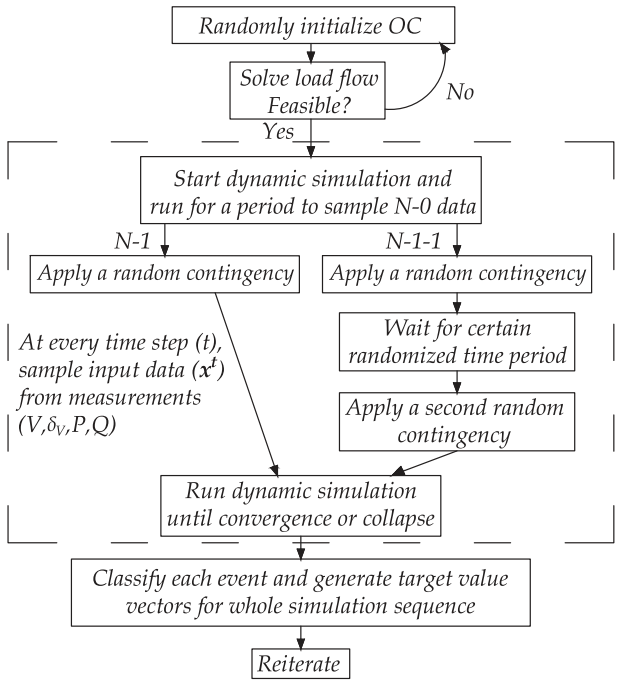


Fig. 4. Flowchart for generating input data and target values.

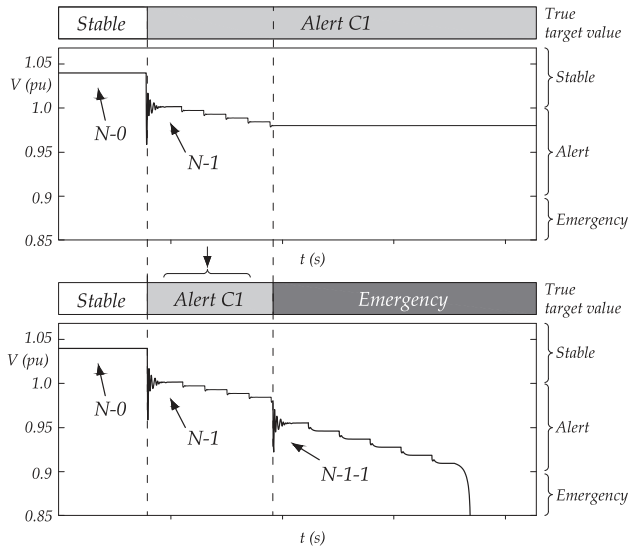


Fig. 5. Example of classification of an $N$-1 and an $N$-1-1 case.

for 65 seconds to generate a sufficient amount of $N$-0 data for the network to train on. At $t = 66$ seconds, the *same* first contingency was applied to both of the cases. After an additional uniformly distributed random time in $[10 - 30]$ seconds after the first contingency, a secondary consecutive contingency was applied for the $N$-1-1 cases. Events resulting in several (near-)simultaneous contingencies were not taken into account ($N$-$k$ events).

The considered contingencies in the simulations were either (i) tripping of a generator, or (ii) a three-phased fault during 0.1 seconds, followed by tripping the faulted line, which was then kept tripped during the remaining time of the simulation. The first contingency was chosen to be a major fault, meaning a fault on any transmission line connecting the different main areas in the system (excluding the "Eq." area, see Fig. 3), *or* any larger thermal generator in the "Central" area. The second contingency, for the $N$-1-1 cases, included tripping of *any* transmission line in the whole system, excluding lines in the "Eq." area. No variations of load and generation were taken into account during the dynamic simulations as these, in the relatively short time of the simulations, are presumed to have a small impact on the system stability.

*4) Sample Inputs and Run Until Stopping Criteria:* For each of the two cases, an input vector $\boldsymbol{x}^t$ consisting of measurements of all bus voltage magnitudes ($V_{mag}$) and angles ($V_\theta$), active and reactive power flows ($P_{flow}$, $Q_{flow}$), were sampled every second ($\Delta t = 1\,s$) and saved in a data file. No information regarding the type and location of applied the contingencies were sampled, as this information implicitly can be learned by the LSTM network. For instance, the LSTM network should be able to correlate a zero power flow in a transmission line with that line being out of service.

Each dynamic simulation ran for a total of 560 seconds, but was, in the case of a major voltage collapse, stopped in advance. The simulation interval of 560 seconds was chosen to allow time for *all* dynamic events to occur and for the system to either fully stabilize or collapse. It should be noted that systems with different dynamics may require longer or shorter simulation times. To reduce the computational burden when generating the training set for a real power system, more intricate methods to

determine whether the system has stabilized can be adopted. For instance, by monitoring the actions of components with slow dynamics, such as load tap changers or excitation limiters of generators, a more efficient way of determining whether the system has been stabilized can be developed. If none of these components has acted in a time frame of the component with the longest activation time, the power system can be assumed to have fully stabilized.

*5) Classification:* For each case, a sequence of true target value vectors $\boldsymbol{y}^1, \ldots, \boldsymbol{y}^{560}$ was generated for every time step in the time-domain simulation. Each $\boldsymbol{y}^t$ in these sequences represents the classification of the system if the system is allowed to run from time $t$ up until 560 seconds without any changes to the current system. As time progresses and new events occur, the class of $\boldsymbol{y}^t$ may change. The sequences consist of multidimensional vectors where the actual class is encoded using one-hot (binary) encoding.

The classification was performed according both to the severity and the location of the system degradation at the *end* of the time-domain simulation. The system was defined as stable if *all* transmission bus voltage magnitudes were above or equal to 1 pu, in an alert state if *any* transmission bus voltage magnitude ranged between $0.9 < V < 1.0$ pu, and in an emergency state if *any* transmission bus voltage magnitude was below 0.9 pu. Overvoltages were not taken into account.

The target values for the *alert* cases were also classified according to *where* the lowest bus voltage magnitudes were found at the end of each dynamic simulation.

The Nordic32 test system is predefined into four different regions, namely: "Eq," "North," "Central," and "South" [23]. The regions "North," "South," and "Eq." were found to be stable regions, and no alert events were found in these regions for any of the simulated cases. To test the capability of the network to also indicate where instability emerges in the system, the "Central" area was divided into three separate regions (indicated by **C1**, **C2**, **C3** in Fig. 3). The classification for each time step of each simulation belonged then to one of 5 different possibilities. Either the whole system was predicted stable; it ended up in an emergency state; or an alert state was predicted in one of the three defined regions (**C1**, **C2**, or **C3**) where the *lowest* occurring transmission bus voltage was found.

The classification process is illustrated in Fig. 5. The target values are always classified as stable up until the first contingency. From different combinations of OCs and contingencies, the system may then end up being in a stable state, an alert state in area **C1**, **C2**, or **C3**, or in an emergency state. For the $N$-1 case, the sequence of true target value vectors from the time of the contingency to the end of the simulation are classified depending on which of these five states the systems end up in. For the example of the $N$-1 case in Fig. 5, the system ends up in an alert state in the **C1** area. For the $N$-1-1 case, the target values are classified as stable up until the first contingency. The target values are then gathered from the $N$-1 case, using the end state of that simulation for classifying the state *between* the first and the consecutive contingency. After the second consecutive contingency, the system runs until it either collapses or until 560 seconds. Depending on this final state, the sequence of true target value vectors from the second contingency until the end of the simulation is classified. In the example in Fig. 5, an emergency state is reached. Note that the scales in Fig. 5 are different from those in the simulations for easier interpretation.

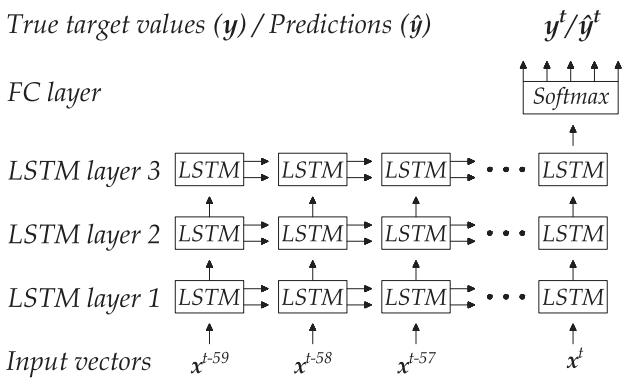


Fig. 6. The proposed LSTM network architecture.

It should be noted that the classification of the different states (stable, alert, emergency) could be performed more intricately to satisfy other criteria of stability. For instance, these could be related to a minimum level of loadability of the system in its post-disturbance state. The loadability limit could then be computed by, for instance, parameterized continuation methods such as the continuation power flow (CPF) method [26], or by certain line indicators [27]. Other stability criteria could include the capability of the system in its post-disturbance state to handle yet another disturbance.

*6) Reiteration:* The described steps are reiterated until a sufficiently large training set is generated.

### *B. Architecture of the LSTM Network*

The proposed LSTM network architecture, shown in Fig. 6, is generally referred to as a "many-to-one" architecture, where previous measurements in the time sequence are used for the classification in the final block. The network consists of three stacked LSTM layers which are used to capture different levels of features from the inputs. Each LSTM block consists of 32 individual LSTM cells. The first layer of LSTM-blocks takes a generated sequence of input vectors as inputs; then by mathematical operation as presented in Section II, the output of each block is forwarded both to the following block in the sequence, as well as to the upper layer of LSTM-blocks. The inputs to the deeper layers consist only of the hidden states of LSTM blocks of previous layers, while both the hidden state and the cell state memory is passed along the time sequence between LSTM blocks of the same layer.

The LSTM network is designed to take sequences of 60 time steps of measurements as inputs. The internal architecture of each LSTM cell and functionality of the nonlinear gating units as presented in Section II, allows the LSTM network to fully utilize and pass forward the information from the first to the final time step in the sequence. The third layer of LSTM-blocks only passes the output forward along the time sequence. The output layer at time $t$ is a fully connected network with softmax

activation for classification. In training, the network uses the true target vector $\boldsymbol{y}^t$ at time $t$, while during the test or prediction phase, the network estimates a prediction vector $\hat{\boldsymbol{y}}^t$ at time $t$. The interpretation of the prediction problem is further explained in Section III-D.

### C. Training the LSTM Network

Different data sets were used for training, validation, and testing of the method on a mix of $N$-1 and $N$-1-1 cases. The training data set has the dimension $(135,000 \times 364 \times 560)$, where the dimension represents the number of training cases, the number of inputs, and the total interval in seconds for each simulation, respectively.

Before training, a process generally referred to as sequence preprocessing was performed to prepare batches of sequences with suitable length. The network is designed to take a sequence of 60 time steps of measurements as inputs and subsequences with a length of 60 time steps $(\boldsymbol{x}^{t-59}, \ldots, \boldsymbol{x}^t)$ were thus extracted from the 560 seconds long simulation intervals, for different values of $t$. For each subsequence of input vectors, a corresponding target value $(\boldsymbol{y}^t)$ at time $t$ was gathered. The sequence preprocessing was performed 120 times for *each* training and validation case by varying $t$ between values of $t = [60, 180]$. The lower bound of $t$ is required to always allow historic data to be included into the sequence. The LSTM network could have been trained on the whole simulation interval by increasing the upper bound of $t$ from 180 to 560. However, since the method is proposed to be used in fast VIP applications, there is less usefulness of predicting instability long after the contingencies have occurred.

The generated subsequences were then used to train the LSTM network. Due to memory limitations, a method called mini-batch gradient descent was utilized where mini-batches of 1000 subsequences were used separately to train the network. The training was performed for a maximum of 500 epochs. An epoch is finished when all generated batches have been used to update the network parameters. Adam [28], an adaptable algorithm suitable for gradient-based optimization of stochastic objective functions was used in training the network. The algorithm used default parameters according to [28], except for the learning rate which was tuned. The loss function on which the optimizer is applied is the categorical cross-entropy function, which is suitable for multi-classification problems. To avoid overfitting the data, two regularization techniques were used during the training. First, early stopping was implemented, and the training of the network was stopped in case the performance on the validation set did not improve after six epochs. Second, a technique called dropout was applied, where a certain percentage of the connections between inputs and the LSTM cells were randomly masked (or "dropped") to reduce overfitting on the data. Both conventional dropout and recurrent dropout between consecutive blocks were applied during the training phase.

All other parameters related to the training of the network are presented in Table I. The LSTM network was trained and implemented in Python, using the Keras library with TensorFlow backend. The architecture and parameters used to train the network have been iteratively tuned to increase the classification accuracy. It should be noted that the tuning could be extended even further to allow an even better classification accuracy.

TABLE I
DESIGN AND HYPERPARAMETERS USED IN TRAINING

| | Parameter | Values and size |
|---|---|---|
| *Data* | Simulation interval | 560 |
| | Input dimension | 364 |
| | Input data type | $V_{mag}$, $V_\theta$, $P_{flow}$, $Q_{flow}$ |
| | Target classes | 5 |
| | Training cases ($N$-1+$N$-1-1) | 45,000 + 90,000 |
| | Validation cases ($N$-1/$N$-1-1) | 5,000 / 10,000 |
| | Test cases ($N$-1/$N$-1-1) | 10,000 / 10,000 |
| *Architecture* | LSTM layers | 3 |
| | LSTM sequence length | 60 |
| | FC activation function | Softmax |
| | LSTM hidden cells | 32 |
| | LSTM Activation function | Tanh |
| *Training* | Max Epochs | 500 |
| | Learning rate ($\alpha$) | 0.0001 |
| | Dropout & recurrent dropout | 50 % / 50 % |
| | Optimizer | Adam [28] |
| | Loss metric | Categorical cross-entropy |

### D. Interpretation and Intuition of the VIP Problem

By the proposed training and architecture of the LSTM network, a classification problem is solved where the *current* system state space is separated into different regions. Every state on a trajectory to a stable, alert (in **C1**, **C2**, or **C3**), or emergency state is labeled accordingly. The LSTM network is then trained on this data to implicitly learn these asymptotic properties of solutions and the trajectories of the system state. Once trained, the network can correlate the inputs, current and historic measurements, with a certain state-space region and trajectory, allowing warnings of voltage instability only moments after a contingency have occurred in a system. The classification is performed under the assumption that the current system is unchanged, meaning that no additional contingencies or changes in generation and load configuration will occur. However, as time progresses, new observations are used as inputs to the LSTM network to continuously update and incorporate such changes in the system.

This VIP problem should be interpreted as a fixed horizon prediction problem, where the prediction horizon always is the final state given by the trajectories of the (dynamical) system. This interpretation assumes that the simulation horizon of the generated time-domain simulations are sufficiently long so that extending the simulation horizon even further, for this particular system beyond 560 seconds, would not change the partitioning of the state space.

## IV. RESULTS AND DISCUSSION

### A. Test Results

The developed VIP methodology was tested on two separate test sets, one containing only $N$-1 cases, the other containing $N$-1-1 cases. Each test set was composed of 10,000 cases of dynamic simulations. The test results of the predictions are

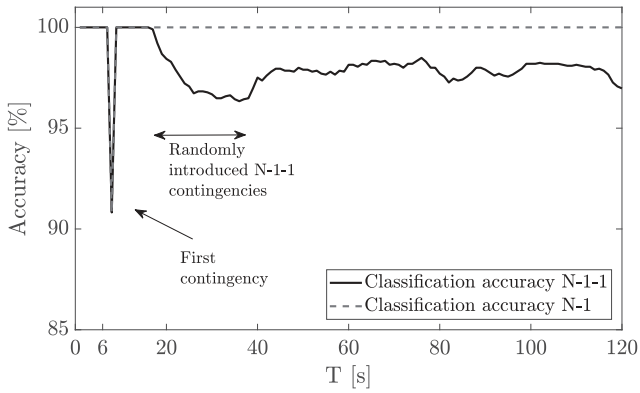


Fig. 7. Classification accuracy over time for the proposed LSTM network.

presented using categorical accuracy, where the *indices* of the true target values are compared to the argument maxima of the predictions. The accuracy at *each* time step is then calculated over time for each of the two test sets.

The data were fed into the network in the form of a rolling window, with subsequences generated in the same manner as described in Section III-C. As time $t$ progresses, new measurements entered the network from the rightmost block in the input layer and were shifted to the left in each time increment. Since the LSTM network require a sequence of 60 time steps of data, no predictions were made before $t = 60$. To facilitate the presentation in the following figures, a new time index $T$ is introduced here. The relationship between the two time-indices is $T = t - 60$. The LSTM network's performance for VIP is not only tested during the short JAD state but during a longer period of the dynamic trajectory the system takes following the disturbances. This is performed to test the network's capability to incorporate new observations and improving its assessment as time progresses throughout a voltage instability event. The classification accuracy is only plotted for 120 seconds after $T$ to better visualize the changes in accuracy after the contingencies.

The classification accuracy *over time* is presented in Fig. 7. The classification accuracy for the $N$-1 test set dropped significantly at $T = 6$ seconds, which is the same instant that the first contingency is applied. The large drop in classification accuracy can be attributed to low bus voltages instantaneously following the first contingency, which the LSTM network has learned to correlate to a voltage instability event. After the first contingency, the classification accuracy increased and remained constant at 100 % for the rest of the simulations.

The classification accuracy for the $N$-1-1 test set was identical up until the time when the consecutive contingencies were randomly applied. During this time, illustrated by the arrows in Fig. 7, the classification accuracy decreased slightly. Since these contingencies do not occur at the same time instant in each test case, the same instant drop in accuracy as for the $N$-1 cases was not seen. The accuracy then gradually increased and stabilized at around 97-98%.

The results show that the LSTM network can classify and predict future stability almost perfectly for the N-1 contingency cases and with good accuracy for the N-1-1 cases. To examine which cases were misclassified, the prediction accuracy for the two test sets, evaluated at $T = 50$ seconds, are presented in Table II in the form of a confusion table. Each number in the column in the table represents instances of the predicted classes and each number in the row represents the instances of the actual classes. The (empirical) conditional probabilities of correctly classifying a certain state is presented in the column furthest to the right. Similarly, the conditional probability of a state *actually* belonging to the predicted state is presented in the bottom row of the table. The total accuracy is presented in the lower right corner of the table. The accuracy for all $N$-1 cases is 100 % and no cases are falsely classified. For the $N$-1-1 test set, the lowest classification accuracy occurred for the alert states. After inspection of the falsely classified cases, it was found that several of these were borderline cases where the transmission bus voltage magnitude used in the classification were very close to what was used in the other classes. The highest classification accuracy occurred for the emergency cases with 99.8%.

It should be noted that the test and training sets were weighted with more cases ending up in certain classes than others. It is thus probable that the results are slightly biased with higher accuracy for these classes, and that the classification accuracy of the other classes may be lower as an effect.

### B. Impact of Sequence Length

In this section, the performance of the sequence-based approach is tested and compared against a conventional feedforward NN, which only uses a single snapshot of measurements as inputs. Further, to test the impact of a *shorter* time sequence, the results of an LSTM network using a time sequence of 30 time steps, instead of 60, are presented.

To allow a fair comparison between the two approaches, the feedforward NN used in this comparison was designed to be as similar as possible to the LSTM network. Essentially, the design of the NN in the comparison is identical to the *final* time step in the LSTM network presented in Fig. 6, with the difference that each layer consists of a hidden layer of neurons. The designed NN has thus three hidden unit layers, each layer with 32 hidden nodes. The same FC layer with a softmax activation function was used. The training for the NN was performed identically as for the LSTM network, with the exception that instead of a sequence of input values, a single snapshot was used. The LSTM network using a shorter time sequence was trained identically to that of the longer LSTM network with the exception that a shorter sequence of 30 instead of 60 time steps was used.

In Fig. 8, the classification accuracy on the $N$-1-1 test set is presented for the two LSTM networks with the different time sequence length and for the conventional NN. The classification accuracy for the conventional NN was around 93% after all the consecutive contingencies had been applied, while that of the proposed LSTM network is around 97-98%. The results show that the performance of the LSTM network using 60 time steps in the sequence significantly exceeded that of the conventional NN, generally providing better classification accuracy over the whole time frame of the simulation cases.

The classification accuracy of the LSTM network using a shorter sequence was similar to the one using a longer sequence, with the difference of a large drop in classification accuracy

TABLE II
CONFUSION TABLE SHOWING PREDICTION RESULTS AND ACCURACY OF THE LSTM NETWORK EVALUATED AT $T = 50$ SECONDS

| | | | *Predicted states ($N$-1 / $N$-1-1)* | | | | | |
|---|---|---|---|---|---|---|---|---|
| | | | **Stable state** | | **Alert state** | | **Emergency state** | **Accuracy** |
| | **Classification** | | All areas | C1 | C2 | C3 | All areas | |
| *Actual states* | **Stable state** | All areas | 2766 / 1147 | 0 / 36 | 0 / 11 | 0 / 8 | 0 / 8 | 100 / 94.8 % |
| | **Alert state** | C1 | 0 / 0 | 856 / 562 | 0 / 3 | 0 / 0 | 0 / 5 | 100 / 98.6 % |
| | | C2 | 0 / 5 | 0 / 5 | 1874 / 1222 | 0 / 0 | 0 / 109 | 100 / 91.1 % |
| | | C3 | 0 / 0 | 0 / 0 | 0 / 12 | 0 / 208 | 0 / 0 | - / 94.5 % |
| | **Emergency state** | All areas | 0 / 0 | 0 / 0 | 0 / 10 | 0 / 0 | 4504 / 6649 | 100 / 99.8 % |
| | **Accuracy** | | 100 / 99.6 % | 100 / 93.2 % | 100 / 97.1 % | - / 96.3 % | 100 / 98.2 % | **100 / 97.9 %** |

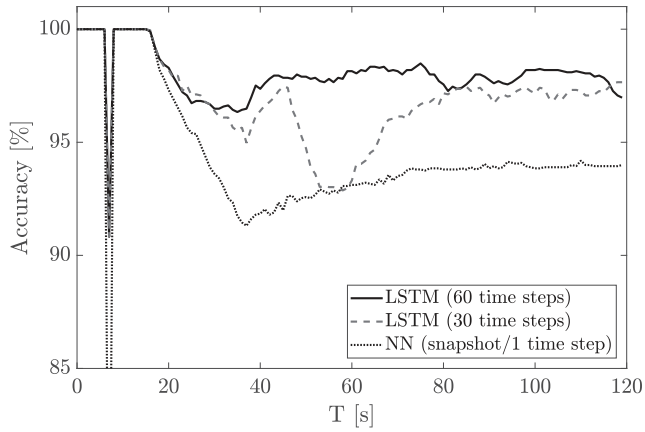


Fig. 8. Impact of sequence length on classification accuracy.

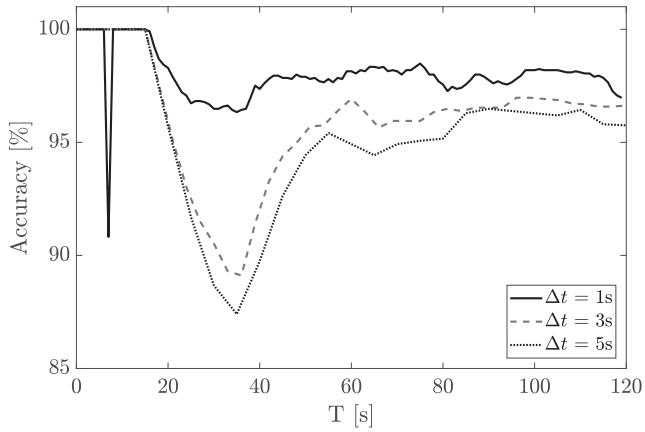


Fig. 9. Classification accuracy over time for different values of $\Delta t$.

occurring at around $T = 46$ seconds, see Fig. 8. The accuracy declined for 20 seconds and was then restored to around 97% accuracy. A similar decline in classification accuracy, though less significant, can be noted for the LSTM network using the longer time sequence at $T = 76$. Thus, a decline in classification accuracy started exactly 60 respectively 30 seconds after the consecutive contingencies were introduced (at $T = 16$) for the two networks, corresponding to the network's respective sequence length. One explanation of these results is that the LSTM networks utilize information concerning the contingency and *pre-contingency* state to enhance the classification accuracy. When the networks starts to lose the information about the pre-contingency state, the chance of a misclassification increases. The results strengthen the hypothesis that a long sequence LSTM network could be used to enhance the state signal to provide better classification accuracy. Theoretically, an even longer sequence could be used to increase the accuracy even further. However, this would increase the computational cost of training, and a balance between classification accuracy and computational cost should be sought.

### C. Impact of Measurement Update Rate

The performance of the LSTM network is in this section tested for different values of the measurement update rate. The performance is compared between the previously assumed available measurement update rate of $\Delta t = 1\ s$ and the slower update rates of $\Delta t = 3\ s$ and $\Delta t = 5\ s$. Due to the slower update rates, the architecture and the number of LSTM blocks along the time sequence had to be reduced accordingly. The original LSTM network was designed to take subsequences of 60 time steps of measurements as inputs. Thus, for the LSTM network adapted for $\Delta t = 3\ s$, the number of LSTM blocks along the time sequence was reduced to a third (20 blocks along the time sequence), while the number of blocks for the LSTM network adapted for $\Delta t = 5\ s$ was reduced to a fifth (12 blocks along the time sequence). The LSTM networks adapted for the new measurement update rates were then trained identically to the original LSTM network, with the difference that now only every third, respectively fifth, measurement in each generated subsequence were passed on the networks.

The classification accuracy for the different values of $\Delta t$ is presented in Fig. 9 using the same $N$-1-1 test set as in previous sections. The results show that the performance when using a measurement update rate of $\Delta t = 1\ s$ exceeds those using a slower update rate. The largest difference can be identified during the period when the second consecutive contingencies are applied, which indicates that a lower value of $\Delta t$ is especially valuable for classification during the short time that follows a disturbance. It should be noted that due to the slower update rates of $\Delta t$, there is no dip in the classification accuracy following the first contingency.

TABLE III
AVERAGE TIME TO PREDICT THE ONSET OF VOLTAGE INSTABILITY

| | *Measurement update rates* | | |
|---|---|---|---|
| | $\Delta t = 1s$ | $\Delta t = 3s$ | $\Delta t = 5s$ |
| Average prediction time [s] | 6.6 | 8.7 | 10.7 |

A larger value of $\Delta t$ may also increase the *time* it takes to accurately predict instability, as new measurements are being passed less frequently to the LSTM network. In Table III, the average time, after a contingency, to accurately predict the future state of the system is presented for the different values of $\Delta t$. The average time is only presented for the time it takes to correctly classify the system states following the *second* consecutive contingency, since correct classification following the first contingency was almost instantaneous in all test cases. The time was computed as the averaged passed time after the second contingency, up until the time when the LSTM network could consistently and accurately predict the state of the system. For cases that took *longer* time than 100 seconds to be correctly classified, a detection time of 100 seconds was assumed to avoid skewed averaged values.

The average time to correctly predict the system state was found to be 6.6 seconds for the proposed LSTM architecture using a measurement update rate of $\Delta t = 1\ s$. The corresponding values for the LSTM networks using the slower update rates of $\Delta t = 3\ s$ and $\Delta t = 5\ s$, were 8.7 seconds and 10.7 seconds, respectively. The longer time longer time to accurately predict instability for the slower update rates of $\Delta t$ can be attributed partly to a lower classification accuracy, and partly to the fact that measurements are being updated less frequently.

### D. Generalization Capability and Training Set Requirement

The generalization capability of a ML method refers to the capability to generalize the learning from the actual training set to other, yet unseen, cases. Such capability is especially valuable in overcoming the combinatorial increase of complexity in the training when $N$-1-1 cases are also considered [29].

In Fig. 10, the classification accuracy is presented on the $N$-1-1 test set when the LSTM network have been trained on three different training sets. The results are presented when the network was trained on i) the full training set with all $N$-1 and $N$-1-1 cases included, ii) a smaller training set with all $N$-1 cases but where only a small batch (5,000) of $N$-1-1 cases have been included, and iii) a training set where the network is *only* trained on $N$-1. The same training approach as previously described were used. According to Fig. 10, the classification accuracy was significantly reduced when no $N$-1-1 cases are included in the test set. When including the small batch (5,000) of $N$-1-1 cases, the classification accuracy increased significantly. However, the accuracy is still lower than when the full training set is used. Thus, the importance of obtaining a representative training set is still imperative if a high classification accuracy is to be achieved.

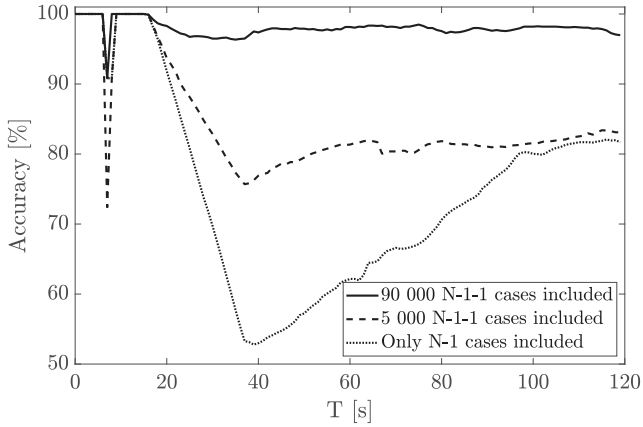


Fig. 10. Classification accuracy over time when varying the number of $N$-1-1 cases included in the training data.

### E. Practical Applications and Requirements

The method is proposed to be used as an online tool for system operators to monitor the current state of a power system. It should be stressed that the method is not proposed to replace conventional voltage instability detection methods, but rather function as a supplementary tool to provide early warnings. The instantaneous prediction capability of the proposed method has to be weighed against the possibility of misclassification of the system's future stability. When comparing the proposed method to other conventional indicators for voltage instability detection (see [2]), it is important to remember that these might be more accurate once instability detected, but generally take *significantly* longer time to indicate instability, thus reducing the time frame that system operators have to steer the system back into stable operation.

The proposed method is mainly intended for predicting mid-term or long-term voltage instability where system operators will have the possibility to act on the warnings provided by the network. Theoretically, the method could be adapted to also handle short-term voltage instability. However, this would require more frequent measurement updates to ensure that the onset of short-term instability is detected in time. Because of the difference in the dynamical trajectories of the system for the two different types of instability events, training a separate LSTM network would likely provide better performance. Furthermore, the signals provided by the network would have to automatically trigger emergency controls, since the available time for system operators to act on the signals would be too short for manual control actions.

For the proposed method to be effective in long-term voltage instability, measurement updates should be available within a few seconds. In this paper, a measurement update rate each second have been assumed to be available. As was found in Section IV-C, slower measurement update rates lead both to lower classification accuracy and slower predictions. To assure that errors and missing values are filtered out, measurements should always be preceded by a state estimator. However, state estimates from a non-linear state estimator based on remote terminal units

may be too slow to be effective. Thus, time-synchronized measurements from wide-area phasor measurements filtered through a linear state estimator would be preferred.

The softmax classifier of the LSTM network outputs a probability vector, where each class is given a certain probability. It should be noted that this probability vector does not provide a *true* representation of the model confidence. However, it can still be useful as a proxy by system operators to track the network's confidence in each prediction. Thus, the operator can use the probability vector directly in an online interface to track the network's belief in each prediction. Alternatively, argument maxima or other functions could be used to present the most probable prediction of the network, or, for instance, to avoid predictions of falsely labeled stable states.

The *practical* classification accuracy of the proposed method will be affected by many aspects and will generally be lower than on a simulated test set. One of the more important aspects are modeling errors, including erroneous system parameters or inaccurate modeling of parameter values for dynamic models. Such aspects will introduce a difference between the simulated and the actual dynamic response after a contingency. However, it should be noted that such limitations are not limited only to ML based approaches for VIP. All methods for DSA require that the dynamic models used in assessing the system response are accurately modeled.

High penetration of variable generation may also impact the proposed ML methodology; primarily by increasing the combinatorial difficulty in generating a representative training set. To reduce the dimensionality of the state space that the power system can operate in, it is thus required that smaller variable generation units can be merged and modelled as equivalent units. Such simplifications are already to an extent required in the modelling of large power systems, where underlying distribution grids are often reduced to single load buses. However, it is important to verify that such simplifications of the simulation models do not affect the dynamical trajectories the system can take under the different contingency scenarios.

## V. Conclusion and Future Work

This paper presents a new approach for online voltage instability prediction using an LSTM network capable of utilizing a sequence of measurements to improve classification accuracy. Once trained, the LSTM network can allow system operators to continuously assess and predict whether the present system state is stable, or will evolve into an alert or an emergency state in the near future. The network is also adapted to be able to indicate *where* instability emerges, allowing system operators to perform more cost-effective control measures.

The LSTM network was proposed to improve the available state signal by implicitly learning the dynamical trajectories of a power system following a disturbance. The LSTM architecture and the operation of the gating units ensure that the network is capable of capturing the long-term dependencies that are common in voltage instability events. The results presented in the paper are highly encouraging and the proposed method is shown to have high accuracy in predicting voltage instability only seconds after a disturbance.

The impact of sequence length of the LSTM network was tested and showed that a longer sequence provided a significantly better classification capability than both a feedforward NN and a network using a shorter sequence. The paper also examined the generalization capability of the proposed LSTM network, where the classification accuracy on $N$-1-1 cases was assessed when the system was only trained on $N$-1 cases. It was found that this reduced the classification accuracy significantly, whereas including a smaller subset of $N$-1-1 cases into the training set resulted in significantly better performance.

Future research work includes examining the impact that emergency control have on the prediction accuracy of the method. Although emergency control will generally be activated too slowly to affect the system in the time frame it takes for the LSTM-network to predict instability, it will affect the following predictions after the control actions have been issued. If such control aspects are included in the training scenarios, the LSTM network could also be used to assess whether the emergency actions indeed succeeded in restoring the system to a stable state again, or if further actions would be required. Moreover, further studies are required in examining how the generalization capability of the LSTM network can be improved. Methods to also evaluate the accuracy of the predictions, such as providing a confidence estimate of the predictions, would also be valuable to ensure the robustness of the method.

## References

[1] P. Kundur *et al.*, "Definition and classification of power system stability IEEE/CIGRE joint task force on stability terms and definitions," *IEEE Trans. Power Syst.*, vol. 19, no. 3, pp. 1387–1401, Aug. 2004.

[2] M. Glavic and T. Van Cutsem, "A short survey of methods for voltage instability detection," in *Proc. IEEE PES Gen. Meet.*, Detroit, MI, USA, Jul. 2011, pp. 1–8.

[3] I. Konstantelos *et al.*, "Implementation of a massively parallel dynamic security assessment platform for large-scale grids," *IEEE Trans. Smart Grid*, vol. 8, no. 3, pp. 1417–1426, May 2017.

[4] T. Van Cutsem *et al.*, "Decision tree approaches to voltage security assessment," *IEE Proc. C - Gener., Transmiss. Distrib.*, vol. 140, no. 3, pp. 189–198, May 1993.

[5] Y. Mansour, A. Y. Chang, J. Tamby, E. Vaahedi, B. R. Corns, and M. A. El-Sharkawi, "Large scale dynamic security screening and ranking using neural networks," *IEEE Trans. Power Syst.*, vol. 12, no. 2, pp. 954–960, May 1997.

[6] K. Sun, S. Likhate, V. Vittal, V. S. Kolluri, and S. Mandal, "An online dynamic security assessment scheme using phasor measurements and decision trees," *IEEE Trans. Power Syst.*, vol. 22, no. 4, pp. 1935–1943, Nov. 2007.

[7] H. Khoshkhoo and S. M. Shahrtash, "Fast online dynamic voltage instability prediction and voltage stability classification," *IET Gener., Transmis. Distrib.*, vol. 8, no. 5, pp. 957–965, May 2014.

[8] C. Liu, F. Tang, and C. L. Bak, "An accurate online dynamic security assessment scheme based on random forest," *Energies*, vol. 11, no. 7, 2018.

[9] C. Vournas and T. Van Cutsem, "Online voltage security assessment," in *Real-Time Stability in Power Systems - Techniques for Early Detection of the Risk of Blackout*. Berlin, Germany: Springer, Jul. 2014, ch. 10, pp. 305–333.

[10] R. F. Nuqui, "State estimation and voltage security monitoring using synchronized phasor measurements," Ph.D. dissertation, Virginia Tech, Blacksburg, VA, USA, 2001.

[11] R. Diao *et al.*, "Decision tree-based online voltage security assessment using PMU measurements," *IEEE Trans. Power Syst.*, vol. 24, no. 2, pp. 832–839, May 2009.

[12] H. Khoshkhoo and S. M. Shahrtash, "On-line dynamic voltage instability prediction based on decision tree supported by a wide-area measurement system," *IET Gener., Transmiss. Distrib.*, vol. 6, no. 11, pp. 1143–1152, Nov. 2012.
[13] H. Nguyen Duc *et al.*, "A novel approach for early detection of impending voltage collapse events based on the support vector machine," *Int. Trans. Elect. Energy Syst.*, vol. 27, no. 9, 2017, Art. no. e2375.
[14] M. L. Scala, M. Trovato, and F. Torelli, "A neural network-based method for voltage security monitoring," *IEEE Trans. Power Syst.*, vol. 11, no. 3, pp. 1332–1341, Aug. 1996.
[15] H. Hagmar, L. A. Tuan, O. Carlsot, and R. Eriksson, "On-line voltage instability prediction using an artificial neural network," in *Proc. IEEE Milan PowerTech*, Jun. 2019, pp. 1–6.
[16] R. S. Sutton and A. G. Barto, *Reinforcement Learning: An Introduction*. Cambridge, MA, USA: MIT Press, 2015.
[17] P. Geurts and L. Wehenkel, "Early prediction of electric power system blackouts by temporal machine learning," in *Proc. ICML98/AAAI98 Workshop Predicting Future: AI Approaches Ser. Anal."*, 1998, pp. 24–26.
[18] L. Wehenkel *et al.*, "Probabilistic design of power-system special stability controls," *Control Eng. Pract.*, vol. 7, no. 2, pp. 183–194, 1999.
[19] P. Geurts and L. Wehenkel, "Temporal machine learning for switching control," in *Proc. Eur. Conf. Principles. Data. Mining. Knowl. Discovery.*, 2000, pp. 401–408.
[20] K. Greff, R. K. Srivastava, J. Koutník, B. R. Steunebrink, and J. Schmidhuber, "LSTM: A search space odyssey," *IEEE Trans. Neural Netw. Learn. Syst.*, vol. 28, no. 10, pp. 2222–2232, Oct. 2017.
[21] D. E. Rumelhart, G. E. Hinton, and R. J. Williams, "Learning representations by back-propagating errors," *Nature*, vol. 323, no. 6088, pp. 533–536, 1986.
[22] S. Hochreiter and J. Schmidhuber, "Long short-term memory," *Neural Comput.*, vol. 9, pp. 1735–80, Dec. 1997.
[23] T. Van Cutsem *et al.*, "Test systems for voltage stability analysis and security assessment," IEEE/PES Task Force, Tech. Rep. PES-TR19, Aug. 2015. [Online]. Available: http://resourcecenter.ieee-pes.org/pes/product/technical-publications/P ESTR19
[24] PSS®E 34.2.0 Model Library, Siemens Power Technologies International, Schenectady, NY, USA, Apr. 2017.
[25] F. Thams, A. Venzke, R. Eriksson, and S. Chatzivasileiadis, "Efficient database generation for data-driven security assessment of power systems," *IEEE Trans. Power Syst.*, vol. 35, no. 1, pp. 30–41, Jan. 2020.
[26] V. Ajjarapu and C. Christy, "The continuation power flow: A tool for steady state voltage stability analysis," *IEEE Trans. Power Syst.*, vol. 7, no. 1, pp. 416–423, Feb. 1992.
[27] S. Yari and H. Khoshkhoo, "A comprehensive assessment to propose an improved line stability index," *Int. Trans. Elect. Energy Syst.*, vol. 29, no. 4, 2019, Art. no. e2806.
[28] D. P. Kingma and J. Ba, "Adam: A method for stochastic optimization," 2014, *arXiv:1412.6980*.
[29] P. Mitra, V. Vittal, B. Keel, and J. Mistry, "A systematic approach to $n$-1-1 analysis for power system security assessment," *IEEE Power Energy Technol. Syst. J.*, vol. 3, no. 2, pp. 71–80, Jun. 2016.

**Hannes Hagmar** (Student Member, IEEE) received the M.Sc. degree in electric power engineering from the Chalmers University of Technology, Gothenburg, Sweden in 2016. Between 2016 to 2017, he worked at RISE Research Institutes of Sweden with research in electric transmission systems and measurement technology. He is currently pursuing the Ph.D. degree at the Chalmers University of Technology. His research interest includes power system dynamics and stability, integration of renewables, and machine learning.

**Lang Tong** (Fellow, IEEE) is the Irwin and Joan Jacobs Professor of engineering at Cornell University and the Cornell Site Director of Power Systems Engineering Research Center (PSERC). He received the B.E. degree from Tsinghua University and the Ph.D. degree in electrical engineering from the University of Notre Dame. He was a Postdoctoral Research Affiliate at the Information Systems Laboratory, Stanford University held visiting positions at Stanford University, the University of California at Berkeley, the Delft University of Technology, and the Chalmers University of Technology in Sweden. Lang Tong's current research focuses on optimization, machine learning, AI, and economic problems in energy and power systems. He received several IEEE society transaction prize papers and conference best paper awards. He was a Distinguished Lecturer of the IEEE Signal Processing Society and the 2018 Fulbright Distinguished Chair in Alternative Energy.

**Robert Eriksson** (Senior Member, IEEE) received the M.Sc. and Ph.D. degrees in electrical engineering from the KTH Royal Institute of Technology, Stockholm, Sweden, in 2005 and 2011, respectively. He held an Associate Professor position at the Center for Electric Power and Energy, DTU Technical University of Denmark, from 2013 to 2015. He is currently with the Swedish National Grid, Department of Markets and System Development. His current research interests include power system dynamics and stability, automatic control, HVDC systems, and DC grids.

**Le Anh Tuan** (Member, IEEE) received the M.Sc. degree in energy economics from the Asian Institute of Technology, Bangkok, Thailand, in 1997, and the Ph.D. degree in power systems from the Chalmers University of Technology, Gothenburg, Sweden, in 2004. He is currently a Senior Lecturer with the Division of Electric Power Engineering, Department of Energy and Environment, Chalmers University of Technology. His current research interests include power system operation and planning, power market and deregulation issues, grid integration of renewable energy, and plug-in electric vehicles.

# On-line Voltage Instability Prediction using an Artificial Neural Network

Hannes Hagmar, Le Anh Tuan, Ola Carlson
*Department of Electrical Engineering*
*Chalmers University of Technology*
Gothenburg, Sweden
hannes.hagmar@chalmers.se

Robert Eriksson
*Market and System Development*
*Svenska Kraftnät*
Sundbyberg, Sweden
robert.eriksson@svk.se

***Abstract*—In this paper, a predictive method to detect voltage instability using an artificial neural network is presented. The proposed method allows transmission system operators to predict long-term voltage instability far before the system voltage stability has been degraded, allowing swift and cost-effective control actions. The predictor is tested and trained on the Nordic32 test system for a wide range of different contingencies. The predictor proves to be accurate in providing early warnings of impending voltage instability, allowing 96.3 % of all test cases being correctly classified only seconds after a contingency. The method is proposed to be used as an effective tool for supplementary voltage instability detection for transmission system operators.**

***Index Terms*—Voltage instability prediction, artificial neural networks, voltage stability, synchronized phasor measurements, emergency control**

## I. Introduction

Ensuring and maintaining voltage stability are challenges that transmission system operators (TSOs) continuously face in their daily activities. The ability for TSOs to act quickly and with the correct control measures is imperative during an event causing voltage instability. Due to equipment in electric power systems, such as overexcitation limiters (OELs), load tap changing transformers (LTCs), and other load restoration dynamics, the time frame of a typical voltage collapse can range from a few seconds up to even a couple of minutes [1].

In the literature, there has been a significant development of different kinds of voltage stability indices (VSIs) suitable for real time assessment [2]. In general, VSIs aimed for *preventive applications* calculate stability margins and precontingency security limits ensuring that the system can handle a credible set of contingencies, thus meeting the N-1 stability criterion [2]. VSIs aimed for *corrective applications* are instead used for voltage instability detection (VID) and they are intended to be used when a contingency has occurred or if the system has drifted close to the instability region, allowing TSOs to as soon as possible detect an impending voltage collapse.

Machine learning (ML) has for several years been proposed to be used in the field of voltage stability assessment. One of the major advantages of using ML in voltage stability assessment is that high effort computations and training of the algorithm can be performed off-line, allowing almost instantaneous estimations once the algorithm is trained. In for example [3] and [4], ML algorithms are used to allow accurate estimation of the N-1 voltage stability margins in real-time. Using conventional methods for estimating voltage stability margins will require a high computational effort, resulting in the estimations not being possible to perform in real-time. In an other paper [5], ML techniques are used for VID, where accurate although more time consuming VSIs can be computed in real-time, allowing more accurate detection of voltage instability than using other more simplified VSIs.

In case the preventive VSIs fails, or larger contingencies in the system occurs, the TSOs have to rely on corrective VSIs. For most corrective VSIs presented in the literature, the aim is to, as soon as possible, detect *when* the system has become unstable. However, when instability is detected, the system is often already severely degraded and the time until a voltage collapse may be either too short for TSOs to act, or the related costs with controlling the system back into stable operation may have significantly increased.

The evolution of a typical bus voltage at a transmission bus is illustrated in Fig. 1 for different severity of contingencies. For the case leading to a system collapse, the voltage instability is gradually developed, driven by components such as LTCs and OELs. At some point, the mechanism of load power restoration has caused the system to deteriorate to such a point that the total total power consumed in the system is reduced instead of restored [1]. Thus, Fig. 1 illustrates the problem of VID: that when the system stability has started to degrade, it evolves quickly and the time for TSOs to react and control the system back into stable operation is highly limited.

The most optimal VID method should allow prediction of voltage instability instantaneously after a contingency has occurred. That would allow TSOs to, directly after a contingency, get a notification whether the system is under too large stress and allow quick and effective control responses to steer the system back into stable operation. An early prediction method based on that approach was presented in [6], where a decision tree (DT) approach was used to predict unstable situations, just after a disturbance. The decision tree approach has been further developed in several papers, such as in [7]–[9].

However, despite the fact DTs are both intuitive and easily interpreted, the accuracy is generally not the highest of all ML algorithms. Artificial neural networks (ANNs) are not new in VIP [10]–[12], but their advantages have been reduced by large

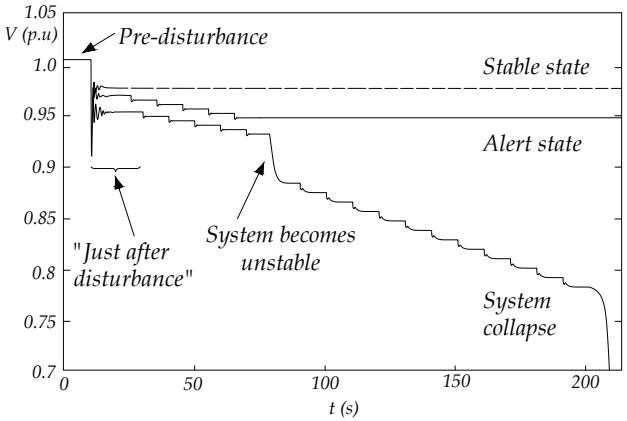


Fig. 1. Evolution of a voltage collapse for different contingencies

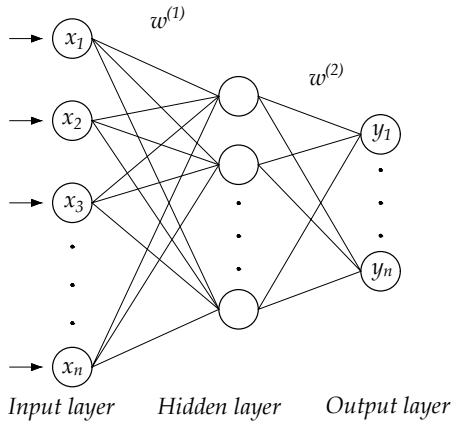


Fig. 2. Architecture of an ANN with a single layer of hidden neurons

requirements of training data. Due to the rapid development of computational power, the popularity of using ANNs in various applications has increased significantly in the last decade [13]. Although generally requiring more training data, they should theoretically allow more accurate modeling of arbitrary non-linear functions, resulting in a higher accuracy of the classification, provided that sufficient data is available.

This paper develops a new approach of voltage instability prediction using a single hidden layer feedforward ANN. The method, in this paper denoted as the on-line voltage instability prediction method (O-VIP), will allow TSOs to not only predict voltage instability, but also to pinpoint *where* the weakest areas in the system are located, allowing local and more cost-effective control measures. Further, the paper suggests suitable parameters and input data for the architecture and training of the ANN, and provides a procedure to generate the training data using the dynamic simulations.

The paper is organized as follows. In Section II, the proposed method is presented along with the relevant theory and the steps of developing the training data and the training of the ANN. In Section III, the results of the method is presented. Section IV discusses possible applications and practical aspects, while concluding remarks are presented in section V.

## II. Method for on-line predictive voltage instability detection

The O-VIP is based on performing off-line training of an ANN with the aim to, within only a few seconds after a disturbance, be able to predict whether that disturbance is going to cause a voltage collapse in the near future. The method is based on the notion that it is possible to deduct, from measuring the system states just after a disturbance, whether the system will end up being stable, in an alert state, or cause a system collapse. Due to the dynamics of voltage instability (mainly caused by OELs, LTC, etc.), the system may appear to be in a stable condition for a rather long time before a more rapid degradation of the system stability occurs.

### A. ANN overview

Feedforward ANNs, also known as multilayer perceptrons, are the foundation of deep learning methods [13]. The strength of these methods, from here on denoted as ANNs, lies in their capability of accurately learning and approximating non-linear functions ($f^*$) from a set of training data without requiring any prior information. Thus, from a set of inputs ($x_n$) and corresponding target values ($y_n$) the ANN is capable of estimating the weights ($w$), or the parameters, mapping the inputs to the target values.

In Fig. 2, the structure of an ANN with a single layer of hidden units is presented. Between each layer there is a set of weights ($w^{(1)}$ & $w^{(2)}$) connecting each node in the system. A deeper architecture, i.e. more layers with hidden units, is often used in applications with more complicated functions and input-output mappings. Each of the nodes in the hidden layer consists of activation functions, such as the sigmoid-function or the rectified linear unit-function, simulating the response of real neurons in the human brain.

The learning of the ANN is performed using an algorithm called backpropagation, which iteratively adjusts the weights between each node and layer based on the adjustments that minimizes a cost function. The cost function is defined as the error between the estimated output and the actual target value. Once either the cost function has been minimized, or other stopping criteria has been met (for example maximum number of iterations reached), the ANN is fully trained.

### B. Generating training data

The simulated system in this paper is the Nordic32 test system which has been tested and used in several previous voltage stability simulations [14]. The method is based on generating a large set of data using dynamical simulations, which will be the training base for the ANN. The steps of the method is illustrated as a flowchart in Fig. 3 and can be summarized as follows:

1) *Randomly chosen power flows*: To simulate a large number of possible power flow states in the system, the system power flows are randomly initiated. For these simulations, the loads are first randomly chosen from a uniform distribution around the original loads (90 % of original load as lower limit, 105 % of load as upper limit). The change in load is then distributed randomly among all the

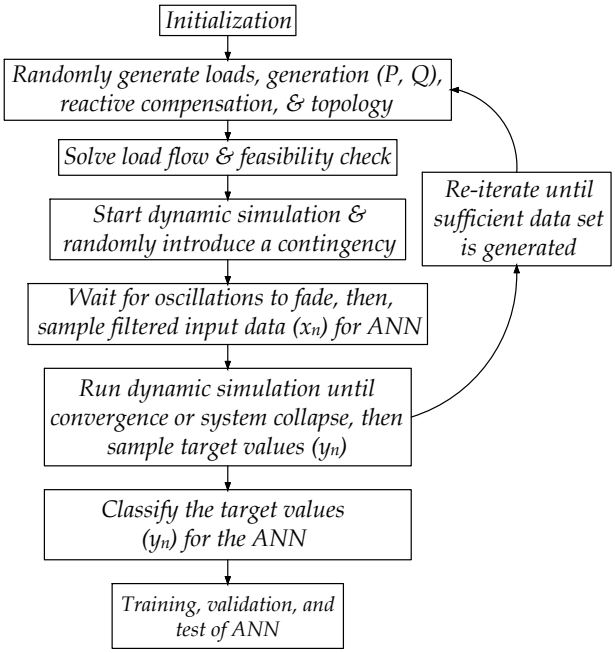


Fig. 3. Flowchart of the procedure of generating data and training the ANN

generators in the system. More configurations are possible, for instance, different levels of reactive compensation and different topologies, but this is not simulated in this paper. All power flow calculations and the dynamical moderation simulations in this paper are performed using PSS®E version 34.2.0 with its in-built dynamical models [15].

2) *Solve and check for feasibility*: The randomly generated system is solved with a power flow simulator, which serves as a starting point for the dynamical simulation. If the load flow does not converge, the initial operating condition is re-initialized.
3) *Start dynamic simulation and introduce contingency*: A dynamic simulation is then started, including all relevant dynamic models of the system. For the simulations in this paper, only line faults are examined. To illustrate a possible contingency, a line fault is applied for 0.1 s, which is then cleared by tripping the faulted line. Any of the lines in the Nordic32 system is randomly chosen for the contingency.
4) *Sample inputs $x_n$ for the ANN*: Before the inputs to the ANN is sampled, the initial oscillations caused by the fault should be allowed to dissipate. If not, the inputs may be inconclusive and cause a more uncertain classification of the system state. To reduce the impact of small oscillations, the inputs are filtered using the mean value of three different samples registered with a few seconds interval 10 seconds after the fault is cleared.
5) *Run until convergence or collapse*: The dynamic simulation is then continued, and runs either until the system converges or crashes. The transmission bus voltage magnitudes are then sampled as a base for generating the target values/classification of the different cases.
6) *Classification of data*: The data is classified into different

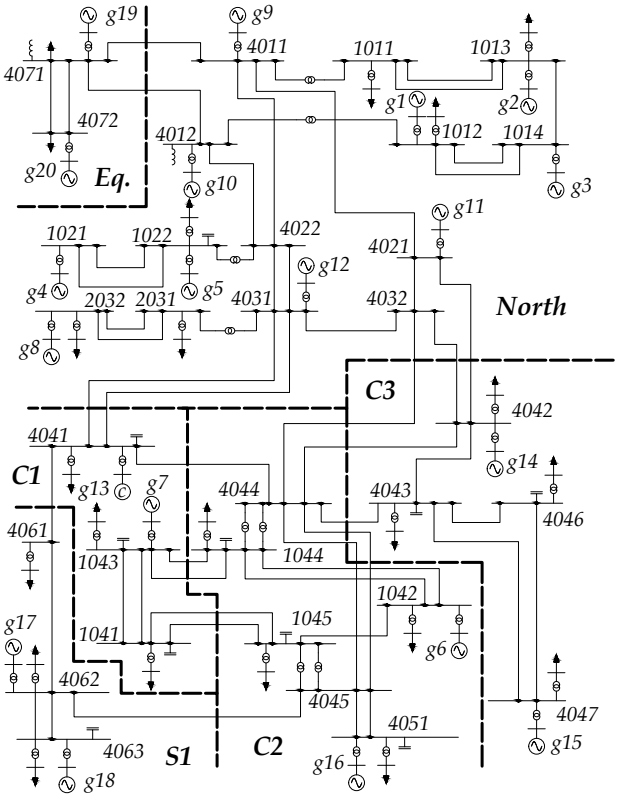


Fig. 4. One-line diagram of Nordic32 test system with new subareas

categories according to the severity and location of the system degradation. The system stability is defined as stable if all transmission bus voltage magnitudes in the system are above 0.95, in an alert state if any transmission bus voltage magnitude ranges between 0.9 - 0.95 pu, and in an emergency state if any transmission bus voltage magnitude is below 0.9 pu:

$$Stable : |V_{mag}| \geq 0.95pu$$
$$Alert : 0.9 \leq |V_{mag}| \leq 0.95pu$$
$$Emergency : |V_{mag}| \leq 0.9pu$$

The cases are also classified according to *where* in the system the lowest bus voltage magnitude is found at the end of the performed dynamic simulation. The Nordic32 system has therefore been divided into different regions, as illustrated in Fig. 4. The regions "North" and "Eq." are more stable regions and no alert events nor emergency events were found in these regions for any of the simulated cases. Thus, for the classification, only the other four regions (C1, C2, C3, S1) were used. The classification for each of the simulations belongs consequently to one of 9 different classes: either the whole system is stable or, an alert or an emergency state is identified in one of the four regions where the lowest occurring transmission bus voltage is identified. The classification is further illustrated in the result section in Table I.

7) *Re-iterate until sufficient data set is generated*: The steps

should be reiterated and the inputs and target values should be saved until a sufficient data set is generated. The required amount of data is highly dependent on the range of possible states in the system and the number of different contingencies being taken under consideration. A more thorough discussion regarding the need of a large data set is given in section IV.

### C. Training and architecture of the ANN

Once a sufficient amount of training data is generated, the ANN is trained. For the results in this paper, an ANN with a single layer of hidden neurons is used, developed in the MATLAB Neural Network Toolbox [16]. The optimization is performed using the scaled conjugate gradient backpropagation. The training was terminated when either a maximum of 1000 epochs was reached, the training mean-squared error falls below 1e-6, or until 10 validation checks are performed. A validation check is given when the validation performance fails to decrease, which is a method to avoid overfitting.

To find the best combinations of inputs to the ANN, 5 different input features sets are tested. These cases include:

Case 1: Voltage mag.
Case 2: Voltage mag. & generated power (P & Q)
Case 3: Voltage mag. & phase angle
Case 4: Voltage mag., P & Q branch flow
Case 5: Voltage mag., P & Q branch flow & phase angle

A total of 100 000 dynamical simulation samples are generated for each feature set. The data is divided into an 80-10-10 % training, validation, and test set, respectively. The most appropriate number of hidden neurons with respect to accuracy, over-fitting, and computation time was found to be 16 hidden neurons. This number is based on the results presented in section III. Due to random sampling and different initializations of the weights in the ANN, the performance varies slightly when training the ANN multiple times. To find the lowest test error, the ANN was trained for a total of ten times, and only the best performance is presented in the paper.

## III. Simulation results

### A. Performance of the O-VIP

The lowest test error achieved in the simulations was 3.7 % using 16 neurons in the hidden layer and inputs according to case 4. In Table I, the classification test results are represented by a confusion matrix for case 4. Each column in the table represents instances of the predicted classes, and each row represents the instances of the actual classes. The total accuracy is presented in the lower right corner of the table.

According to the table, the accuracy of the O-VIP in the case of stable states is 96.2 %, and 3.8 % of all stable cases were thus misclassified to belong in the alert state. None of the actual stable states were classified as emergency states. All of the misclassification for the emergency states were either for other regions, or ended up being classified as an alert state but in the correct region. A 100 % accuracy was achieved for the classification of emergency state in S1, although only a single sample were generated for this class. This region of the Nordic32 test system was thus significantly less prone to voltage instability compared to other regions. The lowest accuracy were for the alert state in S1, 85.2 %, where several samples were misclassified as being in a stable state.

It is likely that for a majority of all cases being misclassified as stable, although actually being in an alert state, the O-VIP would be able to classify these correctly if the measurement values were sampled a longer time after the contingency occurred, allowing the system to degrade slightly more. Hence, there exists a balance between a fast classification and accuracy. Specific threshold values could be applied such that only a certain amount of falsely positive classified cases are accepted, or that only classifications with a certain probability are accepted.

### B. Choice of input features

Five different set of input feature combinations were tested to find the best suitable. The performance for each of the five cases are presented in Table II. The best performance is achieved for case 4, where the input data consists of bus voltage magnitudes and active and reactive branch flows. Thus, in contrast to what is presented in [4], the voltage magnitude and the phase angles do not present the best input to the ANN for this application. One explanation for this outcome could be the fact that during faults, the angle difference for certain buses may vary significantly depending on the actual contingency, providing somewhat inconclusive information to the ANN. Thus, if branch power flows are used instead of phase angles, the ANN is provided with more conclusive data and allows a better classification. Another advantage of using branch flow as inputs is that these provide information if a branch is out of service, as the flow always reduces to zero. In case phase angles are used, the ANN will have no indirect information that a certain branch is no longer in service.

For case 5, the error is somewhat larger than for case 4. It is an interesting result, since more input values should at least not increase the error. The probable main explanation is the impact of random sampling of the test set, different initializations of the weights, and that the network might slightly overfit on the training data.

### C. Choice of neurons and training set size

The so-called hyperparameters of an ANN, such as the number of neurons in the hidden layer, or the depth of the network, control the learning of the algorithm and must be chosen before the actual learning process has begun. The design and choice of such parameters is often an iterative process, and will often have to be tuned and changed repeatedly in order to achieve a desirable performance. In the scope of this paper, the sensitivity of all available hyperparameters is not feasible to present, and the focus has instead been to examine a suitable number of neurons in the hidden layer and how the training set size affects the performance of the predictor.

TABLE I
PREDICTION RESULTS AND ACCURACY OF THE O-VIP ALGORITHM (CONFUSION TABLE)

| | | | *Predicted states* | | | | | | | | | |
|---|---|---|---|---|---|---|---|---|---|---|---|---|
| | | | **Stable state** | **Alert state** | | | | **Emergency state** | | | | **Accuracy** |
| | **Classification** | | All areas | C1 | C2 | C3 | S1 | C1 | C2 | C3 | S1 | |
| *Actual states* | **Stable state** | All areas | 4527 | 62 | 0 | 1 | 117 | 0 | 0 | 0 | 0 | 96.2% |
| | **Alert state** | C1 | 77 | 2359 | 1 | 0 | 6 | 1 | 13 | 0 | 0 | 96.0% |
| | | C2 | 0 | 0 | 0 | 0 | 0 | 0 | 0 | 0 | 0 | - |
| | | C3 | 2 | 2 | 0 | 1268 | 0 | 0 | 0 | 4 | 0 | 99.4% |
| | | S1 | 63 | 7 | 0 | 0 | 402 | 0 | 0 | 0 | 0 | 85.2% |
| | **Emergency state** | C1 | 0 | 0 | 0 | 0 | 0 | 1 | 0 | 0 | 0 | 100% |
| | | C2 | 0 | 7 | 0 | 0 | 0 | 3 | 262 | 0 | 0 | 96.3% |
| | | C3 | 0 | 0 | 0 | 3 | 0 | 0 | 0 | 83 | 0 | 96.5% |
| | | S1 | 0 | 0 | 0 | 0 | 0 | 0 | 0 | 0 | 725 | 100% |
| | **Accuracy** | | 97.0% | 96.8% | 0% | 99.7% | 76.6% | 20% | 95.3% | 95.4% | 100% | **96.3%** |

TABLE II
PERFORMANCE OF ANN WITH DIFFERENT INPUT FEATURE SETS

| **Feature case** | **Case 1** | **Case 2** | **Case 3** | **Case 4** | **Case 5** |
|---|---|---|---|---|---|
| Test error [%] | 5.0 | 4.4 | 4.7 | 3.7 | 4.0 |

*1) Choosing number of neurons in hidden layer:*

To find the most suitable number of neurons in the hidden layer, an iterative algorithm was adopted that trained the system with an increasing number of neurons. In Fig. 5, the training, validation, and test error for a range of different numbers of neurons in the hidden layer are presented for case 4. According to the figure, the test error decreases significantly with an increasing amount of neurons up until 16 neurons, where the lowest test error is found. By increasing the number of neurons even further, the test training error keeps decreasing, while both the validation and the test error are increasing, indicating an increased overfitting of the parameters. The suitable number of neurons are highly depending on the application and a different number of neurons for other sizes and configurations of grids is possibly more accurate.

*2) Impact of training data size:* The impact of a sufficiently large training set is illustrated in Fig. 6, where the training, validation, and test error is plotted for case 4, this time with an increasing amount of training data on the x-axis. Generally, an ANN increases its performance with an increasing amount of training data, up to a certain point when the performance converge. As can be seen in the figure, the test performance increases significantly with an increasing amount of data. However, as the training data approaches a larger value, the test error stabilizes at around 4 %.

The training error should converge to a value close zero with an increasing amount of data, given that the provided input values contains sufficient information to differentiate between the post-contingency states. Since this is not fully the case, it is likely that the provided input data is not sufficient to allow accurate classification in the more difficult cases. If other information, such as dynamic values and states of OELs and LTCs, could have been provided to the ANN, the harder cases could possibly be correctly classified as well.

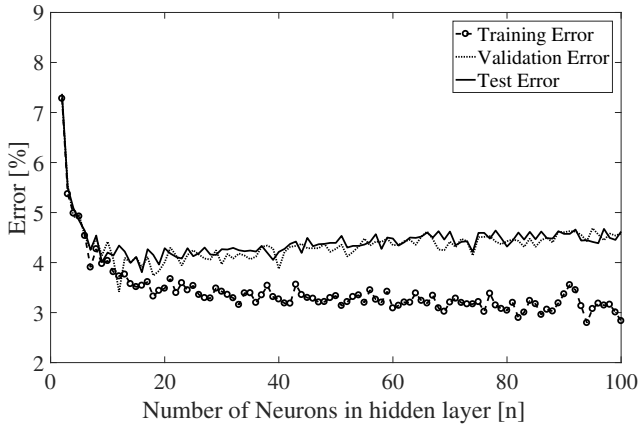


Fig. 5. Training, validation, and test error with varying number of neurons in hidden layer

The requirement of a large data set is also affected by the range of different pre-contingency load flows of the system and the set of credible contingencies taken into account. A system with minor variations in its configurations and its load flows would thus require a smaller set of training data than a system with large variations.

## IV. APPLICATIONS AND LIMITATIONS

### A. Applications and usefulness

The O-VIP could present a powerful tool for TSOs and it is proposed to mainly be used as a supplementary system and to act as a complement to other voltage instability warning systems. For the predictor to be effective, measurement updates should be available in the range of a few seconds (1-10 s), as otherwise too long time between the assessments would occur. Measurements from SCADA systems filtered through a conventional state estimator could thus be too slow to be effective, and preferably, the O-VIP would instead be based on measurements from wide-area phasor measurements, filtered through a (linear) state estimator.

The application can serve as a direct warning system to TSOs, allowing them time to perform suitable control measures to control the system back into stable operation. Alternatively, the application itself could be used to initiate

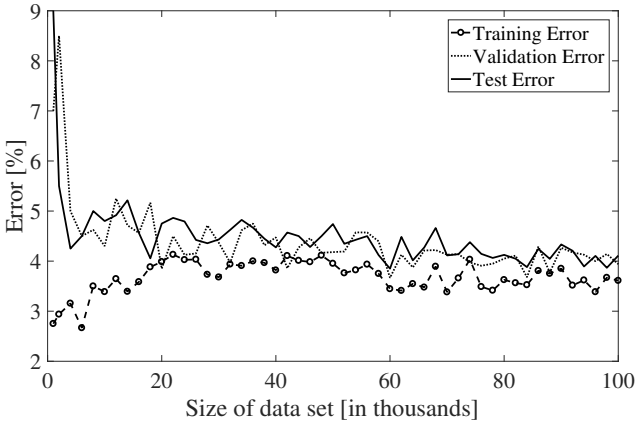


Fig. 6. Training, validation, and test error with varying data set size

system protection schemes to automatically restore stability to the system. Such automatic schemes would in most cases only be used after significant testing and most likely only for the detection and aversion of emergency states.

Another advantage of using an ANN is that it is highly suitable for on-line applications. Using training methods such as stochastic gradient descent, the ANN can gradually increase its performance as more training data is being generated. Connecting an on-line training scheme of the O-VIP with, for example, the SCADA system could allow the method to gradually increase its accuracy while ensuring that no changes in the system are neglected.

### *B. Measurement and model errors*

The performance of any VSI will be affected by both measurement errors and by errors in the model that the VSI is based on. The trueness and precision of measurements in the power system is dependent on both the quality of measurement devices and the level of measurement redundancy in the system. A high level of measurement redundancy increases the accuracy of state estimation algorithms and reduces the impact of such errors significantly, which in turn would increase the accuracy of VID systems. However, it is most likely that the model errors that will affect the accuracy of the O-VIP the most. Not only has regular system parameters, such as line reactance and line resistance to be modeled accurately, but also each dynamic model in the system has to be modeled with sufficient accuracy. This includes modeling of parameters for OELs, time-steps for LTCs, time-delays in different relay equipment, and various load restoring systems. One of the greatest challenges is to *verify* that the O-VIP is in fact accurate. Voltage collapses, although a phenomenon that TSOs always have to plan and take into account, occurs very seldom. Hence, it would prove difficult to, in practice, test the system. Since such tests of the O-VIP would be difficult, the requirement of careful assessment of all different dynamic models in the system becomes increasingly important.

## V. Conclusion

This paper presents a new approach for on-line prediction of voltage instability based on training an ANN. The results presented in this paper is highly encouraging, showing high accuracy (96.3 %) of predicting whether a voltage collapse will develop, only seconds after a contingency in the system. The main benefits of the O-VIP are both the early prediction of voltage instability and the possibilities to pinpoint where in the system the instability is the most severe. This would allow earlier and more cost-effective control actions to steer the system back into stable operation again. The system can be applied and trained using on-line measurement data from the SCADA system, but for real-time detection of voltage instability, measurement from wide-area phasor measurements would be preferred. More studies should be performed regarding the impact of measurement and model errors and how that would affect the accuracy of the O-VIP.

## Acknowledgment

The work presented in this paper has been financially supported by Energimyndigheten (Swedish Energy Agency) and Svenska kraftnät (Swedish National Grid) within the SamspEL program.

## References

[1] T. Van Cutsem and C. Vournas, *Voltage stability of electric power systems*. Boston: Kluwer Academic Publishers, 1998.

[2] M. Glavic and T. Van Cutsem, "A short survey of methods for voltage instability detection," in *Proc. (IEEE) PES General Meeting*, Detroit, MI, Jul 2011, pp. 1–8.

[3] M. L. Scala, M. Trovato, and F. Torelli, "A neural network-based method for voltage security monitoring," *IEEE Trans. on Power Syst.*, vol. 11, no. 3, pp. 1332–1341, Aug 1996.

[4] D. Q. Zhou, U. D. Annakkage, and A. D. Rajapakse, "Online monitoring of voltage stability margin using an artificial neural network," *IEEE Trans. on Power Syst.*, vol. 25, no. 3, pp. 1566–1574, Aug 2010.

[5] G. G. Lage, R. A. S. Fernandes, and G. R. M. da Costa, "Neural-network representation of voltage stability indices at the voltage collapse," in *North American Power Symposium*, Aug 2011, pp. 1–7.

[6] T. Van Cutsem *et al.*, "Decision tree approaches to voltage security assessment," *IEE Proceedings C - Generation, Transmission and Distribution*, vol. 140, no. 3, pp. 189–198, May 1993.

[7] H. Khoshkhoo and S. M. Shahrtash, "Fast online dynamic voltage instability prediction and voltage stability classification," *IET Generation, Transmission & Distribution*, vol. 8, no. 5, pp. 957–965, May 2014.

[8] ——, "On-line dynamic voltage instability prediction based on decision tree supported by a wide-area measurement system," *IET Generation, Transmission & Distribution*, vol. 6, no. 11, pp. 1143–1152, November 2012.

[9] R. Diao *et al.*, "Decision tree-based online voltage security assessment using pmu measurements," *IEEE Trans. on Power Syst.*, vol. 24, no. 2, pp. 832–839, May 2009.

[10] Q. Zhou, J. Davidson, and A. A. Fouad, "Application of artificial neural networks in power system security and vulnerability assessment," *IEEE Trans. Power Syst.*, vol. 9, no. 1, pp. 525–532, Feb 1994.

[11] Y. Mansour *et al.*, "Large scale dynamic security screening and ranking using neural networks," *IEEE Trans. Power Syst.*, vol. 12, no. 2, pp. 954–960, May 1997.

[12] ——, "Large scale dynamic security screening and ranking using neural networks," *IEEE Trans. Power Syst.*, vol. 12, no. 2, pp. 954–960, May 1997.

[13] I. Goodfellow, Y. Bengio, and A. Courville, *Deep Learning*. MIT Press, 2016, http://www.deeplearningbook.org.

[14] M. Stubbe *et al.*, "Long term dynamics - phase II final report ," Cigré Task Force, Tech. Rep. 38.02.08, Mar. 1995.

[15] *PSS®E 34.2.0 Model Library*, Siemens Power Technologies International, Schenectady, NY, Apr. 2017.

[16] M. H. Beale, M. T. Hagan, and H. B. Demuth, *Neural Network Toolbox™ User's Guide*, 1992.

# Integration Aspects of Full Converter Wind Turbines and the Impact on Long-term Voltage Stability

Hannes Hagmar, Le Anh Tuan, Ola Carlson
*Department of Electrical Engineering*
*Chalmers University of Technology*
Gothenburg, Sweden
hannes.hagmar@chalmers.se

Robert Eriksson
*Market and System Development*
*Svenska Kraftnät*
Sundbyberg, Sweden
robert.eriksson@svk.se

***Abstract*—This paper examines how various integration aspects of full converter wind turbines, such as grid code design, control aspects, and placement of turbines, impact the long-term voltage stability of a power system. The simulations are conducted on a modified version of the Nordic32 test system. Different cases have been analyzed and show, for example, that if over-dimensioning of converters is implemented, it is mainly the converters' current capacity that should be increased since the voltage limitation of converters seldom is reached during voltage instability events. Furthermore, a restrictive reactive control scheme is tested, with the aim of minimizing the wear and maintenance of converter components. Although found to generally reduce the voltage stability, the proposed control scheme could be adopted during specific conditions where the local need of voltage support is low. The placement of larger wind farms was found to have the largest impact, both on long-term voltage stability of the system itself, and on the effect that the analyzed design and control aspects had on the system stability. Consequently, the placement of WFs is found be an important factor to consider when designing ancillary services and grid codes for wind power.**

***Index Terms*—Long-term voltage stability, full converter wind power, integration aspects, grid codes, power control schemes**

## I. Introduction

During the last decades, the global wind power market has been the fastest growing energy generation sector in the world [1]. The impact of wind power on long-term voltage stability (LTVS) is becoming an increasingly important topic [2], and in response to these challenges, a range of actions have been proposed in the research and by the industry. The technical requirements, or grid codes, for connecting wind farms (WFs) have been updated and strengthened in several countries in the world [3], [4]. Stricter requirements have led to an increasing adoption of full converter based WFs (FC-WFs) in power systems, mainly due to their flexibility in controlling the output and response of the turbine [5].

The maximum capacity of wind power in a power system is affected by numerous aspects, such as the placement of turbines, control schemes, reactive power support capability, and the availability of reserve power generation. Aspects of wind power generation, ranging from grid integration issues [2], [6], [7], control aspects [8], [9], or possibilities of providing ancillary services [5], [10], have been examined in previous papers. A focus in these previous papers has also been to examine how WFs can be designed to better contribute to the LTVS. However, designing a system that better contributes to the system stability often comes with a cost, be it increased cost for sizing of converters, or increased wear of converters due to increased reactive power support.

The main objective of this paper is to bring new insights in how different integration aspects of FC-WFs affect the LTVS of a power system. Examined design aspects include grid code design, power control aspects, and placement and output of larger FC-WFs. The results are also put into context with economic aspects of, for example, designing grid codes or choosing control schemes for larger WFs. More specifically, the aim of the paper is to determine *when* and *during what conditions* certain design or control aspects are the most important, both with respect to technical and economic aspects.

## II. FC-WF Power Generation Aspects

### A. Modeling of equivalent circuit of WFs

A wind farm consisting of several wind turbines can in power flow studies be simplified into a single equivalent unit, as illustrated in Fig. 1. The impedance of wind farm feeders, filters, collectors, and step-up transformers may then be transformed into an equivalent impedance of a grid connected step-up transformer [5]. The active and reactive power capability of FC-WFs can then be derived from this equivalent circuit.

The grid converter voltage ($V_c$) is controlled by alterations of the modulation index, while the the phase angle ($\delta$) is controlled by changing the switching pattern of the converters. The maximum value of $V_c$ is a design value determined by the size and ratings of the wind turbine converters, and it is an important factor for dimensioning components to meet different grid codes and requirements [5].

### B. Modeling active and reactive power capability

A FC-WF can provide reactive power independently as long as it is operating within the converter limits, while active power output is determined by the actual mechanical power generated by the turbine. The maximum current capability of a converter can be represented by a circle in the $PQ$-plane, given by [5]:

$$P^2 + Q^2 = (V_g I_c)^2 \tag{1}$$

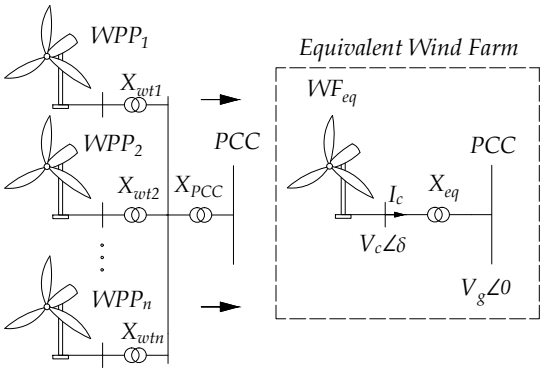


Fig. 1. Equivalent circuit diagram of a wind farm

where $P$ and $Q$ represent the active and reactive power production at the AC grid connection point, and $V_g$ and $I_c$ represent the grid voltage and converter current, respectively. Another limit is constituted by the maximum voltage across the converter transistors, and consequently the difference between the grid converter voltage ($V_c$) and the grid voltage ($V_g$). The relationship between $P$ and $Q$ at the converter limit is given by [5]:

$$P^2 + \left(Q + \frac{V_g^2}{X_{eq}}\right)^2 = \left(\frac{V_c V_g}{X_{eq}}\right)^2 \tag{2}$$

where $X_{eq}$ is the total equivalent reactance of the wind farm. The maximum values of the converter current and voltage ($V_{c,max}$ and $I_{c,max}$) are determined by the ratings of the grid connected converters. The converter current is highest when active and reactive power are at rated values ($P_r$ and $Q_r$), while the grid voltage is at the minimum. This relationship, given in p.u. by simplifying the right-hand side by taking $P_R$ and $Q_R$ as the MVA base of the system, is given by:

$$I_{c,max} = \frac{\sqrt{P_r^2 + Q_r^2}}{V_{g,min}} = \frac{\sqrt{1 + \tan^2\theta_R}}{V_{g,min}} \tag{3}$$

where $\theta_R$ is the rated power factor angle of the converter. The maximum required converter voltage can be derived using (2) and it is highest when the grid voltage and the system frequency are at the maximum level, and the active and reactive power of the WF are at rated values. This relationship in p.u. is given by [5]:

$$V_{c,max} = \frac{f_{max} X_{eq}}{V_{g,max}} \sqrt{1 + \left(\tan\theta_r + \frac{V_{g,max}^2}{f_{max} X_{eq}}\right)^2} \tag{4}$$

where $f_{max}$ and $V_{g,max}$ are the maximum frequency and grid voltage, respectively.

## III. Simulation Approach and Design

### A. Simulation aspects

Several scenarios are simulated, such as varying levels of wind generation, power control approaches, and design aspects

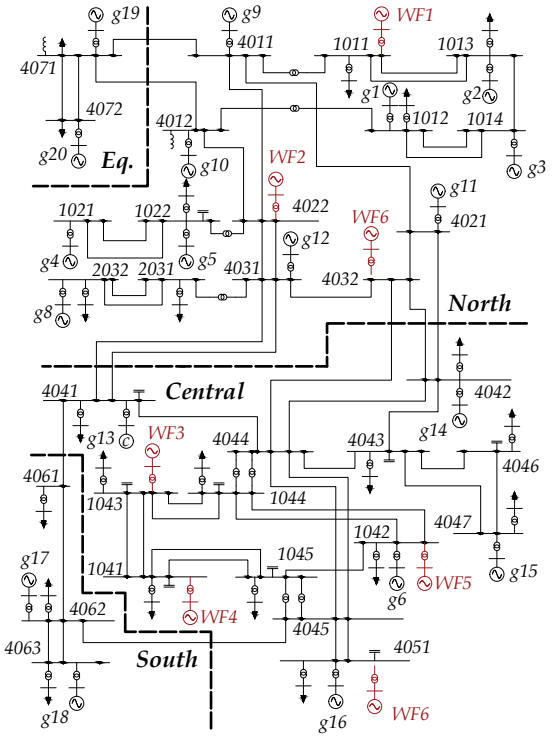


Fig. 2. The modified Nordic32 Test System with inclusion of 6 separate WFs

of grid codes. The simulations are based on a modified version of the Nordic32 test system presented in [11], and the single-line diagram is found in Fig. 2. The following simulations are all based on the unstable version of the system, denoted as the "Operating point A" in the Nordic32 test system and all required parameters can be found in [11]. All the simulations are performed in PSS®E version 34.2.0 with its built-in dynamical models [12].

*1) WF placement and generation:* To simulate a future power system with a higher penetration of WFs, six separate systems (WF1-WF6) have been included into the test system. The placement of the largest system, WF6, is varied in the simulations, and two different cases are examined. The first case is when WF6 is placed in the area denoted as "Central" (bus 4051), and the second when WF6 is placed in the area denoted as "North" (bus 4032), see Fig. 2. Furthermore, the output of the WFs is varied in the simulations, and two cases are examined: a very high wind case when all WFs generate 95 % of rated $P$, and a lower wind case when all WFs operates at 40 % of rated $P$.

*2) Grid code design:* In 2016, the European Union (EU) adopted new regulations regarding connection of power-generator modules such as larger WFs [3]. The regulations state the requirements of providing reactive power while operating at rated capacity and at various levels of grid voltage. The regulations state the maximum reactive power requirements for WF owners, with reactive power requirements as a function between grid voltage and $Q/P_{MAX}$-ratio. The final specific design of the grid codes and the requirements are left to be

decided each country's legislative body. From a societal view, they should be designed both with respect to grid requirements of stability and to economic aspects for the WF owner.

In the simulations, three proposed grid code designs are examined where the capability to provide reactive power under certain operating points are varied. The three grid code designs are illustrated in Fig. 3.

(i) Grid Code 1: Illustrated in Fig. 3 as the red dotted square, the same reactive power requirement is used for any values of grid voltage. This is a stricter grid code, requiring higher capacity of converters to be able to produce reactive power at all operating points.

(ii) Grid Code 2: Illustrated in Fig. 3 as a black step-wise increasing/decreasing function, the adaptive reactive power requirements are reduced step-wise as the grid voltage increases. The adaptive grid code reduces the need of over-dimensioning converters, although not being able to generate as much reactive power during all conditions.

(ii) Grid Code 3: Illustrated in Fig. 3 as the green dashed square, an even less strict grid code is adapted, requiring only 0.15 $Q/P_{max}$ at 1 p.u. grid voltage.

*3) Voltage control approach:* The failure mechanisms of power electronic devices are complex and affected by numerous factors, where thermal cycling is one of the most critical failure causes [13]. The life-time of IGBTs in a FC-WF may be affected both during stable operation and during varying conditions caused by, for example, wind gusts or varying reactive power demand. Higher average operating currents increase the junction temperatures, which in turn make the IGBTs more sensitive to thermal cycling damage [14].

In response to this, two different strategies for voltage control of the FC-WFs are simulated. The first one (in coming simulations denoted as $V_{ctrld}$) is the same as for regular synchronous generators, where the FC-WFs always participate in controlling the voltage to the scheduled level. In the second control strategy (in coming simulations denoted as $V_{reserv}$), the FC-WFs only participate in voltage control when the grid voltage ($V_g$) is equal or less than 0.95 p.u. Thus, in stable conditions, the reactive power is controlled to be minimized. However, as soon as ($V_g$) drops below 0.95 p.u., the reactive power generation is increased to control the voltage back to 0.95 p.u. The benefits of such an approach would be less thermal stress and conduction losses of the converter IGBTs. However, the grid would be less stiff and the the voltage stability could suffer.

### B. System stress level, disturbances, and stability criterion

For all combinations of the design aspects described in the previous section, the system is stressed until a stability criterion is violated. The stability criterion used in the simulations is that the post-contingency state is considered stable if, over a simulation interval of 600 seconds, all distribution bus voltages are restored above 0.95 p.u. The highest system stress level is then found by gradually increasing *all* the loads in the system and applying a contingency that further stresses the system.

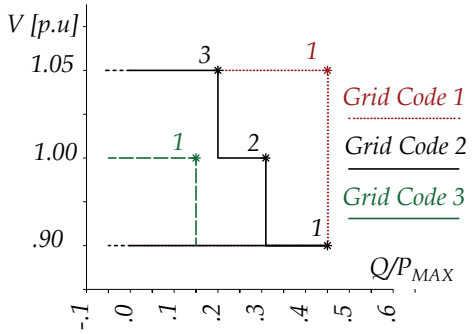


Fig. 3. Three different grid code designs to be tested in simulations

TABLE I
DATA OF ADDED WFS

| Name | Bus | Replaces | Base voltage (kV) | $X_{eq}$ (pu) | $P_{max}$ (MW) | $V_{sched}$ (pu) |
|---|---|---|---|---|---|---|
| WF1 | 1011 | - | 33.0 | 0.3 | 220 | 1.0520 |
| WF2 | 4022 | - | 33.0 | 0.3 | 200 | 1.0170 |
| WF3 | 1043 | g7 | 33.0 | 0.3 | 180 | 1.0141 |
| WF4 | 1041 | - | 33.0 | 0.3 | 110 | 1.0141 |
| WF5 | 1042 | - | 33.0 | 0.3 | 110 | 1.0141 |
| WF6 | 4051 | - | 33.0 | 0.3 | 500 | 1.0531 |
| | | | ***or*** | | | |
| WF6 | 4032 | - | 33.0 | 0.3 | 500 | 1.0531 |

For each of the gradually increasing load levels, different types of contingencies are tested, as different design aspects will cause the system to be sensitive to different faults. To reduce the number of simulations, only tripping of transmission lines that connect either of the different regions (excluding the "Equivalent" region) is tested.

### C. Simulation parameters

All WFs are simulated generically using the built-in models WT4G2 and WT4E2 in PSS®E. The parameters for the dynamic models are gathered from [12], with reference to a Siemens 2.3 MW wind turbine. The total $X_{eq}$ is modeled by a an explicit step-up transformer of 0.3 pu. The power flow data of the WFs are presented in Table I. The control mode for the wind turbines are set to $P$-priority, where the active power is kept to its reference value although a larger reactive power is required to keep the grid voltage constant to the reference value. Despite the control mode, all converter parameters are adapted to still allow the WFs to generate the required amount of reactive power from the present grid codes.

The WF parameter values are dependent on the design values of the grid codes and can computed using Eq. (3) and (4). The dimensioning requirement of $V_{c,max}$ occurs when the grid voltage is the highest and the maximum requirement of generated/absorbed reactive power exists.

*1) Grid Code 1:* The dimensioning requirements occur in the upper right corner of the depicted grid code in Fig. 3, with a power factor of $\cos\theta_R = 0.91$ and with $V_{g,max} = 1.05$. Using this value for $\theta_R$ and assuming $f_{max} = 1.01$, values of $V_{c,max} = 1.21$ and $I_{c,max} = 1.22$ can be computed.

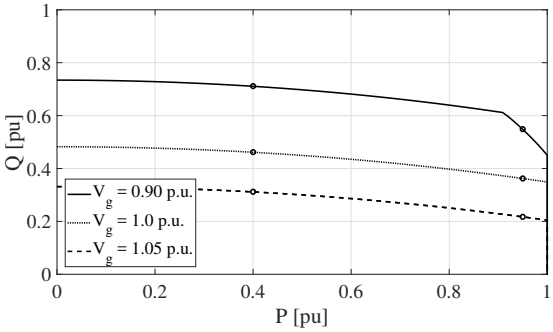


Fig. 4. PQ-capacity diagram under Grid Code 2

TABLE II
DESIGN VALUES FOR GRID CODE 2

| | $V_{g,max}$ | $\cos\theta_R$ | $V_{c,max}$ | $I_{c,max}$ |
|---|---|---|---|---|
| Corner 1 | 0.9 | 0.91 | 1.11 | **1.22** |
| Corner 2 | 1.0 | 0.96 | 1.13 | 1.16 |
| Corner 3 | 1.05 | 0.98 | **1.14** | 1.13 |

*2) Grid Code 2:* The dimensioning requirements can occur in either of the right hand corners of the depicted grid code in Fig. 3. Compared with Grid Code 1, both $V_{g,max}$ and $\theta_R$ vary in this case, causing $V_{c,max}$ and $I_{c,max}$ to vary as well. The three requirements by each corner are evaluated in Table II. The PQ-capacity diagram is found in Fig. (4) with operating points for 40 % and 95 % of maximum P marked out. The largest values of $V_{c,max}$ and $I_{c,max}$ is then dimensioning for the converter. As a comparison, Grid Code 2 allows a smaller dimensioning $V_{g,max}$ compared to Grid Code 1, while the $I_{c,max}$ requirement is constant.

*3) Grid Code 3:* The design values are calculated in a similar manner as for Grid Code 1, resulting in $V_{c,max} = 1.09$ and $I_{c,max} = 1.12$. The parameters for all grid codes are then incorporated into the dynamic models of the WFs.

## IV. SIMULATION RESULTS

The results for the different simulations cases are presented Table III, in which all design aspects are varied: grid codes (type 1 - 3), WF output (High wind and Low wind), and control scheme ($V_{cntrl}$ and $V_{reserv}$). The increase in load in % compared to the base case is represented by $\Delta P_{L,all}$. The last state that the system meets the defined stability criterion is presented as the result in the table.

*1) Impact of grid code design:* The different grid codes was found to have a small effect on the stability of the analyzed system. For instance, Grid Code 1 (with the strictest requirements) only increased the $\Delta P_{L,all}$ by 0.2 % respectively 0.4 % for case type A and B, compared to Grid Code 3 (with the least strict requirements). However, the relatively small stability improvement should be put into relation to the, compared to the whole grid, relatively small increase in reactive power capacity of the WFs.

In Fig. 5, the generated reactive power and l voltage for case 1, 2, and 9 are presented for the same level of increased load (7.9 %), each representing a different grid code. The reactive power output of case 1 and 2 are identical, since neither the current nor the voltage limitation is met. The generated reactive power for case 9 is reduced and the voltage collapses, mainly due to a lower $I_{c,max}$-value and higher converter currents due to lower grid voltages. Although the larger $I_{c,max}$-values only improved the voltage stability marginally in the simulated cases, the actual benefit of more reactive power is highly dependent on other factors such as the level of penetration from wind power in a power system. Since voltage instability in general is correlated to low grid voltages, over-dimensioning $V_{c,max}$ to allow more reactive power output at high grid voltages could be argued to be an inefficient measure to increase stability. Instead, a more adaptive scheme, as for Grid Code 2, would be preferred.

*2) Impact of wind power output:* The most significant impact on the LTVS was the placement of the largest WF, WF6. Not surprisingly, by placing more generation in the "Central" area, closer to the larger load centers, it resulted in a significant enhancement of the stability. However, the impact is highly affected by the output of the WFs and the increase was found to be reduced during occasions of low wind.

Another aspect to consider is that WFs do not always generate full active power, both due to wake effects and wind speed variations. In these cases, the WF has increased possibilities to support the grid with reactive power, even without reducing the active power. In power systems with large penetration of wind power, the system is likely most sensitive to disturbances during occasions of low wind if the active power needs to be transmitted long distances from other areas to compensate the loss of generation. Thus, the ability of a FC-WF to support the grid with reactive power is also highest when the need for reactive power is high.

*3) Impact of proposed voltage control scheme:* The functionality of the proposed control scheme $V_{reserv}$ is illustrated in Fig. 6 for a stable version of Case 5A. In the figure, the reactive power is controlled to zero as long as the grid voltage is above 0.95 p.u. As the grid voltage decreases below 0.95, the WF initiates its reactive power output to stabilize the voltage.

The different control strategies had some impact on the stability of the system and lower levels $\Delta P_{L,all}$ were possible with the proposed control scheme. Again, the impact was lower during both occasions of low wind, and when WF6 was located in the "North" area. Although the proposed control scheme in most cases would not be optimal, the results indicate that it could be utilized during certain conditions. For instance, if a larger WF would be located in an area with low requirements of reactive power, it could be an option to reduce the wear of converter IGBTs to both extend the life-time of the devices and to reduce the need for maintenance. However, this would require that grid codes can be adaptable to allow different requirements on FC-WFs depending on, for instance, the placement of the WF or specific need at the grid cite.

## V. CONCLUSION

This paper analyzes the impacts on long-term voltage stability from different integration aspects of FC-WFs, such as grid codes and reactive power control. The paper has tested

TABLE III
SIMULATIONS RESULTS WITH WF6 LOCATED IN CENTRAL REGION

| *WF6 located in "Central" area* | Case 1A | Case 2A | Case 3A | Case 4A | Case 5A | Case 6A | Case 7A | Case 8A | Case 9A | Case 10A |
|---|---|---|---|---|---|---|---|---|---|---|
| Grid Code | 1 | 2 | 1 | 2 | 1 | 2 | 1 | 2 | 3 | 3 |
| WF Output | High | High | Low | Low | High | High | Low | Low | High | Low |
| Control Scheme | $V_{ctrld}$ | $V_{ctrld}$ | $V_{ctrld}$ | $V_{ctrld}$ | $V_{reserv}$ | $V_{reserv}$ | $V_{reserv}$ | $V_{reserv}$ | $V_{ctrld}$ | $V_{ctrld}$ |
| $\Delta P_{L,all}$ before stability criterion violation (% to base case) | **8.0 %** | **8.0 %** | **1.9 %** | **1.9 %** | **7.1 %** | **7.1 %** | **1.7 %** | **1.7 %** | **7.8 %** | **1.8 %** |
| *WF6 located in "North" area* | Case 1B | Case 2B | Case 3B | Case 4B | Case 5B | Case 6B | Case 7B | Case 8B | Case 9B | Case 10B |
| Grid Code | 1 | 2 | 1 | 2 | 1 | 2 | 1 | 2 | 3 | 3 |
| WF Output | High | High | Low | Low | High | High | Low | Low | High | Low |
| Control Scheme | $V_{ctrld}$ | $V_{ctrld}$ | $V_{ctrld}$ | $V_{ctrld}$ | $V_{reserv}$ | $V_{reserv}$ | $V_{reserv}$ | $V_{reserv}$ | $V_{ctrld}$ | $V_{ctrld}$ |
| $\Delta P_{L,all}$ before stability criterion violation (% to base case) | **5.0 %** | **5.0 %** | **1.3 %** | **1.3 %** | **3.9 %** | **3.9 %** | **1.2 %** | **1.2 %** | **4.6 %** | **1.3 %** |

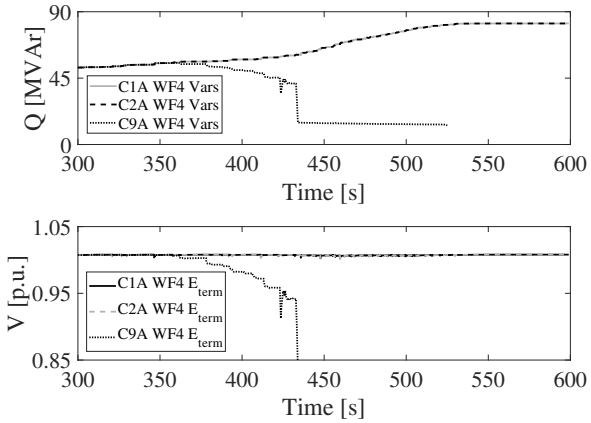


Fig. 5. Generated reactive power and terminal voltage for WF4. Difference illustrated between simulation cases 1, 2, and 9.

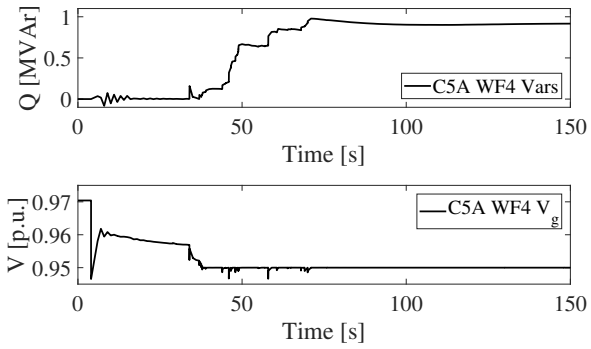


Fig. 6. Generated reactive power and grid voltage ($V_g$) for WF4, case 5A

different cases and shows, for instance, that over-dimensioning of a FC-WF does not in all cases increase the stability. If such over-dimensioning is implemented, it is mainly the $I_{c,max}$-ratings of the converters that should be increased since the voltage limitation of the converters seldom are reached during voltage instability events. A restrictive reactive control scheme is also tested, and although it is found to reduce the stability in some cases, it could be used during certain conditions to reduce maintenance and wear of components. Moreover, the placement of larger WFs is found to have the largest impact on the LTVS of a power system, and the closer larger WFs are located to load centers, the more they contribute to the system stability. Thus, if ancillary services would take into account the *actual* improvement that the FC-WFs is providing, such aspects should be included in the design of those.

## ACKNOWLEDGMENT

The work presented in this paper has been financially supported by Energimyndigheten (Swedish Energy Agency) and Svenska kraftnät (Swedish National Grid) within the SamspEL program.

## REFERENCES

[1] "Global wind report," Global Wind Energy Council, Tech. Rep., 2017.
[2] R. R. Londero, C. d. M. Affonso, and J. P. A. Vieira, "Long-term voltage stability analysis of variable speed wind generators," *IEEE Trans. Power Syst.*, vol. 30, no. 1, pp. 439–447, Jan 2015.
[3] "Establishing a network code on requirements for grid connection of generators," Commission Regulations (EU) 2016/631, European Union, Apr. 2016.
[4] "The grid code," National Grid Electricity Transmission, Mar. 2017.
[5] N. R. Ullah, K. Bhattacharya, and T. Thiringer, "Wind farms as reactive power ancillary service providers—technical and economic issues," *IEEE Trans. Energy Convers.*, vol. 24, no. 3, pp. 661–672, Sept 2009.
[6] R. Billinton *et al.*, "Adequacy assessment considerations in wind integrated power systems," *IEEE Trans. Power Syst.*, vol. 27, no. 4, pp. 2297–2305, Nov 2012.
[7] E. Vittal, M. O'Malley, and A. Keane, "A steady-state voltage stability analysis of power systems with high penetrations of wind," *IEEE Trans. Power Syst.*, vol. 25, no. 1, pp. 433–442, Feb 2010.
[8] M. Chinchilla, S. Arnaltes, and J. C. Burgos, "Control of permanent-magnet generators applied to variable-speed wind-energy systems connected to the grid," *IEEE Trans. Energy Convers.*, vol. 21, no. 1, pp. 130–135, March 2006.
[9] J. V. de Vyver *et al.*, "Comparison of wind turbine power control strategies to provide power reserves," in *2016 IEEE Int. Energy Conf. (ENERGYCON)*, April 2016, pp. 1–6.
[10] M. Triggianese, F. Liccardo, and P. Marino, "Ancillary services performed by distributed generation in grid integration," in *2007 Int. Conf. Clean Elect. Power*, May 2007, pp. 164–170.
[11] T. Van Cutsem *et al.*, "Test systems for voltage stability analysis and security assessment," IEEE/PES Task Force, Tech. Rep. PES-TR19, Aug. 2015. [Online]. Available: http://resourcecenter.ieee-pes.org/pes/product/technical-publications/PESTR19
[12] *PSS®E 34.2.0 Program Application Guide: Volume II*, Siemens Power Technologies International, Schenectady, NY, Apr. 2017.
[13] K. Ma *et al.*, "Thermal loading and lifetime estimation for power device considering mission profiles in wind power converter," *IEEE Trans. on Power Elect.*, vol. 30, no. 2, pp. 590–602, Feb 2015.
[14] D. Zhou *et al.*, "Reliability and energy loss in full-scale wind power converter considering grid codes and wind classes," in *2014 IEEE Energy Conversion Congress and Exposition (ECCE)*, Sept 2014, pp. 3067–3074.

# A Survey of Voltage Stability Indicators Based on Local Synchronized Phasor Measurements

Hannes Hagmar, Le Anh Tuan, Ola Carlson
*Department of Electrical Engineering*
*Chalmers University of Technology*
Gothenburg, Sweden
hannes.hagmar@chalmers.se

Robert Eriksson
*Market and System Development*
*Svenska Kraftnät*
Sundbyberg, Sweden
robert.eriksson@svk.se

***Abstract*—This paper reviews and evaluates the main types of voltage stability indicators (VSIs) based on local measurements and further provides a background to their development. Due to weaknesses during dynamic conditions, the bus VSIs based on Thévenin's equivalent impedance methods are in general found to be unsuitable for most corrective applications, but may instead be used to estimate local loadability margin to voltage instability. Line VSIs, although requiring some data communication, are in general found to be more robust and may in most cases be used both for predictive and corrective applications. Sensitivity-based VSIs are typically more accurate for detecting voltage instability, but are instead sensitive to measurement noise and are highly nonlinear when the system is close to a voltage collapse, consequently being unsuitable for estimating stability margins. The VSIs based on the local identification of voltage emergency situations (LIVES) concept can take into account the delayed effects from load tap changers, making them suitable for corrective applications and to use in local protection schemes.**

***Index Terms*—Voltage stability index, voltage instability, synchronized phasor measurements, instability detection, emergency control, local measurements**

## I. Introduction

Voltage instability is a phenomenon that transmission system operators (TSOs) continuously have to take into account during both planning and operation of the power system. An increasing demand of electric power and the driving force of maximizing economic benefits have pushed the operation of the power system closer to the physical limits [1]. In general, the closer a grid can be operated to these limits, the more economic and efficient it will be. However, this will also make the system more vulnerable to contingencies and disturbances. Hence, there exists a balance between a system that is operated efficiently and one that is operated securely.

Another trend in the electrical power system is the increasing amount of inverter-based renewable generation and other power electronic controlled devices (e.g. FACTS and HVDC) that are being integrated into the power system. These appliances have generally different and significantly faster dynamics compared to more conventional equipment (e.g. synchronous generators). This development will thus with high probability increase the need of developing faster and more efficient methods of assessing the system stability [2].

978-1-5386-7138-2/18/$31.00 © 2018 European Union

In the last decades, the phasor measurement technology has opened several new perspectives and methods for wide-area monitoring and control of the power system [3]. Several voltage stability indices (VSIs) based on phasor measurements have been proposed in the literature. The phasor-based VSIs may mainly be divided into two categories [4]:

1) *VSIs based on local measurements*: These VSIs are based on few or no input from other measurements and are mainly developed using a maximum power transfer theorem or the existence of solutions for the voltage equations.
2) *VSIs based on observability of whole region*: These methods are generally more accurate than the VSIs based on local measurements. However, as the name indicates, they require full observability of the monitored region and the measurements used in these models should preferably be filtered through a state estimator causing increased computation time and complexity.

This paper will perform an extensive review of the development of VSIs based on *local phasor measurements*. The definition of a local VSI is in this paper defined as a VSI relying on measurements from only two or fewer buses. Although PMUs are becoming more widely deployed, few parts of the power systems fulfill the requirement of full observability. Further, all of the VSIs based on local measurements can be extended as the number of PMUs in a power system increases, allowing TSOs to gradually increase the monitoring system as the number of installed PMUs increase.

Previous studies have examined the development of some VSIs, e.g. as in [5], [6]. However, these reviews are more general in their approach and there is no specific focus on phasor-based VSIs using local measurements. This paper examines more the underlying differences and sensitivities to model simplifications between the VSIs and a specific focus is also spent on evaluating practical applications of the different classes. This field of research is also in development and more recent VSIs are lacking in previous reviews. The paper is aimed to provide researchers a good starting point into the field of phasor-based VSIs, as well as giving TSOs an overview of the potential applications and limits. The paper does not strive to evaluate *all* local VSIs, but rather the most prominent and/or

recently developed ones for each class.

The local VSIs may be divided into two main groups, namely; bus voltage stability indices (bus VSIs) and line voltage stability indices (line VSIs). The paper is then organized as follows. In Section II and Section III, the bus and line VSIs are briefly presented. In Section IV, an evaluation and classification of these VSIs are presented, along with a discussion of potential applications. Finally, concluding remarks are presented in Section V.

## II. Bus Voltage Stability Indices

The bus VSIs are in this paper defined as the VSIs only determining the voltage stability in a single bus and by mainly requiring phasor measurements from that bus in the grid. The bus VSIs are based mainly on 3 approaches; either by using (A) Thévenin's Equivalent (TE) impedance methods, (B) sensitivity-based methods using the systems characteristics in the voltage collapse point, or (C) methods based on the so called local identification of voltage emergency situations (LIVES) method [7].

### A. Thévenin Equivalent VSIs

The most common approach for the bus VSIs is to use the TE impedance as a measure of the margin to voltage instability. Considering the simple system in Fig. 1, consisting of a TE and a load bus, it can be shown that the maximum transferable power in the system occurs when $|\overline{Z}_{th}| = |\overline{Z}_L|$. This relationship has been used in several papers, e.g. [8]–[10], to develop a tracking algorithm that uses the TE impedance to estimate the proximity to a voltage collapse. The relationship between the TE equivalents may be stated as:

$$\overline{E}_{th} = \overline{V}_L + \overline{Z}_{th} \cdot \overline{I} \tag{1}$$

where $\overline{E}_{th}$ and $\overline{Z}_{th}$ are the TE voltage and impedance, respectively, and $\overline{V}_L$ and $\overline{I}$ the load voltage and current, respectively. Using the relationship in (1), the values of $\overline{Z}_{th}$ can be estimated. The real and imaginary values of $\overline{E}_{th}$ and $\overline{Z}_{th}$ in (1) results in 4 unknowns, requiring measurements to be taken at two or more times to solve for the unknown parameters. The estimation is based on the assumption that the system is in a quasi-steady-state, where the TE impedance and voltage are constant during the time of the measurements.

*1) Least-squares TE (LS-TE), Impedance Stability Index (ISI), Total Least Squares TE (TE-TLS):* In [8], a least-squares TE method (LS-TE) is introduced, where a larger measurement windows is used to handle measurement noise and the quasi-static TE parameters. The relation between $\overline{E}_{th}$ and $\overline{Z}_{th}$ are then used as the indicator of the proximity to voltage collapse. In [9], the impedance stability index (ISI) is developed by instead using a recursive least-squares algorithm to track these time-varying parameters. The concept is taken further by taking into account and allowing communication of reactive power limits from generators to the local voltage instability predictor relays. In [10], a method based on the total least squares (TE-TLS) was proposed that proved less sensitive to measurement noise to other compared methods.

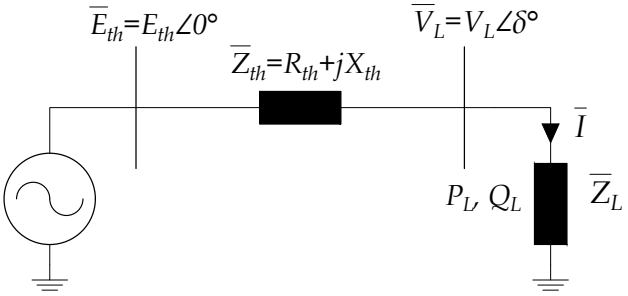


Fig. 1. A Two-bus Thévenin Equivalent Circuit

*2) Adaptive Method (AD):* In [11] and [12], the need for significant system variations between two subsequent measurements and a large data window is addressed. The method, denoted as the Adaptive Method (AD) in previous papers, assumes that $X_{th} \gg R_{th}$, causing the complexity of (1) to be reduced from four unknown variables to three. The proposed algorithm further assumes that $E_{th}$ and $X_{th}$ are constant in the brief interval during their identification, which requires a very short sampling time. The adaptive method then introduces an estimation of $E_{th}$, which allows the TE circuit to be solved directly. From the changes in the $X_{th}$-value the estimated value of $E_{th}$ is then updated. The speed of the adaptive method is depending on how fast the estimation of the $E_{th}$ is allowed to be, where a balance between a fast estimation and a non-oscillatory estimation in general is desired.

*3) Thévenin Equivalent Determination Method (TE-DM):* The assumption of a quasi-steady-state system is not always true, and simultaneous changes in the system side and the load side may cause large errors for TE-methods. In [13], this problem, and the impact of measurement errors, are addressed. The paper proposes a VSI, here denoted as the Thévenin equivalent determination method (TE-DM), based on the following developed relationship:

$$E_{th}^2 = V_L^2 + I^2 Z_{th}^2 + 2P_L R + 2Q_L X \tag{2}$$

where $P_L$ and $Q_L$ are the active and reactive power. Using three different measurements and eliminating $Z_{th}^2$ from the equations allows the equations to be rewritten into:

$$2\Delta P R + 2\Delta Q X + \Delta V_L^2 = 0 \tag{3}$$

where

$$\Delta P = det \begin{bmatrix} 1 & 1 & 1 \\ P_{L(1)} & P_{L(2)} & P_{L(3)} \\ I_{(1)}^2 & I_{(2)}^2 & I_{(3)}^2 \end{bmatrix},$$

$$\Delta Q = det \begin{bmatrix} 1 & 1 & 1 \\ Q_{L(1)} & Q_{L(2)} & Q_{L(3)} \\ I_{(1)}^2 & I_{(2)}^2 & I_{(3)}^2 \end{bmatrix},$$

$$\Delta V_L^2 = det \begin{bmatrix} 1 & 1 & 1 \\ V_{(1)}^2 & V_{(2)}^2 & V_{(3)}^2 \\ I_{(1)}^2 & I_{(2)}^2 & I_{(3)}^2 \end{bmatrix}$$

and where the number index in parenthesis is the measurement number. The three separate measurements can then be used to represent and calculate the TE impedance parameters. To compensate for measurement errors and variations in the system side, additional redundant measurements are proposed to be used to reduce the impact of these factors.

### B. Sensitivity based bus VSIs

*1) S-Difference Criterion (SDC):* There are a number of other Bus VSIs based on other approaches than using the TE-theorem. In [14] and [15], a sensitivity-based method denoted as the SDC is presented. The method is based on using two consecutive measurements of the apparent power on the receiving end of a transmission line. The method is based on the fact that at the voltage collapse point, an increase in the apparent power flow will not increase the received power. The SDC is defined as:

$$SDC = \left| 1 + \frac{\Delta \overline{V}_r^{(k+1)} \overline{I}^{(k)}}{\overline{V}_r^{(k)} \Delta \overline{I}^{(k+1)}} \right| \tag{4}$$

where $\overline{V}_r$ and $\overline{I}$ are the measured phasors of the receiving voltage and current for the measurement $k$ and $k+1$. At the point of voltage instability, the SDC equals zero. In [16] and [17], the validity of such local sensitivity indices are proven by introducing a global index, in the paper called the sensitivity-based Thévenin index (STI). The STI, although requiring data from wide area monitoring systems, are proposed to be used as either validating the results, or for predicting the effects of reactive limits from local indices.

*2) Real-time Voltage Stability Index (RSVI):* In [18], a similar VSI to the SDC is developed, where the relationship between the rate of change of voltage and current magnitudes are used. The RSVI is defined as:

$$RSVI = 1 - \left( \frac{d\left|I_L\right|/dt}{\left|I_L\right|} - \frac{d\left|V_L\right|/dt}{\left|V_L\right|} \right) \tag{5}$$

where $d\left|I_L\right|/dt$ and $d\left|V_L\right|/dt$ are the rate of change of current and voltage magnitudes over a specified period of time ($dt$). In a stable state, the rate of change of voltage is close to zero, resulting in RSVI values less than 1. Near the point of collapse, the RSVI reaches a value of 1 which indicates an impending voltage collapse.

*3) Ambient QV-sensitivity ($\Gamma$-VSI):* Another sensitivity-based method is presented in [19], where a measure based on the slope of the QV-curve is developed. The VSI is based on the fact that, in the voltage collapse point, the slope of the QV-curve will become infinite. The VSI is based on a positive and a negative index, both calculated by the formula:

$$\Gamma_i = \frac{\Delta Q_i}{\Delta V_i} = \frac{\sum_j \Delta Q_{ij}}{\Delta V_i} \tag{6}$$

where $\Delta Q_{ij}$ is the reactive power difference between two measurements for each transmission line connected between two nodes, $i$ and $j$, and $\Delta Q_i$ and $\Delta V_i$ represents the incremental change in reactive power and voltage respectively. The data is split into a positive and a negative subset, which is then used in a weighted mean average to estimate the sensitivities. The methods are further tested in [20], where the sensitivity-based methods are found to be favorable in the sense that that they do not require any model parameters and may be extended to be used in every bus in the grid for higher observability. However, all methods require preprocessing of data as the high sensitivity to noise in the measurements may cause the accuracy of the method to be reduced.

### C. LIVES concept

*1) LIVES and the New LIVES Indicator (LIVES & NLI):* In [7], [21], a method called local identification of voltage emergency situations (LIVES) is introduced and tested. The LIVES stability condition is based on monitoring the change in the secondary voltage after at tap decrease on the primary side ($\Delta r < 0$) of a load tap changing (LTC) transformer, which simplified may be stated as:

$$\frac{\Delta V_2}{\Delta r} < 0 \tag{7}$$

where $\Delta V_2$ is the change in the secondary voltage. Thus, if a tap decrease leads to a negative change in $\Delta V_2$, this indicates an unstable condition. Further, the criterion indirectly takes into account the effect of other taps acting in the system as it can observe the net effect of various LTCs over a cycle of tap operations. In [22], this concept is developed further by monitoring the stability condition of (7), solely from the transformer bus, by assuming that primary voltage and current measurements are available. The decreasing tap change is measured indirectly as an conductance increase seen from the primary side, whilst the secondary voltage is indirectly monitored as an increase of consumed active power, $P$. The new index, denoted as the New LIVES Index (NLI) is formulated as:

$$NLI = \frac{\Delta P}{\Delta G_1} > 0 \tag{8}$$

where

$$G_1 = Re\{\overline{I}_1 / \overline{V}_1\}$$

Simulations shows promise during several different grid conditions and topologies, allowing early indication of impending voltage collapses. The method is further tested in [23], where the method is extended and applied for distance relays of transmission lines feeding weak areas.

## III. Line voltage stability indices

The line VSIs are based on phasor measurements being available from both sides of a two-port transmission line and are mainly based on using one or a combination of three different approaches: (A) maximum power transfer theorem, (B) existence of solutions to the voltage equation, and (C) sensitivity-based line VSIs.

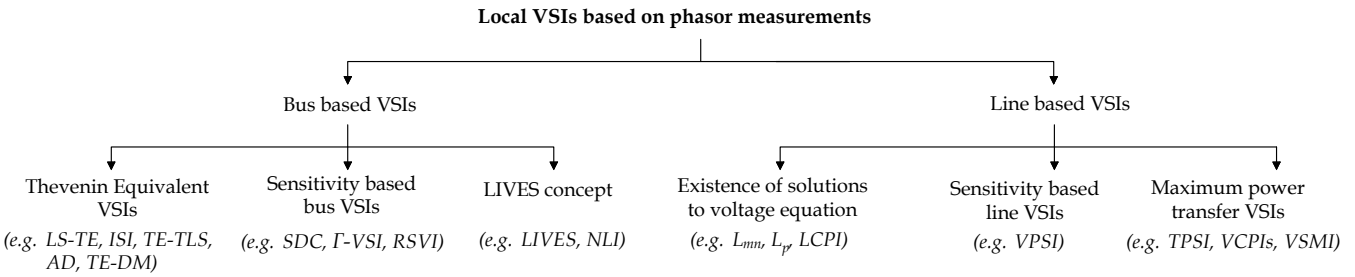


Fig. 2. Classification and some examples of local VSIs based on phasor measurements

### A. Maximum power transfer VSIs

Over the years, several line VSIs based on the concept of maximal transferable power have been developed. These are similar to the TE-based methods for the bus VSIs, with the difference being that phasor measurements are required in each end on of a transmission line.

*1) Transmission Path Stability Index (TPSI), Voltage Collapse Proximity Indicators (VCPIs), Voltage Stability Margin Index (VSMI):* One of the first presented suitable for PMU applications, was the transmission path stability index (TPSI) in [24]. In the TPSI, the maximum power transfer occurs when the voltage drop equals the load-side voltage, according to:

$$TPSI = \frac{V_s}{2} - (V_s - V_r \cos\delta) \tag{9}$$

where $V_s$ and $V_r$ indicates the sending and receiving end voltage, and $\delta$ is the angle difference between the two nodes. This measure is similar to the equal impedance theorem, although it only uses the voltage measurements on each side of a transmission line. Other line VSIs based on similar concepts are the voltage collapse proximity indicators (VCPIs) in [1], where four so called VCPIs are developed, based on the maximum transferable power and the maximum possible line losses that may occur over a transmission line. This is further examined in other papers such as in [25], where similar VSIs based on the same principle are proposed. A simple index, called the voltage stability margin index (VSMI), presented in [26], uses the angle differences between two buses. The VSMI, although showing promise, was found to have limited accuracy for transmission lines with high $Q/P$ ratios.

### B. VSIs based on existence of solutions to voltage equation

The methods based on the existence of solutions to the voltage equation are mainly based on different formulations of the classical power-voltage relationship with negligible line resistance. This relationship may be stated as [27]:

$$V_r = \sqrt{\frac{V_s^2}{2} - QX \pm \sqrt{\frac{V_s^4}{4} - X^2P^2 - XV_s^2Q}} \tag{10}$$

where $P$ and $Q$ is the active and reactive power respectively, and $R$ and $X$ the line resistance and reactance. It can be shown that the maximum power transfer occurs when the value of the inner square root in (10) is zero.

*1) $L_p$, & $L_{mn}$ & Line Collapse Proximity Indicator (LCPI):* In [28] and [29], two popular indices called $L_p$ and $L_{mn}$ are presented, using either the expression for the active or the reactive power and reformulating with respect to solvable values for the discriminant of the voltage equation.

In most of the line VSIs, the shunt susceptance is neglected, which naturally leads to a more restrictive assessment of the proximity to the voltage instability point. This is addressed in [30], where a VSI based on the classical ABCD-matrix of a $\pi$-modeled transmission line is defined according to:

$$LCPI = \frac{4A\cos\alpha(P_L B\cos\beta + Q_L B\sin\beta)}{(V_s\cos\delta)^2} \tag{11}$$

where A and B are the transmission line parameters from the ABCD-matrix, and $\alpha$ and $\beta$ are the respective phase angles of the A and B components. A large amount of other line VSIs based on the similar concept are also presented in other papers.

### C. Sensitivity-based line VSIs

*1) Voltage-Power Sensitivity Index (VPSI):* In [31], the sensitivity of the voltage-to-power characteristics at the voltage instability region is used to form a VSI. The VSI, in this paper denoted as the VPSI, is based on the existence of solutions to the voltage equation and is based on the fact that $dV/dP \to \infty$ at the point of a voltage collapse. The VPSI is then defined as:

$$VPSI = \frac{V_L}{\sqrt{2V_s^2 + 2(P_rR + Q_rX)}} \tag{12}$$

When the system is close to the voltage collapse point, the index of VPSI approaches 1. Although showing effectiveness in simulations, the practical aspects of the VPSI are affected by it being highly non-linear when close to the collapse point. Other events, such as generator capability limits being met, may also affect the accuracy of the VSI.

## IV. Classification and evaluation of VSIs

### A. Classification and attributes

The classification developed in this paper is presented in Fig. 2 and the general attributes are presented in Table I. The inherent local feature of the TE-VSIs is one of the main advantage of that type of indicators, with in principle no requirements of communication from other buses. However, several studies, such as in [32], have shown the weakness

TABLE I
ATTRIBUTES AND EXAMPLES OF LOCAL PHASOR-BASED VSIS

| Type | Subcategory | Index | Attributes & applications |
|---|---|---|---|
| *Bus VSIs* | Thévenin Equivalent VSIs | LS-TE [8]<br>ISI [9]<br>TE-TLS [10]<br>AD [11]<br>TE-DM [13] | Low requirement on data communication<br>Provides information on loadability margins<br>In general unsuitable for corrective applications |
| | Sensitivity-based bus VSIs | SDC [14]<br>Γ-VSI [19]<br>RSVI [18] | Sensitive to measurement noise<br>Nonlinear indicator in collapse point<br>Suitable mostly for corrective applications |
| | Methods based on the LIVES concept | LIVES [7]<br>NLI [22] | Suitable for corrective applications<br>Fast local assessment of voltage stability<br>Used either for weak areas and/or buses with for LTCs |
| *Line VSIs* | Existence of solutions to voltage equation | $L_{mn}$ [28]<br>$L_p$ [29]<br>LCPI [30] | Some data communication requirements<br>Predictive and corrective applications possible<br>Affected by line parameters errors |
| | Maximum power transfer | TPSI [24]<br>VCPIs [1]<br>VSMI [26] | Similar to the VSIs based on existence of solutions to voltage equation |
| | Sensitivity-based line VSIs | VPSI [31] | Similar to sensitivity-based bus VSIs |

of the TE-methods when modeling meshed power systems during nonlinear and dynamic conditions. The fact that the TE parameters are estimated over a time window which has to be wide enough to result in sufficient change in the operating conditions, whilst at the same time narrow enough to assume the quasi-steady state of the system, may also significantly reduce the speed and/or accuracy of these VSIs. Since the line VSIs use measurements from both sides of a transmission line, these are less sensitive to changes in, for instance, system topology. Additionally, they do not have the same requirement for a filtering window as the TE-VSIs.

The sensitivity-based VSIs, both for the bus and the line based, are favorable as they do not require any model parameters. However, they have a drawback of being highly nonlinear when the system is close to the voltage collapse point. The sensitivity-based VSIs are also highly sensitive to measurement noise, which requires some filtering algorithm either on the measurement values or on the signal of the VSI. The VSIs based on the LIVES concept, requires similarly as previous VSIs a filter to reduce noise and short term transients. These method are developed mainly to be applied to either buses with LTCs, or as in the case of the NLI, any transmission bus feeding a weak area.

### B. Potential Applications

The characteristics of the VSIs are of high importance to what kind of practical applications they would be used for. In general, they may either be used for (i) preventive applications, or (ii) for emergency/corrective applications [4]. Preventive applications include the possibility of estimating the local loadability margin, which can be be used by system operators to take preventive actions against voltage instability. Corrective applications include to in real-time detect and warn system operators of voltage instability, as well as initiate local system protection schemes (SPS) that, for instance, can give signals to relays for undervoltage load shedding.

*1) Preventive applications:* The TE-VSIs and for the line VSIs, with the exception of the sensitivity-based VSIs, are mostly suitable for preventive applications. Due to the discussed weaknesses of the TE-VSIs during dynamic conditions, these may in general be unsuitable for corrective and emergency purposes. However, in more stable conditions, the difficulties of estimating the TE parameters, such as the need of using a large time window for filtering, will be reduced. Thus, the TE-VSIs may instead be used to, in near real-time, allow system operators to determine the loadability margin for that specific bus. Such estimations will allow the system operators to track the margin in between the conventional, slower, voltage stability assessments. Most of the line VSIs, being able to both estimate the distance to a voltage collapse, and being more robust during dynamic conditions, allows them to in a larger extent be used for both types of applications.

*2) Corrective applications:* For all categories of the sensitivity-based VSIs, the indicator is mainly useful corrective applications, as those indicators in general are highly nonlinear closer to the collapse point. For corrective applications, speed and accuracy of the assessment is fundamental. However, the inability of most local VSIs to take into account the impact of overexcitations limiters (OELs) and/or the delayed effects of LTC transformers, will cause slower assessments during emergency conditions. This has led recent papers to in a larger extent use so called coupled single-port Thévenin equivalent model (e.g. in [33]), that in a larger extent can take into account the effects of, for instance, OELs. Such methods, although seemingly effective, do require more communication infrastructure and the simplicity of the VSIs based on local measurements are thus lost. For the VSIs based on the LIVES concept, the dynamics of the LTC transformers are being taken into account, allowing them to perform quick identification of impending voltage collapses, and thus being highly suitable for corrective applications and for local SPS.

*3) Practical experience:* Even though PMUs for a quite long time have been deployed into the power system in several countries, practical applications of local VSIs are uncommon and is to a large extent still considered as a "future" application [3]. This notion is confirmed when examining technical reports, where very little practical experience from local VSIs are reported. Although the technology and the methods have been developed for several years, most TSOs seem reluctant of implementing these methods practically. The rather limited practical use of these indicators are, according to the authors of this paper, mainly

due to fact that the robustness of the VSIs still to some extent is undetermined. As blackouts and other major failures are connected with extremely high costs, the robustness of the VSIs are of highest concern to the TSO. Thus, from the view of a TSO, it is more important that a VSI is robust and accurate than having a fast computation time. Furthermore, the overall lack of practical experience may itself deter TSOs to use such methods. Thus, even more research and field testing of the developed VSIs are required.

## V. Conclusion

This paper presents a review of the development of VSIs based on local phasor measurements, and further attempts to classify the VSIs based on their attributes and applications. The TE-VSIs, simple in their design but somewhat inaccurate during dynamic conditions, are mainly proposed to be used to in near real-time monitor the local loadability margin to voltage instability. Line VSIs are in general found to be more robust, whereas the fully local feature is somewhat lost. For the sensitivity-based VSIs, the main drawback is the high sensitivity to measurement noise and the nonlinearity of the indicators. These type of VSIs are thus mainly proposed to be used in corrective assessments, allowing warnings to in real-time be communicated to the system operators. The methods based on the LIVES are able to take into account some of the delayed effects from e.g. LTCs, making them suitable for corrective applications and local SPS. The practical implementations of the local VSIs are limited and more accurate estimations of the robustness and accuracy of the methods are required for a more widespread use.

## References


[1] M. Moghavvemi and O. Faruque, "Real-time contingency evaluation and ranking technique," *IEEE Proc. - Generation, Transmission and Distribution*, vol. 145, no. 5, pp. 517–524, 1998.

[2] F. A. Althowibi and M. W. Mustafa, "Line voltage stability calculations in power systems," in *2010 IEEE Int. Conf. Power and Energy*, 2010, pp. 396–401.

[3] J. O. Brien *et al.*, "Use of synchrophasor measurements in protective relaying applications," in *2014 67th Annu. Conf. Protective Relay Engineers*, 2014, pp. 23–29.

[4] M. Glavic and T. V. Cutsem, "Wide-area detection of voltage instability from synchronized phasor measurements. part I: Principle," *IEEE Trans. Power Syst.*, vol. 24, no. 3, pp. 1408–1416, 2009.

[5] J. Modarresi, E. Gholipour, and A. Khodabakhshian, "A comprehensive review of the voltage stability indices," *Renewable and Sustainable Energy Reviews*, vol. 63, no. Supplement C, pp. 1–12, 2016. [Online]. Available: http://www.sciencedirect.com/science/article/pii/S1364032116301204

[6] M. Glavic and T. Van Cutsem, "A short survey of methods for voltage instability detection," in *2011 IEEE PES General Meeting*, 2011, Conference Proceedings, pp. 1–8.

[7] C. Vournas and T. V. Cutsem, "Local identification of voltage emergency situations," *IEEE Trans. Power Systems*, vol. 23, pp. 1239 – 1248, 09 2008.

[8] K. Vu, M. M. Begovic, D. Novosel, and M. M. Saha, "Use of local measurements to estimate voltage-stability margin," *IEEE Trans. Power Systems*, vol. 14, no. 3, pp. 1029–1035, 1999.

[9] M. Begovic, B. Milosevic, and D. Novosel, "A novel method for voltage instability protection," in *Proc. 35th Annu. Hawaii Int. Conference System Sciences*, 2002, pp. 802–811.

[10] J. Lavenius, L. Vanfretti, and G. N. Taranto, "Performance assessment of PMU-based estimation methods of Thevenin equivalents for real-time voltage stability monitoring," in *2015 IEEE 15th Int. Conf. Environ. and Elect. Eng. (EEEIC)*, 2015, pp. 1977–1982.

[11] S. Corsi and G. N. Taranto, "A real-time voltage instability identification algorithm based on local phasor measurements," *IEEE Trans. Power Systems*, vol. 23, no. 3, pp. 1271–1279, 2008.

[12] ——, "Voltage instability alarm by real-time predictive indicators," in *2012 IEEE Power and Energy Society General Meeting*, 2012, pp. 1–10.

[13] S. M. Abdelkader and D. J. Morrow, "Online Thevenin equivalent determination considering system side changes and measurement errors," *IEEE Trans. Power Systems*, vol. 30, no. 5, pp. 2716–2725, 2015.

[14] G. Verbic and F. Gubina, "A novel concept for voltage collapse protection based on local phasors," in *IEEE/PES Transmission and Distribution Conf. and Exhibition*, vol. 1, 2002, pp. 124–129 vol.1.

[15] ——, "A new concept of voltage-collapse protection based on local phasors," *IEEE Trans. Power Delivery*, vol. 19, no. 2, pp. 576–581, 2004.

[16] A. Reddy, R. Matavalam, and V. Ajjarapu, "Validation of the sensitivity based thevenin index on large systems," in *2017 IEEE PES General Meeting*, 2017, pp. 1–5.

[17] A. R. R. Matavalam and V. Ajjarapu, "Sensitivity based thevenin index with systematic inclusion of reactive power limits," *IEEE Trans. Power Systems*, vol. 33, pp. 932–942, 2018.

[18] B. Shakerighadi, F. Aminifar, and S. Afsharnia, "A real-time voltage stability index based on local measurements," *2015 23rd Iranian Conf. on Electrical Eng.*, pp. 1492–1497, 2015.

[19] X. Liu, X. Zhang, and V. . Venkatasubramanian, "Distributed voltage security monitoring in large power systems using synchrophasors," *IEEE Trans. Smart Grid*, vol. 7, no. 2, pp. 982–991, 2016.

[20] H. Li, A. Bose, and V. M. Venkatasubramanian, "Wide-area voltage monitoring and optimization," *IEEE Trans. Smart Grid*, vol. 7, no. 2, pp. 785–793, 2016.

[21] C. Vournas, C. Lambrou, and M. Kanatas, "Application of local autonomous protection against voltage instability to ieee test system," *2016 IEEE PES General Meeting*, pp. 1–1, 2016.

[22] C. Vournas, C. Lambrou, and P. Mandoulidis, "Voltage stability monitoring from a transmission bus pmu," vol. PP, pp. 1–1, 11 2016.

[23] C. Vournas and P. Mandoulidis, "On-line voltage stability monitoring," in *Circuits and Systems (ISCAS), 2018 IEEE Int. Symposium on*. IEEE, 2018, pp. 1–5.

[24] F. Gubina and B. Strmcnik, "Voltage collapse proximity index determination using voltage phasors approach," *IEEE Trans. Power Syst.*, vol. 10, no. 2, pp. 788–794, 1995.

[25] Y. Gong, N. Schulz, and A. Guzmán, "Synchrophasor-based real-time voltage stability index," in *2006 IEEE PES Power Syst. Conf. and Exposition*, 2006, pp. 1029–1036.

[26] T. He, S. Kolluri, S. Mandal, F. Galvan, and P. Rasigoufard, "Identification of weak locations in bulk transmission systems using voltage stability margin index," in *IEEE Power Eng. Society General Meeting, 2004.*, 2004, pp. 1814–1819 Vol.2.

[27] T. V. Cutsem and C. Vournas, *Voltage stability of electric power systems*. Boston: Kluwer Academic Publishers, 1998.

[28] M. Moghavvemi and F. M. Omar, "Technique for contingency monitoring and voltage collapse prediction," *IEE Proc. - Generation, Transmission and Distribution*, vol. 145, no. 6, pp. 634–640, 1998.

[29] M. Moghavvemi and M. O. Faruque, "Technique for assessment of voltage stability in ill-conditioned radial distribution network," *IEEE Power Eng. Rev.*, vol. 21, no. 1, pp. 58–60, 2001.

[30] R. Tiwari, K. R. Niazi, and V. Gupta, "Line collapse proximity index for prediction of voltage collapse in power systems," *Int. J Elec. Power & Energy Syst.*, vol. 41, no. 1, pp. 105–111, 2012. [Online]. Available: http://www.sciencedirect.com/science/article/pii/S0142061512000774

[31] X. Ancheng *et al.*, "On-line voltage stability index based on the voltage equation of transmission lines," *IET Generation, Transmission & Distribution*, vol. 10, no. 14, pp. 3441–3448, 2016.

[32] M. Glavic and T. V. Cutsem, "Wide-area detection of voltage instability from synchronized phasor measurements. part II: Simulation results," *IEEE Trans Power Syst.*, vol. 24, no. 3, pp. 1417–1425, 2009.

[33] H. Y. Su and C. W. Liu, "Estimating the voltage stability margin using PMU measurements," *IEEE Trans. Power Systems*, vol. 31, no. 4, pp. 3221–3229, 2016.